Temperature Dependent Behavior of Optical Loss from Hydrogen Species in Optical Fibers at High Temperature

Elizabeth Ann Bonnell

Thesis submitted to the faculty of the Virginia Polytechnic Institute and State University in partial fulfillment of the requirements for the degree of

Master of Science

In

Materials Science and Engineering

Gary R. Pickrell, Chair

Daniel S. Homa

Christopher R. Winkler

7 April 2015

Blacksburg, VA

Keywords: Hydrogen, Fiber Optics, OH Species, Temperature Dependence, Glass Structure, Infrared Spectroscopy, Diffusion

Temperature Dependent Behavior of Optical Loss from Hydrogen Species in Optical Fibers at High Temperature

Elizabeth Ann Bonnell

ABSTRACT

This study reports on the behavior of silica based optical fibers in a hydrogen environment at high temperatures. The hydrogen response in the form of optical loss in the wavelength range of 1000-2500 nm of a germanium doped graded index 50/125 graded index fiber was examined in the temperature range of 20–800 °C. When the fiber was exposed to hydrogen at 800 °C two absorption bands appeared: ~1390 nm assigned to the first overtone of the hydroxyl stretch and ~2200 nm band with complex assignments including the combination mode of the fundamental hydroxyl stretch with SiO_4 tetrahedral vibrations and the combination mode of SiOH bend and stretch. The growth rate of the 1390 nm band fits the solution to the diffusion equation in cylindrical coordinates while the 2200 nm band does not. Absorption for both bands persisted as the fiber is cooled to room temperature. Temperature dependent behavior was observed in that as temperature increases from room temperature, the absorption intensity decreases and band shifts slightly to longer wavelengths. Temperature dependence is repeatable and reversible. However, if no hydrogen is present in the environment at temperatures greater than 700 °C, the 1390 nm band will permanently decrease in intensity, while the 2200 nm band does not change. Changes in the structure of the glass appear to be causing this temperature dependent behavior. Other necessary conditions for structural changes to cause this temperature dependent behavior are examined

Dedication

Without the prayers and encouragement of the following people this work would not have been possible: Jeananne Knies, Brit Hoskins, Dave Duckett, Gwen Reese, Kearah Donato, Anita Walz, Adriana Balcazar, Phillip Tweedy, Erika Holoub, Mary Westerman, Laura Dase, Mary McDonald, and many others. Constant support, cheerleading, and proofreading by my family made this work a success. Thanks to Megan Bonnell, Patricia Bonnell, David Bonnell.

Acknowledgements

There were many people who contributed academically to the success of this work. I would like to thank Dr. Bill Reynolds of the MSE department for constant support in computational interpretation of my data. In all his help and support he never ceased to shine the light of Christ into my life. I would like to thank Dr. Chris Winkler and Dr. Dan Homa from MSE for guiding me in the right direction for experimentation and theoretical foundations in addition to serving faithfully on my committee. Thanks to Dr. Anbo Wang, from the Center for Photonics Technology (CPT) in Electrical Engineering, for generously granting me access to the equipment I needed to conduct experimental work and for always graciously addressing my requests. I would like to thank Li Yu from CPT in Electrical Engineering for training me in optical measurements, experimental setup, and data processing. His contributions and example have been integral to the success of this work and my growth as a scientist and engineer. Thanks to Dr. Michael Buric and Dr. Paul Ohodnicki from the National Energy Technology Laboratory for providing mentoring and the funding for the research that sparked this work. Thanks to Dr. Al Wicks of Mechanical Engineering and Dr. Kathleen Meehan of Electrical Engineering who gave me my start in graduate school whose mentorship was the foundation upon which my career as a student has been built. And a most important final thanks to my adviser Dr. Gary Pickrell. His faith in me as a student, dedication to my success through advising, selecting me for the project that started this work, provision through funding, and high standards for excellence has been the cornerstone of my academic success. Thank you.

This technical effort was performed in support of the National Energy Technology Laboratory's ongoing research under the RES contract DE-FE0004000.

Disclaimer

This project was funded by the Department of Energy, National Energy Technology Laboratory, an agency of the United States Government, through a support contract with URS Energy & Construction, Inc.

Contents

Figures

Tables

1. Introduction

Fiber optic sensing technology is a growing field home to a vast array of current research and applications. Sensing capabilities span the range of applications including chemical [14], temperature [15], and mechanical sensing [16]. This comprehensive sensing range and robust qualities like small footprint, EMI immunity, corrosion resistance, and high operating temperatures make fiber optic sensors a favorite for harsh environment sensing solutions. To best assure sensor system reliability the harsh environment response of fused silica optical fibers must be understood as well. Although the phenomenon of hydrogen darkening, that is degradation of optical signal by hydrogen penetration, is well known, its temperature dependent behavior is not understood. The characterization of this temperature dependent behavior, especially at high temperatures, is essential for designing robust sensing systems.

Hydrogen penetration in optical fibers causes absorption peaks at vibrational frequencies of the hydrogen species present, some of which occur in the operating range of most fiber optic applications. The diffusion rate of hydrogen in glass is very fast, room temperature diffusivity $D_{H_2} \approx 1.163 \times 10^{-11} cm^2 \cdot s^{-1}$ [11], the rate increasing with increasing temperature; hence the performance of optical fiber can be degraded quickly in a hydrogen environment. In his review paper, "Reliability of optical fibers exposed to hydrogen", Lemaire [17] shows that hydrogen exposure can cause significant signal degradation in a matter of hours. Figure 1, generated from this work, shows that the signal through only 15 cm of optical fiber can show prominent peaks in just 30 minutes at 800 °C and also increase over time.

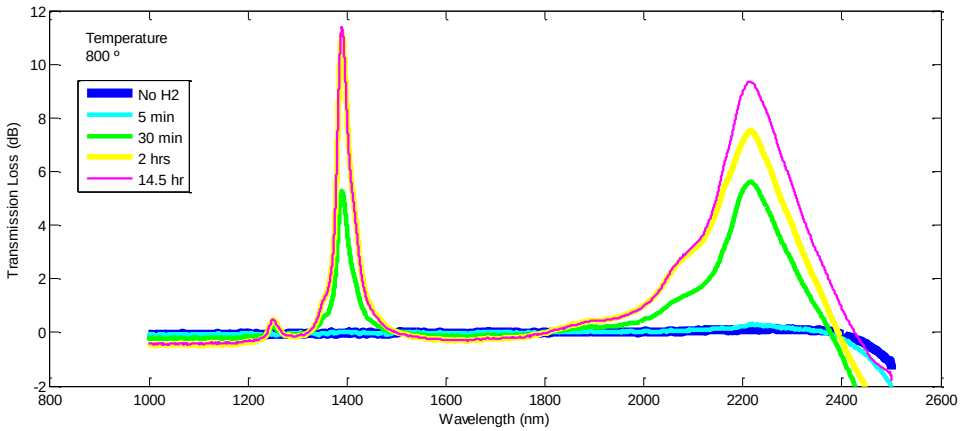

Figure 1 Absorption in Ge doped graded index 50/125 optical fiber at different lengths of time of hydrogen exposure

At low temperatures the primary hydrogen species is physically dissolved hydrogen molecules occupying interstitial space in the glass network [11, 18]. Absorption due to physically dissolved hydrogen is often referred to as "reversible" because the hydrogen can be caused to diffuse back out of the fiber, for instance when the source of hydrogen is removed [11, 17] At higher temperatures (above 150 °C [17]) the rate at which dissolved hydrogen will react with the glass network increases, usually resulting in hydroxyl formation, such that absorption due to reacted hydrogen species dominate. Absorption due to species formed by reaction is called permanent or irreversible [11, 17] (although some processes have been

developed to remove it [19, 20]). It is often understood that reactions occur at defect sites in the glass [17] and thus when all defect sites have participated in reactions, the fiber is saturated and no more OH formation is possible at which point the concentration cannot increase [17]. The absorption frequency of the OH stretch lies in the infrared and has overtones in the near infrared. One approach employed to determine the concentration of OH in glass is to examine the size of the absorption peak related to OH vibrational frequencies via infrared spectroscopy [17, 21, 22].

In a study to evaluate silica optical fiber performance in a hydrogen environment at high temperatures, the attenuation of step index pure silica core and graded index germanium doped core multimode fibers was monitored in situ with temperature and hydrogen exposure. Temperature dependent behavior of the IR absorption bands of the hydroxyl groups around 2200 nm and 1390 nm was observed in the range from 20–800°C during the tests. The temperature dependent behavior of the hydroxyl absorption in the two bands, ~1390 nm and ~2200 nm, in silica glass at high temperatures is consistent with other studies [1, 23, 24]. This work expands on the knowledge of the behavior showing its reversibility and repeatability, as well as surprising findings about the differences in the behavior of these two absorption bands over time when hydrogen is removed from the environment. The temperature dependent behavior of these two peaks coupled with the disparity of their time dependent behavior suggest that the entire glass structure is changing with temperature.

2. Theory

2.1 Infrared Spectroscopy

Infrared spectroscopy is a characterization technique which can provide molecular structure information about a sample. A sample is illuminated by a broadband light source containing frequencies in the infrared and the transmitted absorption spectra contains features that are characteristic of the molecular rotation and vibration modes of the molecules present in the sample. It is a technique that is complementary to Raman absorption spectroscopy as they are sensitive to different rotational and vibrational modes and they can be used together to get a more complete picture of the material properties.

2.1.1 Molecular Vibrational Modes

Molecules, like atoms, are rather particular about what energies are allowed for their excited states. Like electron states in atoms, molecules have vibrational and rotational states whose energy levels are quantized. This quantization of vibrational energies arises from the differential equations and boundary conditions that describe them and the requirements of quantum mechanics. Differential equations with boundary conditions always yield quantized results which, for this discussion, mean specific vibrational modes with specific frequencies. Quantum mechanics provides boundary conditions for the molecular vibrational modes in the same fashion as it does for electronic energy states in an atom. This section will consider some of the consequences of these quantized solutions.

2.1.2 Normal Vibrational Modes

Molecules have bonds that can be considered classically like springs that follow Hooke's law [25]:

$$F = -kx \tag{1}$$

Where **F** is the force on the mass, **m,** attached to the spring, **k** is the spring constant, and **x** is the direction of displacement of the system. Equation (1) can be re-written in the form of the following differential equation [25]:

$$\ddot{x} = -\frac{k}{m}x \tag{2}$$

The solution to Equation (2) yields a normal frequency for each set of coordinates, $\vec{x}$.

The number of atoms in a molecule, **N**, will determine how many coordinates are needed to specify the orientation of this molecule in space, **3N**, and will thus specify the number of vibrational frequencies the molecule will have. That system of coordinates can be reduced to its most simplified set by specifying the

location in space of the center of mass of the molecule and then specifying the orientations of the atoms with respect to the center of mass reducing. The vibrational modes resulting from the solution to Equation **(2)** in the center of mass coordinate system are called normal modes. Since linear molecules require one less angular coordinate to specify the location of the center of mass in space, five coordinates instead of the six coordinates needed for non-linear molecules. Expressions to determine the number of normal vibrational modes for a molecule of **N** atoms can be stated as

$$3N - 5 \tag{3}$$

for linear molecules and

$$3N - 6 \tag{4}$$

for non-linear molecules.

Molecular vibrational modes are then energy states of a molecule not dissimilar from electronic energy states in an atom. Rotational modes exist as well whose mathematical treatment is similar to the vibrational modes. Rotational modes are modeled with ridged rotator physics and yield similar quantized results. These two types of molecular energy levels can combine to create combination modes. When the frequency of any of these energy levels falls in the infrared range and if the mode has an oscillating dipole moment it can interact with infrared radiation at that frequency by absorption of the radiation.

2.1.3 Normal Vibrational Modes Examples

Water Molecule

Consider a water molecule: it is a non-linear molecule with three atoms in it. Using Equation (4) the number of vibrational modes works out to be 3 (3*3-6=3). The three modes for water, symmetric stretching ($\mathbf{v}_1$), bending ($\mathbf{v}_2$), and antisymmetric stretching ($\mathbf{v}_3$), are illustrated in Figure 2. Each mode has its own frequency, which is related to the masses of the atoms and the strengths of the bonds between them. The parameters that control frequency come into the math via the **k/m** coefficient in Equation (2) for each of the coordinate sets needed to describe the molecule. All of these modes for the water molecule

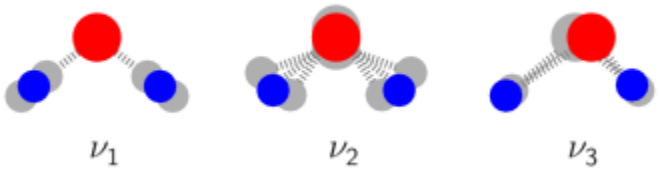

Figure 2 Water molecule vibrational modes.
Stefan.Water is blue ... because water is blue. 2009 [cited 2014 3 June 2014]. Reproduced under fair use 2015. [6]

have an oscillating dipole moment, which means they will absorb radiation of the same energy as that of their mode.

Silicate Molecule

Now consider the silicate molecule: SiO_4. It is a non-linear molecule composed of five atoms. Using Equation (4) the number of vibrational modes works out to be 9 (3*5-6 =9). Similar to the water molecule there are stretching and bending modes. But recall that the frequencies of normal modes are determined by the masses of the atoms involved and the strength of the bonds. Since SiO_4 is a tetrahedral molecule with Si in the center and O on each corner, there are several normal modes with the same vibrational frequency because the masses and bond strengths involved are the same. When modes have the same frequency they are said to be degenerate. For the SiO_4 molecule there are only four distinct frequencies even though there are nine normal modes. The modes are as follows: Mode one is the totally symmetric stretching mode (or breathing mode), modes two and three are the doubly degenerate bending mode, modes 4, 5, and 6 are the triply degenerate antisymmetric stretching mode, and modes 7,8, and 9 are the triply degenerate antisymmetric bending mode, as shown in Figure 3. In the isolated silicate molecule all modes are all Raman active and but only the ν_3 and ν_4 vibrations are active in the infrared. In other symmetries the ν_1 and ν_2 vibrations can display infrared activity [10, 26].

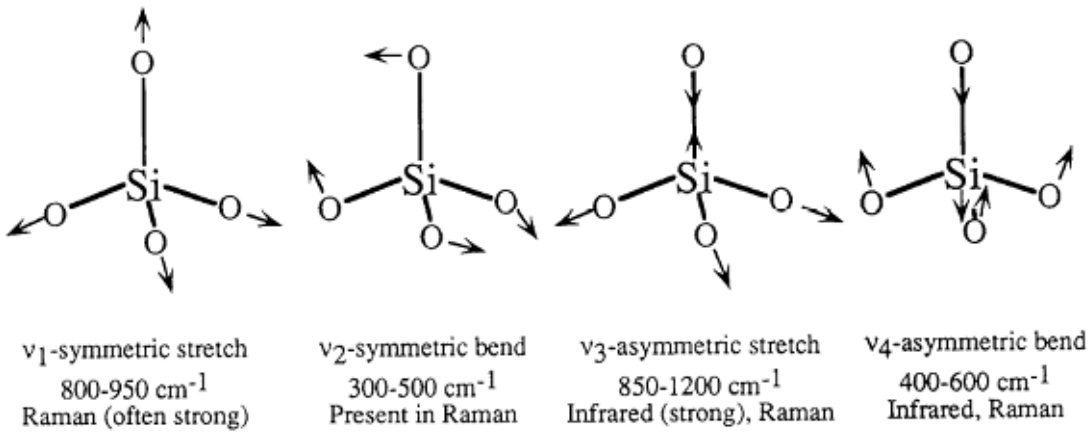

Figure 3 The normal modes of vibration of an SiO_4-tetrahedra. Within isolated tetrahedra, all vibrations are Raman-active, while only the ν_3 and ν_4 vibrations are active in the infrared. However, environments with no-tetrahedral symmetries frequently produce infrared activity in the ν_1 and ν_2 vibrations in silicate minerals.
Williams, Q., Infrared, Raman and Optical Spectroscopy of Earth Materials, in Mineral Physics & Crystallography: A Handbook of Physical Constants. 2013, American Geophysical Union. p. 291-302. Used with permission from John Wiley and Sons. [10]

2.1.4 Classical Electrodynamics

A classical electrodynamics treatment will be sufficient to connect the normal vibrational modes of molecules to the absorption of infrared radiation, which is the basis of infrared spectroscopy. As previously stated quantum mechanics is necessary to get specific energy level distribution and spectrum intensities, but it will not be necessary to get to get to why vibrational modes absorb light. To begin the discussion it will be useful to review some classical electrodynamics theories.

2.1.5 Electric Fields in Matter

Recall from electrodynamics that when a dielectric is in the presence of an electric field the electric field pulls the nucleus of the atoms and the electron cloud apart, thus polarizing the atoms or molecules of the material. This slight shifting around of charge in the direction of the electric field, $\vec{\boldsymbol{E}}$, is called an induced dipole moment, $\vec{\boldsymbol{p}}$. The induced dipole moment is proportional to the electric field by a constant of proportionality called the polarizability of the molecule, $\tilde{\boldsymbol{\alpha}}$, which is a symmetric tensor. The polarizability of a material is the ease with which the electron density distribution of the molecules can be distorted by an electric field. This polarizability tensor plays a greater role in Raman activity which requires that the vibrational mode have a change in polarizability. Infrared activity requires the vibrational mode to have a change in dipole moment. Equation (5) shows that the magnitude of the dipole moment induced by an electric field is the product of the polarizability tensor and the electric field [27]:

$$\vec{\boldsymbol{p}} = \tilde{\alpha}\vec{\boldsymbol{E}} \tag{5}$$

2.1.6 Oscillating Electric Field

Light is an oscillating electromagnetic field, which means it has an oscillating electric field component. Consider the following oscillating electric field [27]:

$$E = E_0 \cos(2\pi\nu t) \tag{6}$$

Writing the induced dipole moment in terms of this oscillating electric field yields [27]:

$$p = \alpha E_0 \cos(2\pi\nu t) \tag{7}$$

Equation (7) indicates an interesting situation about how light can interact with matter: incident radiation induces an oscillating dipole moment. But from the treatment of molecular vibrational modes (and rotational modes and rovibrational modes) we know that the energy levels of these modes are quantized. Combine this result with the quantum nature of light, i.e., Equation (8)

$$E = h\nu \tag{8}$$

and incident light of the same energy as vibrational modes that have an oscillating dipole moment will be absorbed. Thus if the mode energy levels of species are known, then the presence of those species in a sample can be characterized by studying the infrared absorption spectra of the sample.

2.1.7 Infrared Spectroscopy Materials Characterization

The infrared spectroscopy material characterization technique capitalizes on molecular preference for absorbing specific wavelengths. Collecting the spectrum transmitted through a sample illuminated by a broad band light source will provide composition information about the sample. The relationship between the absorbance at a specific wavelength and the concentration of the absorbing species is given by the Beer's law

$$A(\lambda) = \epsilon(\lambda)cx \tag{9}$$

where $\boldsymbol{A(\lambda)}$ is the absorbance at the band maximum, $\boldsymbol{\epsilon(\lambda)}$ is the molar extinction coefficient, $\boldsymbol{c}$ is the concentration of the absorbing species, and $\boldsymbol{x}$ is the optical path length through the sample [22, 28-30]. If the value of $\boldsymbol{\epsilon}$ is known for a species at a specific wavelength the concentration can be identified. Even if the exact concentration cannot be calculated, the presence of a species can be determined by the presence of its characteristic absorption peaks in the spectra of the sample. Infrared spectroscopy is dependent on the absorption of specific wavelength of light by a specific vibrational energy state of the absorbing species. The local environment of a species affects its bond energies which in turn affect its vibrational frequencies thus broadening the absorption peak into an absorption band. This peak broadening can make it more difficult to interpret absorption spectra for sample composition. If two or more species have absorption energies near each other, the spectral resolution may not be able to provide differentiation between spectral lines of different species. Deconvolving peaks to try to sift out this information is not trivial. Although the infrared absorption spectra provides a composition fingerprint for a sample, interpreting the spectra, especially in the case of a solid sample, which will considerably broaden the absorption bands, is not always simple.

The selection rules which come from the values that the quantum numbers in the solution to the Schrödinger equation for the harmonic oscillator govern which transitions are permitted. These selection rules restrict the value for the vibrational quantum number of the harmonic oscillator to

$$\Delta v = \pm 1 \tag{10}$$

Equation (10) then requires that the frequency of absorbed light be exactly the same as the vibrational frequency. However, in infrared spectroscopy, overtone frequencies of the same vibrational state are seen. In other words light is absorbed at two, three, and so on multiples of the vibrational frequency of the mode. This seeming violation of quantum mechanics is due to the fact that the vibrational modes were derived from a simple harmonic oscillator model which is oversimplified for the physical molecular system.

References [22, 27, 28]

2.2 Fiber Optics

Understanding the basics of fiber optic operation is a necessary foundation for understanding how the reliability of fiber optic systems are affected and degraded by hydrogen exposure. This section will build a skeletal framework for the principles governing the operation of fiber optics. Some topics, such as solving Maxwell's equations for cylindrical waveguides, polarization, and mode theory, are essential for a comprehensive understanding of optical laws governing fiber optics but are superfluous for the optical foundation needed here. A ray optics treatment for wave theory will suffice for understanding fiber optic operation and the quantum nature of light will be used without rigorous derivation.

2.2.1 Optical Theory and Definitions

Light, is an oscillating electromagnetic field thus a material's response to electromagnetic radiation, is of critical concern when understanding its optical properties. Light, as a wave, has a wavelength and frequency whose product is the speed of light. Those properties in vacuum are usually used to characterize the light, but light does not travel at the same speed in a material as it does in a vacuum. The ratio between the speed of light in a vacuum and the speed of light in a material is known as the index of refraction, **n**, which is the chief optical property of a material:

$$n = \frac{c_{vac}}{c_{mat}} \tag{11}$$

The speed of light in a vacuum is

$$c = \lambda f \tag{12}$$

where $\boldsymbol{\lambda}$ is the wavelength and $\boldsymbol{f}$ is the frequency. In a material the speed of light is smaller than in vacuum thus the index of refraction, **n** is usually greater than 1. The wavelength is also smaller in a material; however the light is usually described by its wavelength in vacuum. It is the wavelength that changes and not the frequency because of the quantum nature of light, namely

$$E = h\nu \tag{13}$$

where **E** is the energy of the photon and $\boldsymbol{h}$ is Planck's constant and $\boldsymbol{\nu}$ is the frequency. Energy is related only to the frequency, and the medium does not change the energy of light, thus it is the wavelength of light in a material that is changed along with the speed and not the frequency. But this relationship also shows that the index of refraction of a material is wavelength dependent. Usually only the index of refraction for the normal operating wavelength of an optical material is specified.

In ray optics, light does not change course unless it encounters a boundary between two different indices of refraction. Consider two materials of different indices of refraction placed together with a flat boundary. When a ray of light traveling in one material encounters the material boundary part of it will be

reflected and part of it will be refracted. The reflected portion travels back through the original material while the refracted portion changes course as it crosses the boundary. The angle of incidence is known as the angle between the incident ray and normal to the boundary as depicted in Figure 4. This angle of incidence and the different indices of refraction are the essential components for understanding what happens at the material boundary from a geometric optics perspective. The relationship describing the behavior of the ray at the boundary is known as Snell's law given by

$$n_1 \sin \varphi_1 = n_2 \sin \varphi_2 \tag{14}$$

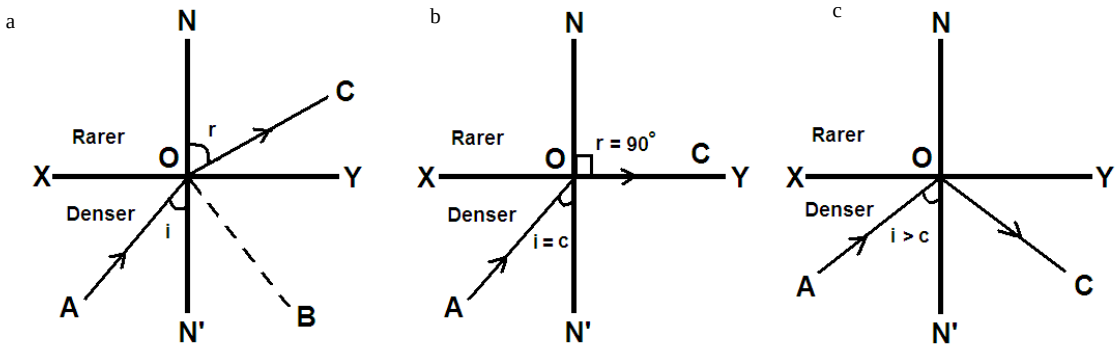

Figure 4 (a) representation of refraction and reflection of a light ray at a material boundary; (b) representation of the critical angle of reflection; (c) representation of total internal reflection.
Refraction, reflection, and what is total reflection? 2015; Available from: http://physics.stackexchange.com/questions/37731/refraction-reflection-and-what-is-total-reflection. Reproduced under fair use. [8]

where $\mathbf{n_1}$ is the index of refraction of the first material; $\boldsymbol{\varphi_1}$ is the angle of incidence at the boundary of the light ray traveling through the first material; $\mathbf{n_2}$ is the index of refraction of the second material; and $\boldsymbol{\varphi_2}$ is the angle of refraction for the light refracted across the boundary into the second material. The angle of refraction, like the angle of incidence, is measured from normal to the boundary. Figure 4 (a) depicts the scenario of a ray of light encountering a material boundary. The portion of the ray reflected back into the first material is reflected 90° across the normal from the incident ray. The path of the refracted ray, transmitted into the second material, is bent (again measured from normal) and related to the incident angle and the indices of refraction of the two materials on either side of the boundary via the Snell's law relationship stated in Equation (14). [31, 32]

When the index of refraction of the first material is greater than the index of refraction of the second material $(\boldsymbol{n_1 > n_2})$ there exists an angle of incidence, $\boldsymbol{\varphi_c}$, for which $\mathbf{\sin \varphi_2 = 1}$. That means the light is refracted at 90° to normal or along and parallel to the material boundary. This angle is known as the critical angle, shown in Figure 4 (b). The critical angle is defined by the following relationship:

$$\sin \varphi_c = \frac{n_2}{n_1} \tag{15}$$

For all incident angles greater than the critical angle the left hand side of Equation (15) approaches one while $\frac{n_2}{n_1}$ cannot increase further and is always less than one because $n_1 > n_2$. Thus for light incident at any angle greater than the critical angle there will be no refracted ray and all of the incident ray will be reflected back into the first material. This case is known as total internal reflection and is depicted in Figure 4 (c).

The phenomenon of total internal reflection can be exploited to create a kind of conduit where light will be guided.

2.2.2 Architecture of Optical Fiber

It is impossible to rigorously describe waveguide technology and treat mode theory without solving Maxwell's equations for the geometry of the waveguide. Nonetheless, a ray optics version of a cylindrical waveguide can suffice for understanding the architecture of an optical fiber.

Although many exotic structures exist, a conventional optical fiber is a solid dielectric material, frequently silica glass, with cylindrical geometry. It consists of a core and a cladding where the core has a higher index of refraction than the cladding such that light can totally internally reflect at the core-cladding boundary and be guided down the length of the fiber. Although both the core and cladding are typically silica glass (SiO_2) either the core, cladding, or both are doped to adjust their respective indices to create the necessary material boundary. The boundary between their indices of refraction can either be abrupt as in a step index profile or graded such that the index changes gradually from the higher index of the core to the lower index of the cladding.

A further demarcation of fiber types, beyond index of refraction profiles, is that of single-mode (SM) and multimode (MM). A typical ray optics drawing suggests that multiple total internal reflection paths available to entering light rays might delineate the difference between SM and MM fibers.

Fibers are fabricated by drawing a glass rod called a preform into a fiber. The preform is fabricated, often by vapor axial deposition (VAD) or modified chemical vapor deposition (MCVD), such that its core and cladding have the same properties as the desired fiber. Although the preform is much larger than the eventual fiber, it has the same relative dimensions which are scaled down as the fiber is drawn from it. The preform is lowered into a furnace and heated to drawing temperature and drawn into a fiber. Modern technology has provided many successful process control measures that allow for uniform fiber drawing controlling dimension to nanometer precision.

A fiber is often described by the dimensions of its core diameter and total fiber outer diameter which are usually on the scale of microns. For example, a fiber whose core is 50 μm in diameter and total outer diameter is 125 μm will be characterized as a 50/125 fiber. The index of refraction profile will be specified as well with the two standard options being step index and graded index. Usually the doping compound of the core and cladding will be specified but the concentrations and indices of refraction are frequently proprietary. Instead of specifying index of refraction for the core and cladding the numerical aperture is specified. Numerical aperture (NA) is a physical specification for coupling light to the fiber and may be approximated by a relationship between the indices of refraction for the core and cladding as given by Equation (16) [32].

$$NA = \sqrt{\left(n_{core}^2 - n_{cladding}^2\right)}$$

(16)

Because numerical aperture is a physical parameter needed for optical system design and operation fiber manufactures usually specify only numerical aperture keeping core and cladding indices of refraction as proprietary information.

2.2.3 Optical Signal

The purpose of optical fibers is to send optical signals from one end of the fiber to another. This signal is usually measured in a dimensionless power ratio of decibel denoted dB. It requires a logarithmic comparison of the optical power measured to some reference optical power as shown by

$$Power\ in\ dB = 10log\frac{P_2}{P_1}$$

(17)

An alternative but similar unit of measurement is dBm, which follows the same logarithmic power ratio comparison as Equation (17) but the reference power, or $\mathbf{P_1}$, is equal to 1 mW (miliWatt). Transmission loss is known as attenuation. Because the signal is guided through the core signal attenuation generally comes from either the core properties or the core-cladding interface. Evanescent modes are transmitted through the cladding and can interact with the modes guided in the core. The intensities of these modes are much lower than that of the modes guided in the core. In a graded index fiber the shape of the radial signal intensity from core to cladding is parabolic resulting in even more signal intensity transmitted through the cladding. Impurities can cause absorption attenuating the signal with impurities present in the core having a larger attenuating effect than those present in the cladding. Absorption can be thought of as plucking a photon out of the total number propagating thus lessening the power of the signal. Scattering related attenuation can occur from the bulk of the core or form non-uniformities in the core-cladding interface. Scattering can be thought of as redirecting rays of light such that they escape the core and are no longer guided or, in other words, follow a path that will not totally internally reflect at the core-cladding interface. Impurities can cause scattering or absorption. Defects in the core cladding interface will cause scattering.

References [31, 32]

2.3 Diffusion

Diffusion describes the transportation of matter from one area of a system to another on the molecular level. The mathematical description of diffusion will be treated here.

2.3.1 The Diffusion Equation

Mass must move in the opposite direction of greatest change of chemical potential which is linearly proportional to the net velocity of the particles when the driving force is small [33] thus the flux of particles is

$$\vec{J} = -CM\vec{\nabla}\mu \tag{18}$$

where **C** is concentration, **M** is particle mobility, and **μ** is chemical potential. Writing the chemical in terms of concentration and using the chain rule the flux can be rewritten as

$$\vec{J} = -CM\frac{\partial \mu}{\partial C}\vec{\nabla}C \tag{19}$$

Fick's laws are the laws describing the diffusion processes. Fick's first law is concerned with relating the flux of particles to the change in concentration of particles with space. They are related by a parameter called diffusivity, **D**, which collects the concentration, mobility, and the change of chemical potential with concentration factors together into one term. Fick's first law (in an isotropic medium) can be written as:

$$\vec{J} = -D\,\vec{\nabla}C \tag{20}$$

where $\vec{J}$ is the flux vector, **D** is the diffusivity or diffusion coefficient, and **C** is the concentration. Flux is the number of particles (or moles) passing through an area per time. The diffusion coefficient is dimensioned in length squared per time and the concentration is the number of particles (or moles) per unit volume. Fick's first law describes multiple transport phenomena like Ohm's law which is the transport of electric charge, and Fourier's law for the transport of heat.

The number of particles is conserved in diffusion thus a conservation relationship can be derived. Consider a test volume through which a particle flux flows. If the particles are conserved the following holds:

$$inflow - outflow = accumulation\ (or\ loss)rate \tag{21}$$

Although the derivation of the conservation expression is fairly straight forward by relating flux components per unit area to concentrate change rate, only the final form will be shown here [5, 34].

$$-\vec{\nabla}\cdot\vec{J} = \frac{\partial C}{\partial t} \tag{22}$$

Putting Equations (20) and (22) together yields Fick's second law, which is the diffusion equation.

$$\frac{\partial C}{\partial t} = \vec{\nabla} \cdot \left(D \vec{\nabla} C\right)$$

(23)

Fick's second law is analogous to Fourier's law of heat transport with a conservation of energy expression and the time dependent Schrödinger equation. Solutions to the diffusion equation show the change of concentration with time. Like all differential equations solutions require input of geometry, boundary conditions, and initial conditions.

2.3.2 The Diffusion Equation in Cylindrical Coordinates

Rewriting the diffusion equation for cylindrical coordinates for the geometry of a fiber and simplifying for diffusion of particles only in the radial direction, the diffusion equation takes the form:

$$\frac{\partial C}{\partial t} = \frac{1}{r}\frac{\partial}{\partial r}\left(rD\frac{\partial C}{\partial r}\right)$$

(24)

Solving Equation (24) for non-steady state solid cylinder of radius **a** where the concentration at the surface is zero and for a uniform concentration inside the cylinder the solution simplifies to this dimensionless concentration expression:

$$\frac{\mathrm{C} - C_1}{C_0 - C_1} = 1 - \frac{2}{a}\sum_{n=1}^{\infty}\frac{e^{(-D\alpha_n^2 t)} J_o(r\alpha_n)}{\alpha_n J_1(a\alpha_n)}$$

(25)

With **C** being the concentration at **r**, $\mathbf{C_1}$ is the initial uniform concentration inside the cylinder, $\mathbf{C_0}$ is the initial concentration at the surface, **D** is the diffusivity, **a** is the radius of the cylinder, and $\boldsymbol{\alpha_n}$ is the nth root of the zero order Bessel function of the first kind. Equation (25) is normalized to the difference between the concentration at the surface and the uniform concentration inside the cylinder. Since the boundary conditions in solving Equation (24) included that the concentration outside the cylinder was zero, Equation (25) actually works for the reverse circumstance of diffusing into the cylinder when the initial concentration inside the cylinder is zero and the concentration at the surface is held constant. The dimensionless concentration distribution across the cylinder follows the contours displayed in Figure 5.

The dimensionless concentration is plotted against **r/a**, the dimensionless radius inside the cylinder. The contour lines are for different constant values of $\mathbf{Dt/a^2}$. This important plot helps depict how the concentration will change in a solid cylinder. Close the center of the cylinder the concentration profile is nearly flat. This observation is shows that during the diffusion process the core region of an optical fiber will have a very nearly uniform concentration profile provided the core diameter is sufficiently small compared to cladding diameter.

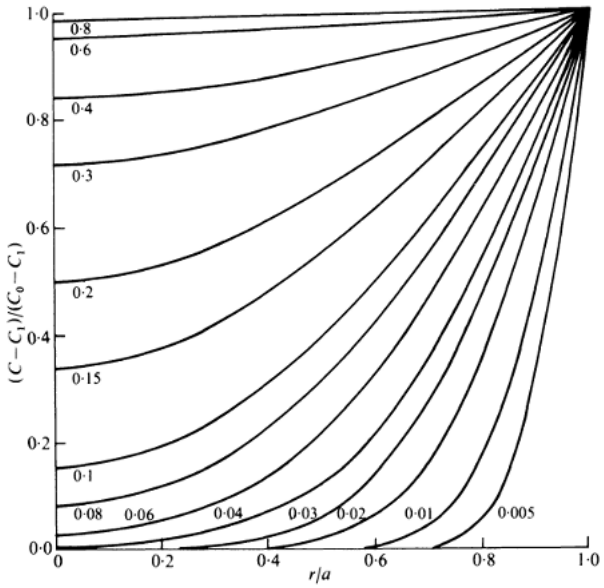

Figure 5 Concentration distributions at various times with initial concentration C_1 and surface concentration C_0; Numbers on curves are values of Dt/a^2.
Crank, J., The Mathematics of Diffusion: 2d Ed. 1975: Clarendon Press. Reprinted with permission from Oxford University Press. [5]

2.3.3 Diffusivity

The diffusivity or diffusion coefficient, **D**, is defined by Fick's first law given by Equation (20). The diffusion coefficient is then, by definition, the rate of transfer of a diffusing substance across a unit of area divided by the gradient of the concentration per unit volume. This definition necessarily gives the diffusion coefficient units of area per time. Under many circumstances the diffusion coefficient is given in experimental units of cm^2/s.

Although this definition sheds light on the physical meaning of diffusivity it does not provide a practical expression for it. The expression for diffusivity is empirical and dependent on temperature and activation energy. It is expressed in the form of an Arrhenius equation

$$D = D_0 e^{\left(\frac{-Q}{RT}\right)} \quad \textbf{(26)}$$

where $\mathbf{D_0}$ is the diffusivity when the temperature is infinite, **Q** is the activation energy of the diffusion process, **R** is the gas constant, and **T** is absolute temperature. Equation (26) can be manipulated into a linear relationship where the natural log of the diffusivity is plotted against **1000/T**, which is plotted on an Arrhenius, where $\mathbf{lnD_0}$ is the y-intercept, and **–Q/R** is the slope.

$$lnD = lnD_0 - \frac{Q}{RT} \tag{27}$$

If diffusivity is measured by way of concentration at different temperatures the slope of the line is the activation energy of the diffusion process. $\mathbf{D_0}$ is consequently then an extrapolation of Arrhenius plot to infinite temperature.

References [5, 34]

3. Literature Review

3.1 Literature Review Introduction

Hydrogen penetration is known to cause attenuation in the infrared in silica glass and is thus of concern in fiber optic applications. “Hydrogen Darkening” is the name often used to describe signal degradation in optical fibers caused by hydrogen exposure. The performance of telecommunications and sensing systems exposed to hydrogen often become compromised over time. Research exploring and characterizing the effects of hydrogen exposure on fiber optics has positively impacted the design and reliability of these systems. The findings from the literature thus far as to the cause, conditions under which this attenuation is observed, the characterization thereof, and factors that affect this attenuation will be discussed here.

The loss observed due to hydrogen ingress is usually categorized by two different mechanisms. The first is often called the “gas in glass” phenomenon [11, 35] or reversible [13, 17] hydrogen related absorption. This reversible absorption mechanism is attributed to molecular hydrogen which is physically dissolved in the glass having diffused through the interstices of the glass network. It is considered reversible because this loss can be removed when the hydrogen source is removed and the molecular hydrogen is allowed to diffuse back out of the fiber [11, 17]. The second is attributed to reactions between dissolved hydrogen and the glass network. This mechanism is called irreversible or permanent although methods have been developed to remove reacted hydrogen [36].

3.2 Molecular Hydrogen

The diffusivity and solubility of molecular hydrogen in silica glass is well studied [11, 13, 17, 18, 35, 37-39]. Losses in optical fibers occur only when hydrogen is present in the light guiding region of the fiber. It is important to study both the characteristic absorption due to interstitial hydrogen and to study the diffusion and solubility behavior of hydrogen in glass for the prediction of long term performance of the fiber.

3.2.1 Characteristic Absorption of Interstitial Hydrogen

Even though there has been much debate as to which of the molecular rotational and vibrational modes contribute to the observed absorption losses due to unreacted hydrogen in silica fibers, losses due to molecular hydrogen have been well documented in the literature [13, 18, 35, 37-43]. Discrepancies include suggestions that the same absorption band may be due to H_2 vibrational absorption, H_2 rotational absorptions, combinations of vibrational and rotational H_2 modes, and combinations with the SiO_4 vibrational modes. The H_2 rotational frequencies coincide with the SiO_4 fundamental vibrational frequency and the fundamental H_2 vibration coincides with the Si-H fundamental vibration [13]. Mochizuki, et al. [13] characterized the complex loss spectrum due to molecular hydrogen absorption with combination modes of fundamental H_2 vibration and SiO_4 vibrations including some combination modes of the first overtones of each. The absorption spectrum is shown in Figure 6 and assignments are

shown in Table 1. Lemaire [17] shows a similar complex spectrum in the 1-1.6 μm range although the rotational and vibrational modes are not assigned.

Table 1 H_2 Absorption bands [13] ; K. Mochizuki, Y. Namihira, M. Kuwazura, and Y. Iwamoto, "Behavior of Hydrogen Molecules Adsorbed on Silica in Optical Fibers," *Ieee Journal of Quantum Electronics,* vol. 20, pp. 694-697, July 1984 1984. Used under fair use 2015

Wavelength (μm)	Frequency
~36.4	ν_1
~21.0	ν_2
~12.5	ν_3
~9.1	ν_4
2.42	ν_H
2.24	$\nu_1+ \nu_H$
2.14	$\nu_2+ \nu_H$
2.04	$\nu_3+ \nu_H$
1.88	$\nu_4+ \nu_H$
1.78	$\nu_1+ \nu_3+ \nu_H$
1.70	$\nu_2+ \nu_4+ \nu_H$ or $2\nu_2+ \nu_H$
1.63	$\nu_3+ \nu_4+ \nu_H$
1.59	$2\nu_1+ \nu_H$
1.24	$2\nu_H$
1.20	$\nu_1+2\nu_H$
1.17	$\nu_2+2\nu_H$
1.13	$\nu_3+2\nu_H$
1.08	$\nu_4+2\nu_H$

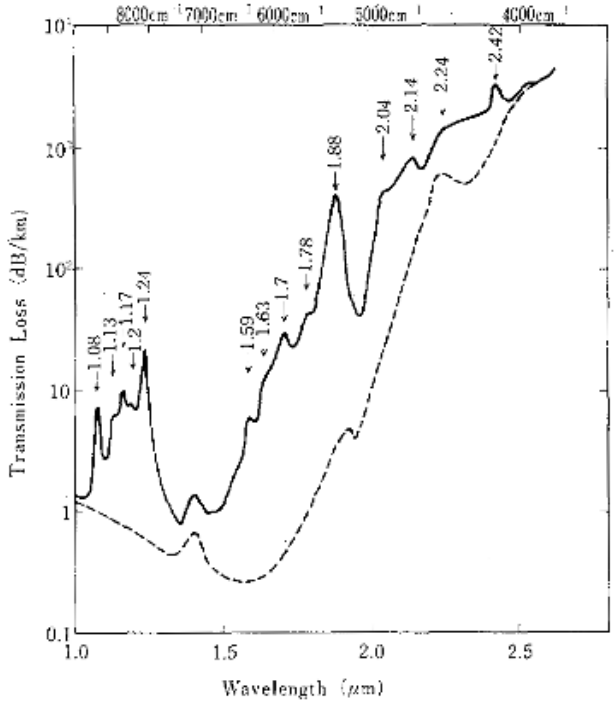

Figure 6 Infrared spectra in a silica glass optical fiber containing H_2; Dotted line and solid line show the spectra before and after containing H_2 respectively.
Reprinted with permission from: Mochizuki, K., et al., Behavior of Hydrogen Molecules Adsorbed on Silica in Optical Fibers. IEEE Journal of Quantum Electronics, 1984. 20(7): p. 694-697. [13]

Beer's law relates absorbance and concentration through the intrinsic material property of molar absorptivity as shown in Equation (9) but molar absorptivity is not always known for each vibrational mode. The probabilities of exciting a mode or combination mode are not equal for all modes. Thus, the magnitude of molar absorptivity varies widely with wavelength [22, 28]. But solubility and diffusion can also be used to relate absorption to concentration. Solubility of molecular hydrogen is dependent on partial pressure and changes slowly with temperature. This fact can be used to relate concentration of hydrogen in the light guiding to the absorbance at a specific wavelength [17]. The equilibrium H_2 absorption can be expressed as

$$\Delta\alpha_{H_2}(eq) = A(\lambda)P_{H_2}exp\left(\frac{8.67\ kj/mol}{RT}\right) \quad \textbf{(28)}$$

where **A(1)** is the spectral dependence of losses due to molecular hydrogen and P_{H_2} is the hydrogen partial pressure. Relationships like that expressed in Equation (28) highlights the importance of understanding diffusivity and solubility of hydrogen in silica glass for predicting performance of fiber optic systems exposed to hydrogen.

3.2.2 Diffusion and Solubility of Hydrogen

Even with the high purity fabrication processes available, hydrogen can enter the light guiding portion of the fiber from the environment in which the fiber is employed. Thus, it is important to examine the diffusion rate and solubility of hydrogen in optical fibers. The diffusion of hydrogen has been studied extensively to understand what can be expected with respect to the concentration of hydrogen in the core of the fiber and the long term stability of fiber optic systems. Even fibers exposed to water experience diffusion of molecular hydrogen into the fiber [44]. In analysis of the loss caused by a fiber in a water filled cable it was found that the loss was due to molecular hydrogen generated by metal corrosion, which was then able to diffuse into the fiber [44]. Because the loss spectrum is so well characterized it was determined that the absorption at 1.24 μm that arose from water exposure was due to molecular hydrogen diffusion into the fiber. Many studies on the diffusion and solubility behavior of molecular hydrogen have been conducted [29, 40, 43-46].

It has been seen that loss increase due to molecular hydrogen is virtually independent of the glass structure [18] and is thus only dependent on solubility and diffusion of the hydrogen . In a study examining the physical solubility of molecular hydrogen in fibers of two different manufacturing process, VAD and MCVD at low temperatures (15, 60, 100 °C) good agreement was found between the experiment and the thermodynamic theory at equilibrium [18] . Physical solubility was defined as the number of hydrogen molecules dissolved into silica glass per unit volume. Using

$$\frac{n_s}{p} = (H_2/2\pi mkT)^{3/2} * (kT)^{-1} * N_s * \left[\frac{e^{-\frac{h\nu}{2kT}}}{\left(1 - e^{-\frac{h\nu}{kT}}\right)}\right]^3 * exp(-E_0/RT) \quad \textbf{(29)}$$

where $\mathbf{n_s}$ is the number of hydrogen molecules dissolved per unit volume of the glass, **p** is the hydrogen partial pressure, **h** is Planck's constant, m is the mass of the hydrogen molecule, **k** is Boltzmann's constant, **T** is the absolute temperature, $\mathbf{N_s}$ is the number of solubility sites available per unit volume, **ν** is the vibration frequency of the dissolved hydrogen molecule, **R** is the gas constant, and $\mathbf{E_0}$ is the binding energy [18]. In the temperature range studied the temperature independent cross section was found to be 7.8 x10^{-24} cm^2/molecule [18], a solubility that will provide visible loss due to hydrogen in the light guiding region of the fiber.

Knowing the diffusivity is essential to determining the rate at which hydrogen can diffuse through the fiber. The diffusion process is amply characterized using the diffusion equation, Equation (23), written in cylindrical coordinates for optical fibers, Equation (24), with solution to dimensionless concentration given in Equation (25). The diffusivity is empirically expressed by Equation (26) and has been found to hold true over the entire temperature range from room temperature to 1000 °C but is relatively independent of the type of silica studied, **D** varying by a factor of 10^7 [11] over that temperature range. In earlier work measuring diffusion of hydrogen out of a fiber it was shown that perhaps diffusion of hydrogen in silica glass does not obey simple diffusion but the anomaly was shown to be conversion of OH present in the fibers to H_2 which could then diffuse out of the fiber [37].

Using the diffusivity to determine the hydrogen concentration at the center of the fiber it can be shown that it will approach an asymptotic limit as hydrogen approaches its equilibrium solubility. Using the cylindrical geometry of the fiber an expression showing the time it takes for the hydrogen concentration to reach 95% of its solubility equilibrium is [17]

$$t_{0.95} = 0.6a^2/D_{H_2} \tag{30}$$

with **a** being the radius of the fiber and $\boldsymbol{D_{H_2}}$ being the diffusivity of hydrogen. This expression also represents a concentration profile contour of constant value of $\mathbf{Dt/a^2=0.6}$ as shown in Figure 5. At room temperature the time it takes to reach 95% of solubility equilibrium is about 13 hours [17]. As the diffusivity goes up with temperature the time for saturation becomes much shorter. As can be inferred from planar geometry diffusion shown in Figure 7 hydrogen can diffuse through the diameter of on optical fiber (125 μm) at 800 °C very quickly. Thus loss due to hydrogen can be seen very quickly and saturation occurs much faster at higher temperatures.

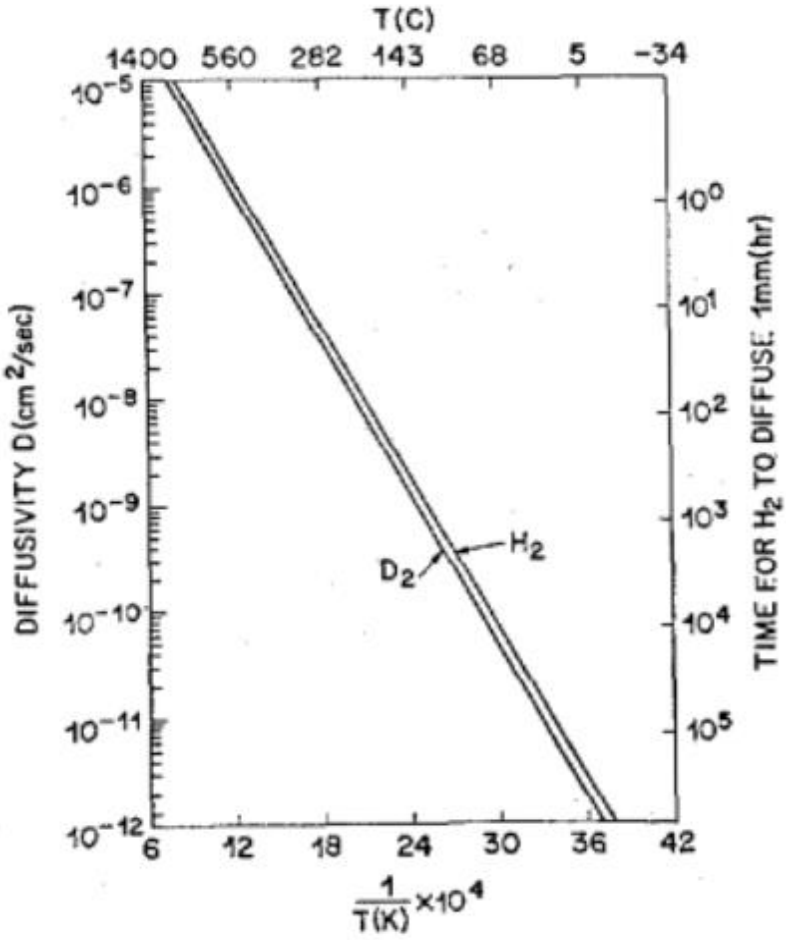

Figure 7 Diffusion coefficient versus 1000/T for H_2 and D_2 in silica, left-hand scale, and characteristic time for H_2 molecule to diffuse 1mm (right hand scale).
Reprinted with permission from: Stone, J., Interactions of Hydrogen and Deuterium with Silica Optical Fibers - a Review. Journal of Lightwave Technology, 1987. 5(5): p. 712-733. [11]

3.2.3 Infrared Activity of Molecular Hydrogen in Silica Glass

Although molecular hydrogen in its gaseous form is not infrared active, losses due to unreacted molecular hydrogen are observed in optical fibers [11, 17, 18]. The most satisfying explanation for this seeming contradiction is presented by Mochizuki, et al. in their study to determine if losses due to molecular hydrogen are due to absorptions by the H_2 molecule itself [13]. Acknowledging that although gaseous H_2 shows Raman activity at 4160 cm^{-1} (1.4 μm) it does not ordinarily show infrared activity. But absorption is seen at 1.24 μm and attributed to absorption of the first vibrational overtone of H_2. To explain how it becomes infrared active it is suggested that H_2 molecule binds weakly to the SiO_2 network polarizing the molecule [13]. The polarization of H_2 distorts the electron density of distribution of the molecule giving it a dipole moment which oscillates when the vibrational mode is excited thus allow it to absorb infrared radiation.

3.3 Hydrogen Reactions

The other means by which hydrogen present in optical fibers can cause attenuation is through reactions with the glass network forming other hydrogen species [47]. Naturally, the wavelengths at which losses will occur are dependent on the frequencies of the infrared active vibrational and rotational modes of the species present. Reactions of hydrogen with the glass network may take place at lower temperatures but they begin to dominate as loss mechanism due to hydrogen ingress at temperatures above 150 °C [12, 17, 46]

The activation for this chemical change is supplied by thermal energy [12]. When glass that already contains molecular hydrogen is heated, the dissolved hydrogen reacts with the glass to create hydrogen species, the most common being OH [12, 17]. The most prominent evidence for this reaction behavior is a change in the observed in the spectra of glass. In a given piece of glass with dissolved hydrogen at room temperature the characteristic spectra of molecular hydrogen absorption can be observed. When the glass is heated, however, the characteristic peaks for molecular hydrogen decrease and the 1.4 μm band characteristic of the first overtone of the OH stretch increases. The 1.4 μm band may be present and larger than the molecular hydrogen absorption bands when molecular hydrogen is absorbed because OH is present in almost all glass and absorbs more strongly than molecular hydrogen. But it can be shown to increase as molecular hydrogen reacts with the glass forming more OH. See Figure 8 for an example from Itoh, et al.'s work exploring the thermal mechanism for the chemical reaction of dissolved hydrogen with the glass network [12].

In addition to being thermally activated, there is another condition for this reaction commonly reported, which is that these reactions occur at defect sites [12, 17]. The most common hydrogen reaction species to form is OH. Corroborating the defect condition, studies have reported that OH forms readily in Ge doped fiber and not in pure silica fiber [12]. The contrast between OH formation in Ge doped fiber and no OH formation in pure silica fiber is explained by the fact that the pure silica fiber has a much lower defect concentration than Ge doped fiber. In this work however, it has been shown that OH does form in pure silica fiber albeit at a much smaller amount than in Ge doped fiber. This result still confirms the hypothesis that reactions of hydrogen with the glass network occur at defect sites. Comparison between crystalline and amorphous silica provide further corroborating evidence.

The amorphous structure of silica glass does appear to play a role in the effects of hydrogen penetration as compared with crystalline silica. Surface studies of porous crystalline silica (average pore diameter p = 7 nm) showed decreasing absorption due to internal molecular hydrogen, hydrogen bonding, and internal hydroxyl groups as it was annealed under vacuum at higher temperatures [48]. These results suggest that crystalline silica does not have the defect centers necessary to produce hydroxyl and hydride species within the crystal. As opposed to hydrogen loaded amorphous silica whose OH absorption peaks increase with annealing.

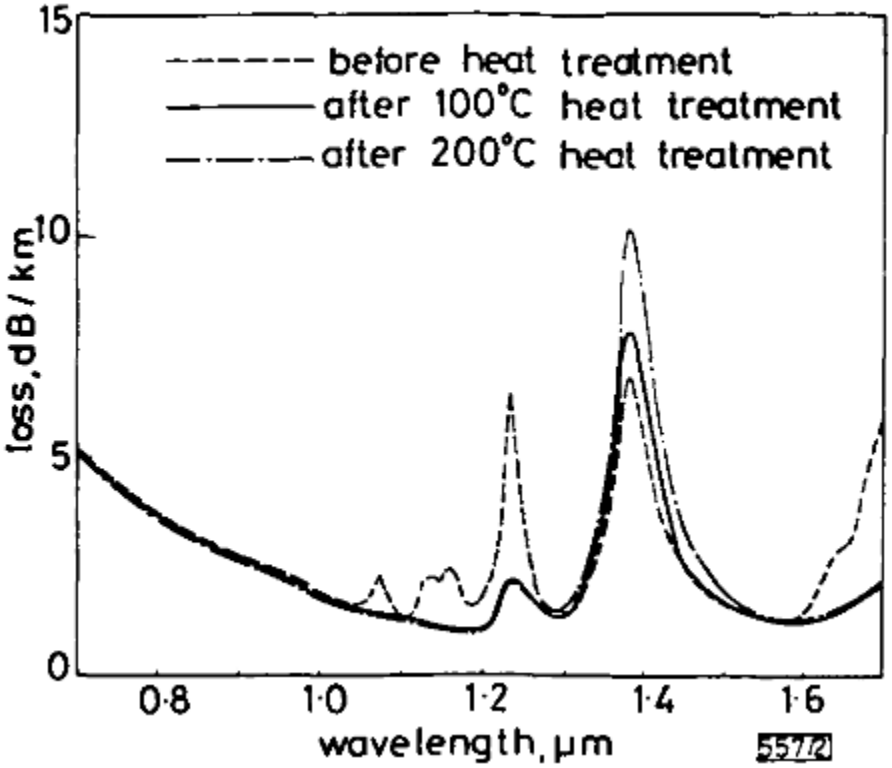

Figure 8 Transmission-loss spectra for GeO_2 doped silica fiber before and after heat treatments. Itoh, H., Y. Ohmori, and M. Nakahara, Chemical change from diffused hydrogen gas to hydroxyl ion in silica glass optical fibres. Electronics Letters, 1984. 20(3): p. 140-142. Reproduced by permission of the Institution of Engineering & Technology via Rightslink. [12]

3.4 Glass Structure and Defects

Glass structure is said to be random or disordered in its amorphous nature in contrast to the ordered nature of a crystal structure, but the disorder does not preclude any structure. The silicon atom has 4 sp^3 electrons to share. The directional nature of p-orbitals favors tetrahedral coordination such that in the case of silica the Si is in the center sharing an electron with four oxygen atoms thus completing its valence shell. The oxygen atoms each desire two electrons fill their valence shells. After sharing one with the silicon in the center of the tetrahedron, each oxygen atom wants for one more electron. The SiO_4^{-4} tetrahedron is the silicate molecule. Because the oxygen atoms each have want of one more electron they are most interested in creating a bond with another silicon atom. Thus the tetrahedron structure is arranged such that each oxygen atom at the corners is shared by two silicon atoms each at the centers of

their own tetrahedron. The simple silica structure can then be considered as repeating tetrahedron sharing oxygen atoms at the corners resulting in the chemical formula of SiO_2. The amorphous nature of glass is such that this repeating pattern is random creating a continuous random network instead of a regular repeating pattern as in crystalline structure. Although no glass structure is known with enormous certainty, some levels of structure can be explored intelligently. This exploration requires the use of a variety of structure investigation techniques including NMR, vibrational spectroscopy, diffraction and other techniques [49].

As the SiO_4 tetrahedron is central to the structure of glass, the O-Si-O bond remains consistently very near to the ideal tetrahedral angle of 109.5° [26, 49] but the Si-O-Si bond angle varies widely. In other words, the corner sharing bond angle between tetrahedrons is allowed a much broader variety of values. The Si-O-Si bond angle is not defined by the tetrahedral structure of the silicate molecule and its freedom to vary over a wide range is a characteristic of the short range order of the continuous random network [50] of vitreous silica. Many studies have been done to characterize this bond angle in vitreous silica [51, 52]. The variation range of the Si-O-Si bond angle is not infinite and most studies have reported the range to be between 146° and 155° for vitreous silica [26, 51, 52]. The random nature of the order of the silicate molecule can result in structures such as an oxygen atom that is not part of two tetrahedrons, two linked tetrahedrons, and closed ring configurations [26, 49].

The many possible structures and tetrahedral configurations in the amorphous nature of glass give rise to the seemly certain fact that it must contain defects. Such defects might include vacancies, interstitials, dangling bonds, overcoordinated atoms, undercoordinated atoms, etc. [50]. Frenkel estimates the concentration of defects in the following way:

$$n \approx (NN')^{1/2} e^{\left(\frac{-E}{2kT}\right)} \tag{31}$$

Where **N** is the number of normal network sites, **N'** the number of interstitial sites, and **E** is the activation energy governing the process [50]. But interpreting this estimation requires many assumptions complicating the topic to such a degree that it becomes nearly impossible to apply to experimental conditions.

3.5 OH Producing Defects

Although there are many possible defect species, the peroxy radical defects are the type that are linked most closely to hydroxyl formation in experiments exploring H_2 permeation in glass [50].

$$\equiv Si - O - O - Si \equiv \rightarrow \equiv Si - O - O^{\cdot} \; Si \equiv \; + e \,. \tag{32}$$

Equation (32) denotes the peroxy radical defect that then can form an OH group with hydrogen exposure and the appropriate activation energy supplied thermally.

$$\equiv Si - O - O - Si \equiv \ + H_2 \rightarrow \equiv Si - OH\ HO - Si \equiv$$

(33)

The activation energy for the reaction shown in Equation (33) is dependent on the fictive temperature of the glass [50].

Should the glass be doped with germanium a host of other OH formation opportunities become possible. The high likelihood of the presence of Ge-E' centers is one such possibility, although their presence necessary to produce and increase in OH [9].

Figure 9 and Figure 10 show some examples of possible reactions [9]. The necessary activation energy is again supplied by thermal energy [12].

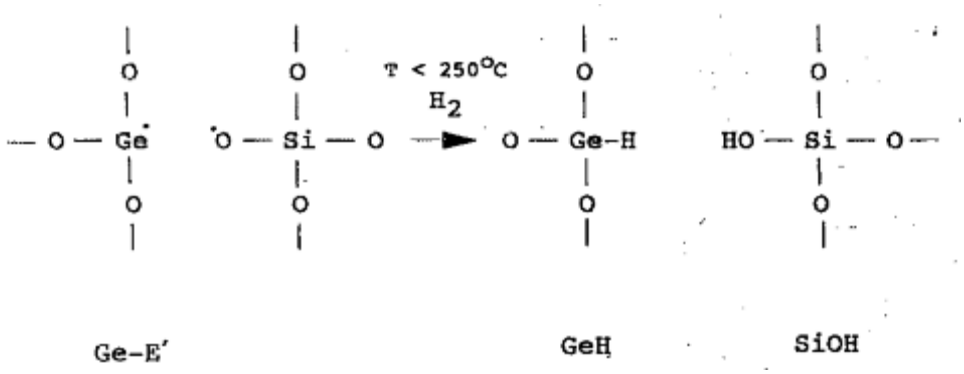

Figure 9 Model of the reaction of H_2 with Ge-E' centers to form the lossy "Ge H" defect and increased OH levels; Si atoms are shown as an example, but Si could also be replaced by Ge.
Reprinted with permission from: Atkins, R.M. and P.J. Lemaire, Effects of elevated temperature hydrogen exposure on short-wavelength optical losses and defect concentrations in germanosilicate optical fibers. Journal of Applied Physics, 1992. 72(2): p. 344. Copyright 1992, AIP Publishing LLC [9]

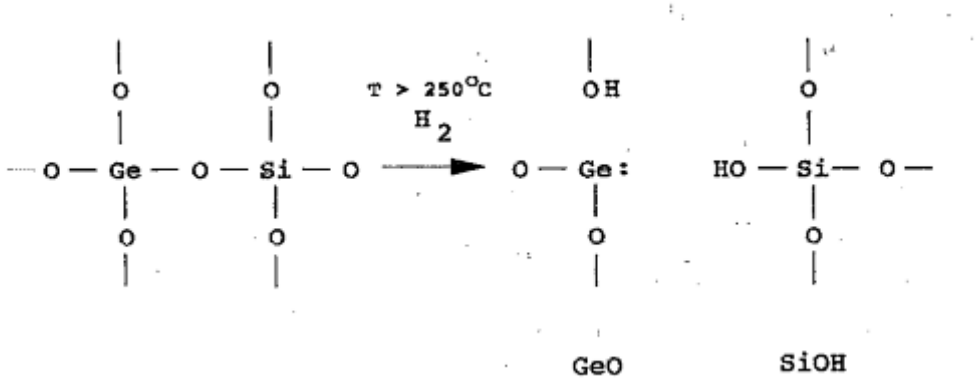

Figure 10 Model of reaction of H_2 with the germanosilicate glass network to form GeO centers and increased OH levels; Si atoms are shown as an example, but Si could also be replaced by Ge.
Reprinted with permission from: Atkins, R.M. and P.J. Lemaire, Effects of elevated temperature hydrogen exposure on short-wavelength optical losses and defect concentrations in germanosilicate optical fibers. Journal of Applied Physics, 1992. 72(2): p. 344. Copyright 1992, AIP Publishing LLC [9]

OH is the most prominent reaction species [53] but it is not the only one that can form. Ge-H, Si-H among others are possible [42]. In a process to remove hydrogen the SiH species is speculated to play a major role [36] as shown in Equation 34 [54].

$$\equiv Si - OH + \equiv SiH \rightarrow \equiv Si - O - Si \equiv + H_2 \quad \textbf{(34)}$$

Molecular water, H_2O is ruled out from being formed in large amounts. Studies of removing hydroxyl from silica glass measured the species released from the glass using quadrupole mass spectrometry finding very little H_2O removed compared with H_2 [36]. In their examination of water diffusion in glass Tomozawa, et al. they asserted that any water that diffuses into the glass reacts with the glass structure and thus becomes immobile [55]. It has also been shown that the diffusion rate of molecular water is much slower than that of OH species making it very likely that molecular water does not exist in large quantities in the silica network [56]. And finally in work done to characterize the speciation of hydrogen in synthetic quartz NIR characterization and IR absorption of frozen quartz suggest that water does not exist in fluid inclusions and any groups must be fewer than a few hundred molecules [19].

3.6 Infrared Spectroscopy Identification of OH Species in Silica Glass

Infrared spectroscopy is the most widely used method of measuring the concentration of OH in glass. Peak area is associated with concentration via a form of Beer's law,

$$\boldsymbol{A(\lambda) = \epsilon(\lambda) bc} \quad \textbf{(35)}$$

where c is the concentration and $\boldsymbol{\epsilon}$ is the molar absorptivity and **A** is the absorbance [22]. Thus an increase in concentration corresponds to an increase in absorbance. The IR absorption bands of OH in vitreous silica have been extensively studied [1-3, 11, 17, 19, 30, 47, 53, 57-62] and are tabulated in Table 2. Table 2 gives a list in order of wavelength of the absorption bands gathered from the literature within the 1000-2500 nm measurement range but includes the fundamental and second overtone of the OH stretch, which lie just outside and on either of this range.

Table 2 OH, H_2O and their combination vibrations in fused silica glass

Assignment	Wave number (cm^{-1})	Wavelength (nm)	Description	Reference
ν_1(OH)	3673	2722	Fundamental OH stretch	[24, 47]
$\nu_{Comb,1}$(OH)	4100	2439	Unidentified OH combination band	[59]

ν_1(OH) + ν_4(SiO_2)	4100	2439	Combination fundamental OH and fundamental SiO_2 vibrations	[2]
ν_{Comb}(XOH) X≠H	4444	2250	Combination Stretch + bend XOH X≠H	[19]
ν_1(OH) + ν_1(SiO_2)	4450	2247	Combination fundamental OH and fundamental SiO_2 vibrations	[2]
$\nu_{comb,2}$ (OH)	4500 4522	2222 2211	Asymmetric distribution of silanol vibration frequencies due to varied degrees of hydrogen-bond	[59]
ν_4(OH) + ν_3(SiO_2)	4520	2212	Combination fundamental OH and fundamental SiO_2 vibrations	[2]
ν_b(SiOH) + ν_s(OH)	4500-4550	2222-2198	Combination bending a stretching of OH in silanol groups	[59]
ν(OH) + ν(SiO_4)	4539, 4505	2203, 2220	Combination OH fundamental mode and SiO_4 vibration	[47]
ν_B (H_2O)$_I$ + ν_{ss}(H_2O)$_I$	5102 shoulder on 5249	1960	Possibly, combination bending and symmetric stretching band of Type I molecular water	[59]
ν(H_2O)	5200	1920	Stretch	[19]
ν_B(H_2O)$_I$ + ν_{AS}(H_2O)$_I$	5249	1905	Combination bending and stretching of molecular water, or more specifically, bending and asymmetric stretching of Type I molecular water	[59]
Both ν(H_2O) & ν(OH^-)	7000	1420	First overtone of Both H_2O and OH^- stretching motions	[19]
ν'(GeOH)	7042	1420	OH vibration bonded to Ge site	[17]

$2\nu_3$(OH)	7100	1408	First overtone OH	[2]
$2\nu_2$ (OH)	7220	1385	First overtone OH	[2]
ν_b(SiOH)	7220	1385	OH vibration bonded to Si site	[17]
$2\nu_s$(OH)	7200-7270	1389-1375	First overtone of OH stretch	[59]
$2\nu_1$(OH)	7260	1377	First overtone of OH stretch	[2]
2ν(OH)	7299, 7278, 7246	1370, 1374, 1380	First overtone of OH stretch	[11, 47]
$2\nu_3$(OH) + ν_2(SiO_2)	7380	1355	Combination first overtone OH and fundamental SiO_2	[2]
2ν(OH) + ν_1(SiO_2)	7874	1270	Combination First overtone stretch and SiO_2 ν_1 mode	[11]
2ν(OH) + ν_2(SiO_2)	7920	1263	Combination first overtone OH and fundamental SiO_2	[2]
$2\nu_1$(OH) + ν_1(SiO_2)	8065	1240	Combination first overtone OH and fundamental SiO_2	[2]
2ν(OH) + ν(SiO_4)	8130, 8065	1230, 1240	Combination of first overtone OH and fundamental SiO_4 vibration	[47]
2ν(OH) + 2ν(SiO_4)	8889	1125	Combination first overtone OH and first overtone SiO_4 vibration	[47]
2ν(OH) + $2\nu_1$(SiO_4)	8928	1120	Combination first overtone OH stretch and first overtone SiO_4 ν_1 mode	[11]
$3\nu_1$(OH)	10526	950	Second Overtone OH stretch	[11]

Notation Table 2

ν denotes vibrational modes of the species in parenthesis following and ν' for OH species bonded to something other than Si. The subscript is information from the reference. If the reference used a number and did not describe the designation other than the number the number is included and the description merely calls out that it is a vibrational mode. The numbers reference distinct vibrational modes for instance ν_2(OH) is distinct from ν_3(OH) but the nature of the mode was not further elaborated. When the

subscript is a letter (B, SS, AS, Comb), it denotes Bending, Symmetric Stretch, and Antisymmetric Stretch, or Comb indicating it is a combined mode respectively, all of which is information that was provided explicitly by the reference but may have been adapted to fit the notation of this table. The information contained in a subscript that is specifically known is also explicitly called out in the description. Subscripts after the species in parenthesis give specific information about that species; for instance, $(H_2O)_I$ indicates type I water molecules. If a description was included in the reference it was transcribed exactly here. If a description was not included the one here was inferred from the context of the reference. Some descriptions provided by references were also adapted to the format of this notation and are thus indicated in the assignment column.

The work of this thesis focuses on the 1–2.5 μm wavelength region. Within this region the 1.4 μm absorption band is the first overtone of the OH stretch [2, 11, 17, 19, 47, 59] whose fundamental frequency is located at around 2.7 μm, just outside the region of interest. The vibrational frequency of OH bonded to Ge will be shifted to slightly longer wavelengths than that of OH bonded to Si, centering at 1420 nm instead of 1380 nm for OH bonded to Si [17]. The 1.4 μm absorption band is the most straight forward absorption band in the region of interest.

The 2.2 μm band is the other major absorption band in the region of interest but the vibrational modes causing it are far less well understood. Some literature sources report that this band is the combination of Si-O-H stretch and Si-O-H bend [19, 59] with one suggesting variation in absorbing frequency is related to the silanol participating in various amounts of hydrogen bonding [59]. Others report that it is a combination mode of the fundamental OH stretch and SiO_4 vibration [2, 47, 59]. SiH fundamental vibration lies near 2190 cm^{-1} [63, 64] which means its first overtone could be close to 4380 cm^{-1}, with wavelength 2283 nm, which would be at the long wavelength side of the 2.2 μm peak. Since SiH is often expected to have formed with SiOH [36, 42, 54], if the first overtone SiH stretch were located near the 2.2 μm peak it would further convolute the makeup of the absorption band. This band is far more complicated than the 1.4 μm band, has great dispute as to its cause in the literature, and is poorly understood in general.

The final OH related band that is observed in this work is the 1.24 μm band. The absorption in this band is commonly considered to be the combination mode of first overtone OH stretch and fundamental SiO_4 vibration [11, 47, 59] and it is also related to the first overtone stretch of H_2 physically dissolved in silica glass [11, 13, 17]. Although absorption at this wavelength occurs for molecular H_2 [11, 13, 17] if no other H_2 related bands are observed the 1.2 μm band can be understood to be primarily OH related [12].

3.7 Temperature Dependence

It has been well documented that heating a fiber exposed to hydrogen increases losses in the infrared spectrum [9, 12, 54, 58, 65] namely in OH related absorption bands. This increase in absorption comes from reactions of molecular hydrogen with the silica network [12]. But in addition to increasing with hydrogen exposure, once the peak is present, and even stable with respect to diffusion, another temperature dependent behavior has been observed. After a fiber has OH peaks present, if it is heated, the absorption due to those peaks will go down [1, 24, 36].

In one study focusing on a process to remove hydroxyl from silica glass, the glass was heated and the fundamental OH peak (located ~3673 cm^{-1}) reduced in intensity until it was almost unmeasurable at 1200 °C [36]. Using quadrupole mass spectra analysis the hydrogen species released from the glass were

measured. It was found that the primary species released from the glass was H_2 and not H_2O. Because the OH related peak showed decrease in intensity it was concluded that the following reaction took place

$$\equiv Si - OH + \equiv SiH \rightarrow \equiv Si - O - Si \equiv + H_2 \quad \textbf{(36)}$$

and H_2 diffused out of the fiber [36]. This process was modeled with diffusion from Fick's second law for their geometry (not the cylindrical geometry of fiber) and activation energies were measured, 254 kJ/mol for 700–900 °C and 32kJ/mol for 900–1200 °C; the activation energy for the lower temperature range having good agreement with prior dihydroxylation process studies and the higher temperature range having good agreement with hydrogen diffusion activation energies. The paper did not show absorption results from when the fiber was cooled back down.

In other studies when glass, with OH peaks already present, is heated the peaks have been shown to decrease in absorption and upon cooling increase again [1, 24, 66]. In one case this behavior is attributed to local structural relaxation around OH in the silica network [24] and in the other it was related to changes in hydrogen bonding states of the OH species [1].

In a study measuring the activation energy for structural relaxation around the OH species the fundamental OH stretch vibrational frequency was investigated to probe the local environment with respect to its participation in hydrogen bonding. The fundamental stretch was divided into high energy and low energy sections with the low energy section relating to hydrogen bonded OH. When the absorption from the high energy portion of the band saturated their detector, the absorption around 4520 cm^{-1} (2212 nm) was used to represent that high energy portion [24] due to its molar absorptivity being proportional to the OH stretch as shown by Davis, et al. [30]. The absorption coefficient at these wavelengths was measured and shown to decrease for this absorption band, and more so for the thinner samples. This reduction in absorption coefficient was attributed to structural relaxation around the OH species in the glass sample. [24]

In another study specifically looking at the temperature dependent behavior of the first overtone OH stretch at 1.39 μm in silica fibers, a reduction in peak height with increase in temperature from room temperature to 650 °C and then a return to the initial absorption with decrease in temperature was observed [1]. Changes in area of the absorption band with temperature were not discussed in this study. The peak at high temperature was also shifted towards longer wavelengths. This temperature dependent behavior was attributed to changes in hydrogen bonding conditions for OH groups in the fiber. The bond of the hydroxyl group whose H is participating in hydrogen bonding will have less energy than one whose H is not participating in hydrogen bonding and thus will have a lower frequency of vibration and will absorb at longer wavelengths. It is commonly understood that an increase in temperature will decrease the amount of hydrogen bonding in which OH groups participate [1]. However, the peak shifted in the direction of longer wavelength when fiber was heated. To address this seeming contradiction the first overtone OH stretch absorption band was fitted to six Gaussians which were analyzed with respect to their temperature response. Two Gaussians in the fit not related to OH, one being the residual from the fit and the other was not affected by OH concentration [1]. The other four were considered related to OH concentration. The first component is the OH stretch when the hydrogen is not bonded to anything other than the oxygen and the other three are different hydrogen bonding configurations between silanol groups.

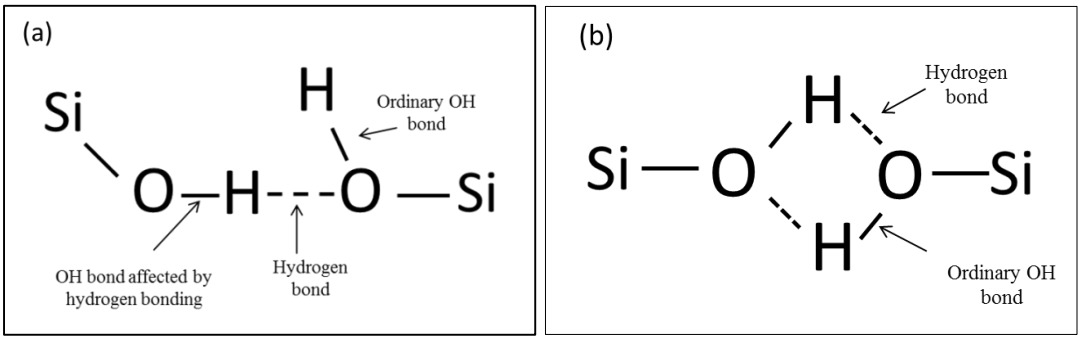

Figure 11 (a) asymmetric bindentate structure yeilding only one linear hydrogen bond with oxygen in neighboring silanol group whose hydroxyl group has an ordinatry OH bond, (b) symmetric bidentate structure where hydrogens of two neighboring silanol groups are close enough to neighboring oxygen to form hydrogen bonds having in-phase and out-of-phase vibrational modes
[1-3]

One such hydrogen bonding scenario is an asymmetric adjoining of two adjacent silanol groups engaging in a linear O-H---O bond which angularly precludes the other proton from participating in hydrogen bonding. The last two hydrogen bonding scenarios both take the same symmetric bidentate structure where the OH vibrations have two states: in-phase and out -of-phase [1]. These four states were first proposed by Walrafen, et al. in their decomposition of the fundamental OH stretch band (~2700 nm) who do not report on temperature dependence [3]. Figure 11 depicts the structures yielding these four states.

The components attributed to the two bonds in Figure 11 (a) varied inversely with temperature where the ordinary OH bond component increased with increasing temperature and the component due to the hydrogen bonded OH group decreased with increasing temperature as predicted by the fact that hydrogen bonding should decrease with increasing temperature. For the two components of the band depicted in (b) the in-phase state contribution decreased with increasing temperature while the out-of-phased state contribution did the opposite [1]. Center wavelengths for fit components for both studies are reported in Table 3.

Table 3 Fundamental and first overtone OH stretch band fit components' center wavelengths [1, 3]; R. T. Yukihiro Yokomachi, Kaya Nagasawa, and Yoshimichi Ohki, "Hydrogen Bond of OH groups in Silica Glass and its relation to the 1.39 um absorption," Journal of Non-Crystalline Solids, vol. 95 & 96, pp. 663-670, 1987.; G. E. Walrafen and S. R. Samanta, "Infrared absorbance spectra and interactions involving OH groups in fused silica," *The Journal of Chemical Physics*, vol. 69, pp. 493-495, 1978. Used under fair use 2015.

Bond	Walrafen, et al. Study [3] component center		Yokomachi, et al. Study [1] component center	
	cm^{-1}	nm	cm^{-1}	nm
Ordinary OH	3690	2710	7350	1361
Hydrogen Bonded OH	3510	2849	7070	1414
In-Phase state ring structure	3665	2729	7250	1379
Out-of-Phase state of ring structure	3615	2766	7204	1388

In all cases when temperature dependence is observed a structural change in the glass is postulated as the cause. When a glass is reheated to the glass-transformation range it may undergo structural relaxation which can change its properties including its volume [34]. Structural relaxation around OH groups is the cause attributed to the temperature dependence shown in the range of 900−1100 °C [24]. At lower temperatures, 20−650 °C the temperature dependence was attributed to a change in hydrogen bonding configurations of the OH group [1].

4. Materials and Methods

The fiber under test used in this study is 50/125 Ge doped silica core, pure silica cladding commercially available optical fiber. The equipment used in the experimental work was the following: MTI GSL-1500X Furnace, Thorlabs OSA203 - Fourier Transform Optical Spectrum Analyzer, an Ocean Optics HL-2000 White Light Source. Other materials used were: 95% N_2 / 5% H_2 gas mixture, and various commercially available 50/125 patch cables and pigtails for appropriate connections to equipment.

The primary fiber used for this work was a 50 μm core, 125 μm cladding germanium doped silica core graded index fiber with pure silica cladding, 0.2 NA. The fiber is commercially available, purchased from Thorlabs, manufactured by Corning. Other fibers used to supplement this work were 50/125 pure silica core fiber step index fibers in low and high OH varieties also with a 0.2 NA. These fibers exhibit the same behavior as shown in the bulk of this work although they are not the focus. The germanium doped fiber showed the best hydrogen response especially in terms of reactions, specifically OH content and was thus used in the bulk of the work.

The size of the section of the fiber under test was 15 cm inside the heated region of the furnace except in one case where 6 cm of the Ge doped graded index fiber were used and the rest of the length made up by pure silica core step index fiber. Although the stock fiber has an acrylate coating, the operating temperature quoted in the specifications for the fiber is 85 °C [7] because the coating burns off at higher temperatures. In these experiments the coating was burned off completely in the 90 minute heating ramp from room temperature to 800 °C from the entire 15 cm section under test. The hydrogen was turned on after achieving 800 °C so any diffusion process was through the silica cladding and core, not through the acrylate coating. See Figure 12 for fiber schematic. In the fiber used in this test the doping concentration is proprietary to the manufacturer as are the core and cladding indices of refraction; only the numerical aperture is specified at 0.2.

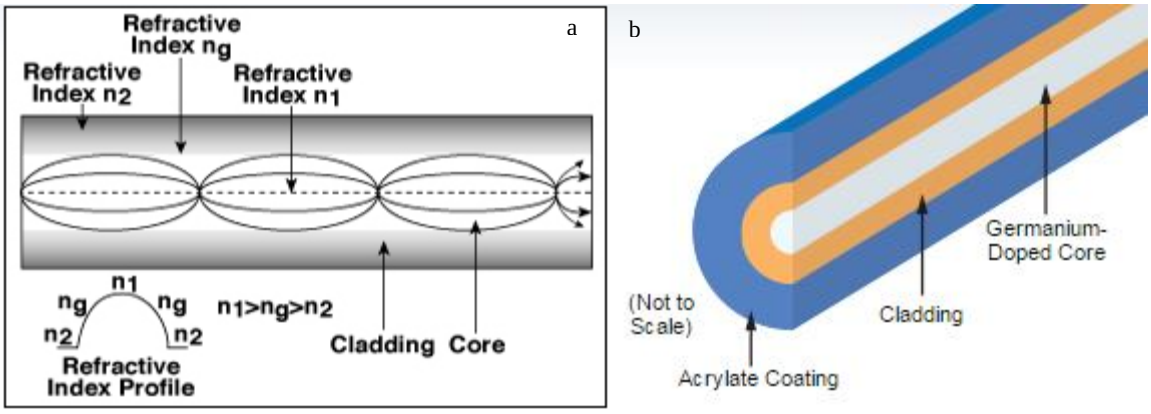

Figure 12 (a) schematic of refractive index profile and light guiding region of Ge doped 50/125 graded index optical fiber; (b) schematic of cross section of fiber.
Thorlabs, 0.20 and 0.27 NA Graded-Index Multimode Fibers. 2015. Reproduced under fair use. [7]

The hydrogen source use was a 5%H_2/95%N_2 gas mixture. This mixture is a non-flammable concentration safe to heat in a furnace, requiring no special safety arrangements for venting. A regulator attached to the tank was set in the range of 20-25 psi and a flow meter governed the flow to greater than 55 sccm (standard cubic centimeter) limit of the flow meter. The exhaust exited through a ¼ inch plastic tube to a bubbler jar of mineral oil which prevented any ambient air at a higher pressure from flowing back into the furnace through the exhaust.

The Ge doped fiber was heated in the furnace at various temperature profiles and exposed to hydrogen while in situ spectra were recorded by the OSA. It was connected to the light source and OSA via splice into pigtails. See Figure 13 for experimental setup.

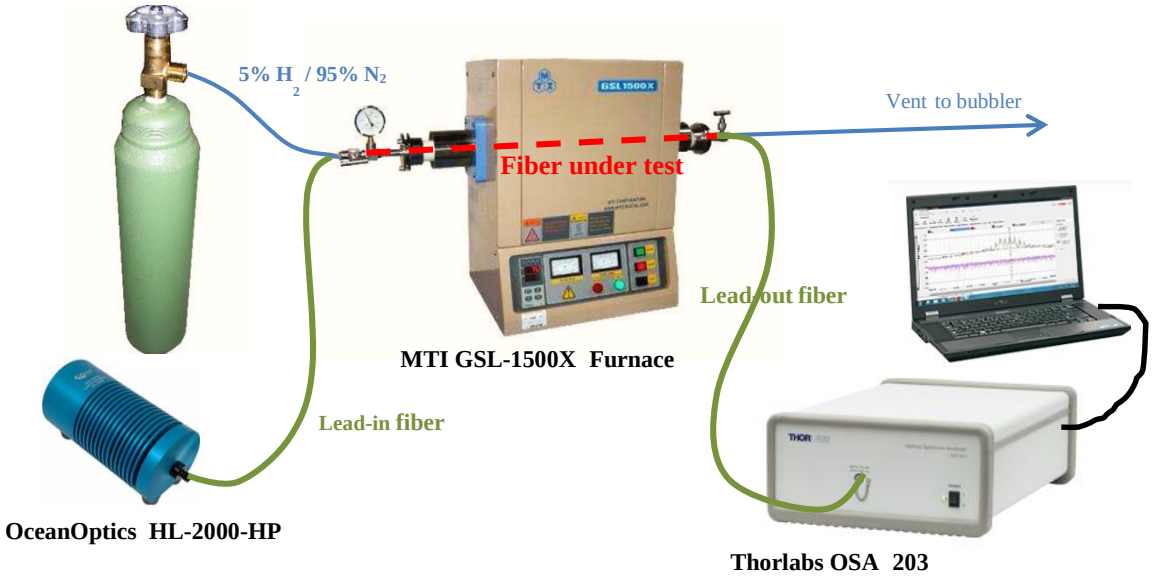

Figure 13 Experimental Setup

Various temperature profiles were used to study the behavior of the fiber once OH was generated in the core. But the initial treatment for each fiber was the same. OH was generated in the fiber by heating the fiber to 800 °C then hydrogen was allowed to flow into the chamber. The furnace was set to dwell for three to six hours at 800 °C before allowing the fiber and furnace to cool to room temperature. The fiber was exposed to hydrogen for the three to six hour period at 800 °C and for the cooling period to room temperature. An example of the temperature profile for this initial treatment is shown in Figure 14.

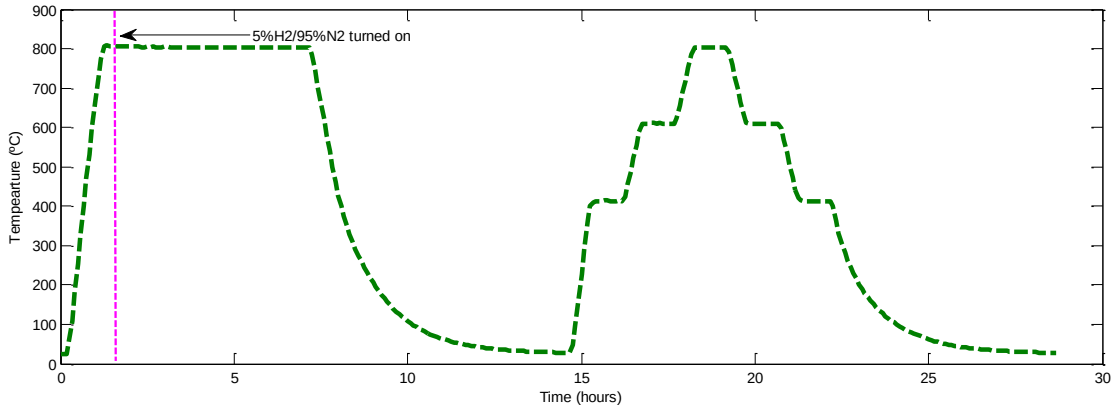

Figure 14 Initial heat treatment and step profile for each fiber

The furnace is capable of heating up from room temperature to 800 °C in five minutes. The cooling was limited by heat exchange rate with ambient environment of the laboratory. The cooling rate is reasonably fast from 800–600 °C (as fast as 5 minutes) and from 600–400 °C (as fast as 10 minutes) but from 400–20 °C the rate is much slower because the furnace does not have any accelerated cooling capabilities. As the rate for cool down was only measured for one data set the cooling segment of the temperature profile is linearly approximated in most figures. The maximum cooling rate from 800 °C to 600 °C when ambient air temperature is at room temperature is ten minutes. Because the cooling rate is not controllable for temperatures lower than 600 °C, the following strategy was employed to ensure the desired lower temperature was actually achieved. When a lower temperature is desired after the ramp period between the high and lower temperature a dwell time was set for the lower temperature such that by the end of the dwell segment the desired temperature had been reached. The programed temperature profile is what is reported in all figures. Thus the cooling segments of profile are linearized estimates for plotting purposes and do not represent the accurate shape of the temperature profile. When a spectrum is reported for a particular temperature it is taken from the end of the dwell time at that temperature ensuring that its reported temperature was its actual temperature. The furnace was able to hold temperatures within a ± 15 °C range of the actual set temperature as measured by a thermocouple.

After this initial heat treatment, a step temperature profile was set in all but one case. This step profile was to step up to 800 °C and back down to 20 °C in 200 ° increments excluding 200 °C with dwell segments at each of 400, 600, and 800 °C. The dwell segment at each incremental temperature was chosen such that the furnace could actually achieve this temperature profile by accommodating for the speed that the furnace could actual ramp up or down. For instance, a dwell of two hours was chosen for 400 °C when ramping down from 600 °C to be sure that the system achieved 400 °C before moving on to

the next temperature step. This step profile had hydrogen flowing in every case. See Figure 14 for depiction of step temperature profile.

Another temperature profile was used after the initial treatment and usually after a step profile as well, to show the repeatability of the phenomenon. In the cycle temperature profile the temperature was cycled between 800 °C and 600 °C six times with varying dwell times at the two temperatures and then ramping back down to room temperature. The ramp time between each temperature was 30 minutes. See Table 4 for details on the various dwell times for the cycle profiles. See Figure 15 for example of cycle profile.

Table 4 Cycle profile dwell and ramp times

Test #	Dwell on 600 °C	Dwell on 800 °C
6	120 minutes	60 minutes
8, 9	30 minutes	30 minutes
10	60 minutes	60 minutes

Additional experiments were performed to verify light source stability, contributions from black body radiation, and OH saturation time. The temperature profiles of those experiments are stated in the sections where their results are discussed.

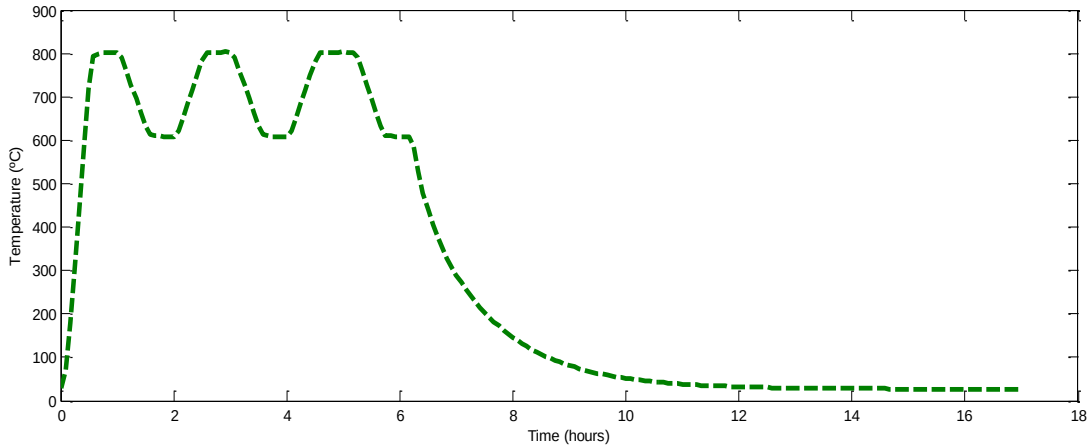

Figure 15 Example of cycle temperature profile, which had a thirty minute dwell times for both 800 °C and 800 °C; Ramp time between temperatures was 30 minutes; This profile has three cycles while most profiles had six

Spectra were recorded in situ by a Thorlabs OSA203 - Fourier Transform Optical Spectrum Analyzer. Measured spectra were recorded at a rate of 5 per minute with 25 spectra taken in a five minute time frame. The twenty five spectra were then averaged over the five minute time period. All data presented and used for calculations is an average over five minutes. OSA output is in dBm. Data was processed using Matlab. Spectra were referenced to spectrum taken from fiber at 20 °C at the start of each experiment. Reference spectrum was subtracted from each spectra converting dBm into dB transmission loss. The five minute averages were smoothed using the smooth function set to a span of 49. A base level from the flattest section of the raw spectra was averaged over all data and subtracted from each spectrum.

5. Results

Through the course of studying this phenomenon over 60 experiments were performed to examine and confirm the observed temperature dependence phenomenon. More than 50 of them were performed in the course of work aimed at understanding the hydrogen response at high temperature of a variety of fibers for the purpose of then exploring possible hydrogen barriers. In the course of examining this hydrogen response at high temperatures a temperature dependent behavior was observed in the OH absorption seen in the fibers. Although that work moved on to barrier considerations, this work focuses on the temperature dependent behavior of the OH related absorption bands. To further study the temperature dependence ten additional tests were performed.

5.1 Initial Loss Increase

The loss caused by the introduction of hydrogen into the environment appears promptly and grows rapidly. Figure 16 shows the spectrum at different times as a fiber is exposed to hydrogen at 800 °C. Three absorption bands appear with maximum height at: 1251 nm, 1389 nm, and 2211 nm in the spectral range of 1–2.5 µm. These absorption bands can all be identified as OH absorption from Table 2. No molecular H_2 bands that do not overlap with OH bands are visible. There are shoulders visible on the short wavelength side of both the 1389 nm band and the 2211 nm band. What is not as visible in this full spectrum is the shoulder on the long wavelength side of 1389 nm band, which can be seen more clearly in Figure 19 as it zooms in on the band. The shoulder on the short wavelength side is actually very small

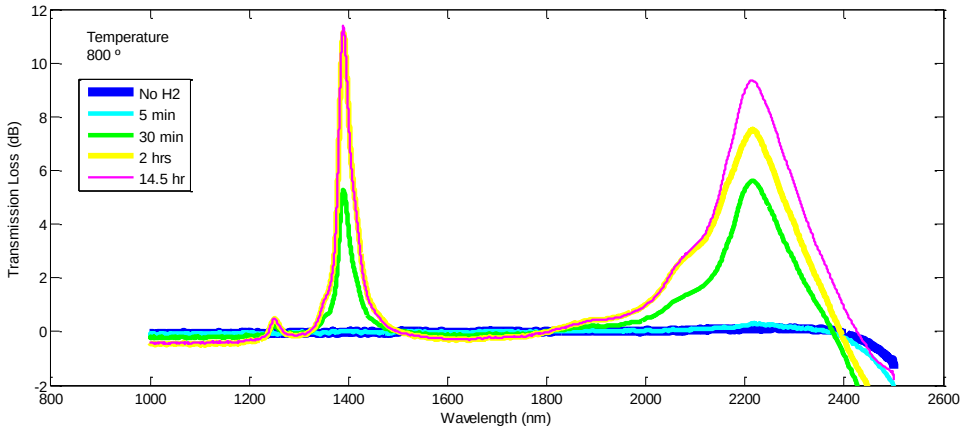

Figure 16 Absorption in Ge doped graded index 50/125 optical fiber at different lengths of time of hydrogen exposure

compared to the one on the long wavelength side. Further peak structure is described later in this section. The 1.24 µm band showed very weak absorption and was not examined in detail. Further results and discussion focus only on the 1389 nm and 2211 nm absorption bands.

What may not be obvious from the spectrum but becomes evident when plotting each peak's maximum value against time as is done in Figure 17, is that the 1389 nm band saturates within about four or five

hours whereas the 2211 nm band continues to increase and does not appear to saturate in the 14.5 hour exposure time from this experiment. It should also be noted that the 1389 nm band has a higher maximum absorption than the 2211 nm band during this initial hydrogen treatment. When the temperature changes, as in lowered and raised again, comparison between maximum peak height for the two peaks becomes even more interesting.

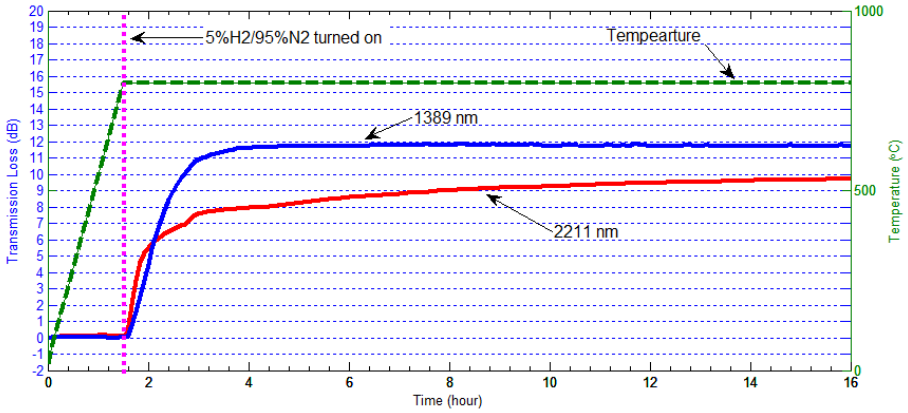

Figure 17 Plotting maximum peak height against time for 14.5 hours of hydrogen exposure

5.2 Temperature Dependent Behavior

In most experiments, the fiber was initially treated with hydrogen at 800 °C, cooled back to room temperature and then subjected to a step profile (see Figure 14) to get better temperature resolution at the selected temperatures of 20, 400, 600, & 800 °C. The fiber is exposed to hydrogen continually from initial exposure through cool down and during the step temperature profile. Figure 18 shows the peak maximum change with time and temperature. 1389 nm peak height maximum is shown in blue and 2211 nm peak height maximum is shown in red. The green dashed line is the temperature profile.

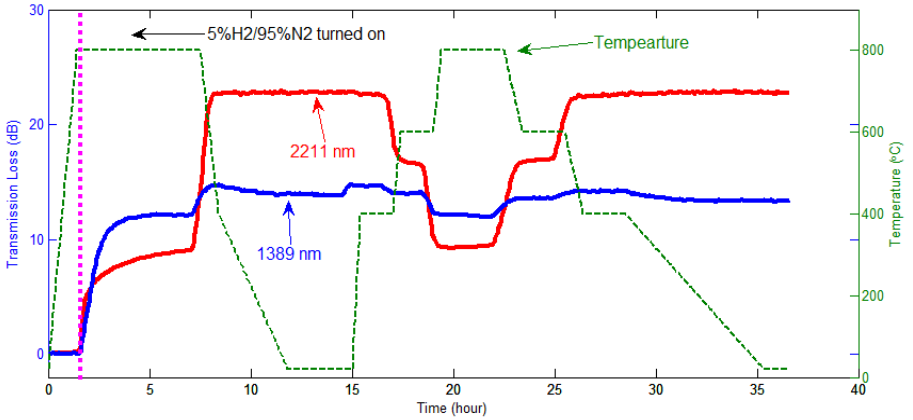

Figure 18 Plotting peak maxium against time through entire temperature profile

Even in the cooling down to room temperature before the step temperature profile, an obvious change in the absorption intensity can be observed. When the fiber was cooled the intensity of absorption in the two most prominent bands, 1389 nm and 2211 nm, increased dramatically with change in temperature. Note

that at 800 °C, the 1389 nm peak height maximum is higher than that of the 2211 nm peak, as they are cooled, even though they both increase, the 2211 nm peak increases more so that its room temperature peak height maximum is much greater than that of the 1389 nm maximum peak height. The difference in peak maxima is greater at room temperature than at 800 °C. When they were heated back up during the step temperature profile following the initial treatment, their absorptions went back down. When returned to 800 °C the maxima of the two peaks return to what they were during the initial treatment at 800 °C. Because the 1389 nm peak had appeared to flatten in the initial treatment this increase in intensity as the fiber is cooled was quite unexpected. On the other hand, the 2211 nm peak while still rising during the initial heat treatment and lower in intensity than the 1389 nm peak, upon cooling became so large that its intensity saturated the detector. Its increase rate upon cooling is much steeper than the initial increase when the fiber was first exposed to hydrogen.

Another important observation is that although the 2211 nm peak showed monotonic reduction with increase in temperature, the 1389 nm peak initially increases as temperature increases to 400 °C and then decreases as temperature increases further through 600 and 800 °C. For the 1389 nm peak the heights at 600 and 800 °C are lower than it is at room temperature. The most dramatic peak height differences are between 600 and 800 °C.

5.3 Peak Structure

To see better how these two peaks changed with temperature and to consider any change to the shape or structure of the bands snapshots of the spectrum from different temperatures are plotted. The 1389 nm peak and the 2211 nm peak are shown independently to better see the structure of each one. The 1.24 μm peak was very weak and is not examined in detail. Heating and cooling are plotted separately for clarity in Figure 19 with heating on the left ((a) and (c)) and cooling on the right ((b) and (d)). The room temperature spectrum after initial hydrogen and heat treatment is shown as a reference in all figures as a blue dashed line.

In (a) and (b) the change with temperature of 1389 nm band is shown. The peak intensity changes as temperature is increased. Initially the peak intensity increases as temperature is increased to 400 °C but then decreases as temperature is increased further to 600 and 800 °C. The center of this peak also shifts slightly to longer wavelengths. The shoulder on the longer wavelength side also shifts such that the structure of the peak does not change as temperature increases. This peak is largely claimed to be due to the first overtone of the OH stretch. The shoulder towards longer wavelengths occupies a wavelength range containing 1420 nm which is the location of the first overtone of the OH stretch that is bonded to Ge, i.e., the OH stretch component of GeOH (see Table 2). There is also a shoulder toward shorter wavelengths. This one is much smaller than the long wavelength shoulder. Its location is near 1350 nm. No molecular hydrogen band is in that area but it could be a combination band of the first overtone OH stretch and a fundamental SiO_4 vibration mode, see Table 2. Both of the shoulders appear to increase very slightly as temperature increases.

In (c) and (d) the 2211 nm band is shown. Its peak intensity changes dramatically with temperature, monotonically decreasing as temperature increases. In other words, transmission in this wavelength range improves as temperature is raised. The difference between high temperature and low temperature is dramatic that at lower temperatures its absorption intensity is so much that it reaches the detection limits

of the OSA used for the measurement across a large portion of the band. The flat part seen in the lower temperature curves is the result of the attenuation being greater than the detection limits of the OSA. Saturation of the detector makes it impossible to see if the intensity of this peak at 400 °C is greater than it is at room temperature as was seen for the 1389 nm peak. However, this saturation problem can be overcome by using a shorter piece of Ge doped fiber making up the rest of the length with pure silica core step index fiber. Figure 19 e and f shows the peak structure of the 2211 nm band from a shorter piece of fiber such that its room temperature intensity does not saturate the spectrum. There it can be seen that the peak at 400 °C is lower in intensity than room temperature. As the peak intensity goes down as the temperature increases the shoulder on the long wavelength side becomes less distinct as a tail on the band seems to form. As can be seen in this plot there appears to be another band forming beyond 2350 nm and the distinction between the two bands smears out as temperature increases. This longer wavelength band whose tail encroaches on the long wavelength end of the 2211 nm band is often understood to be the end of the fundamental OH stretch situated near 2700 nm, which is beyond the spectral limits of this detection system. It may also be a combination band of the fundamental OH stretch with a SiO_4 vibrational mode near 2439 nm which would be a combination mode with a different silicate vibrational mode than that of the 2211 nm combination band.

The only exception to the decrease as temperature increases is a very small shoulder on the short wavelength side of this peak near 2065 nm. That wavelength is not identified as either a molecular hydrogen absorption peak or an OH related peak (see Table 1and Table 2). This shoulder appears to go up in absorption intensity as temperature increases. At room temperature this shoulder looks almost like a second peak. As the temperature increases the entire 2211 nm band broadens and this second peak looks more like a shoulder.

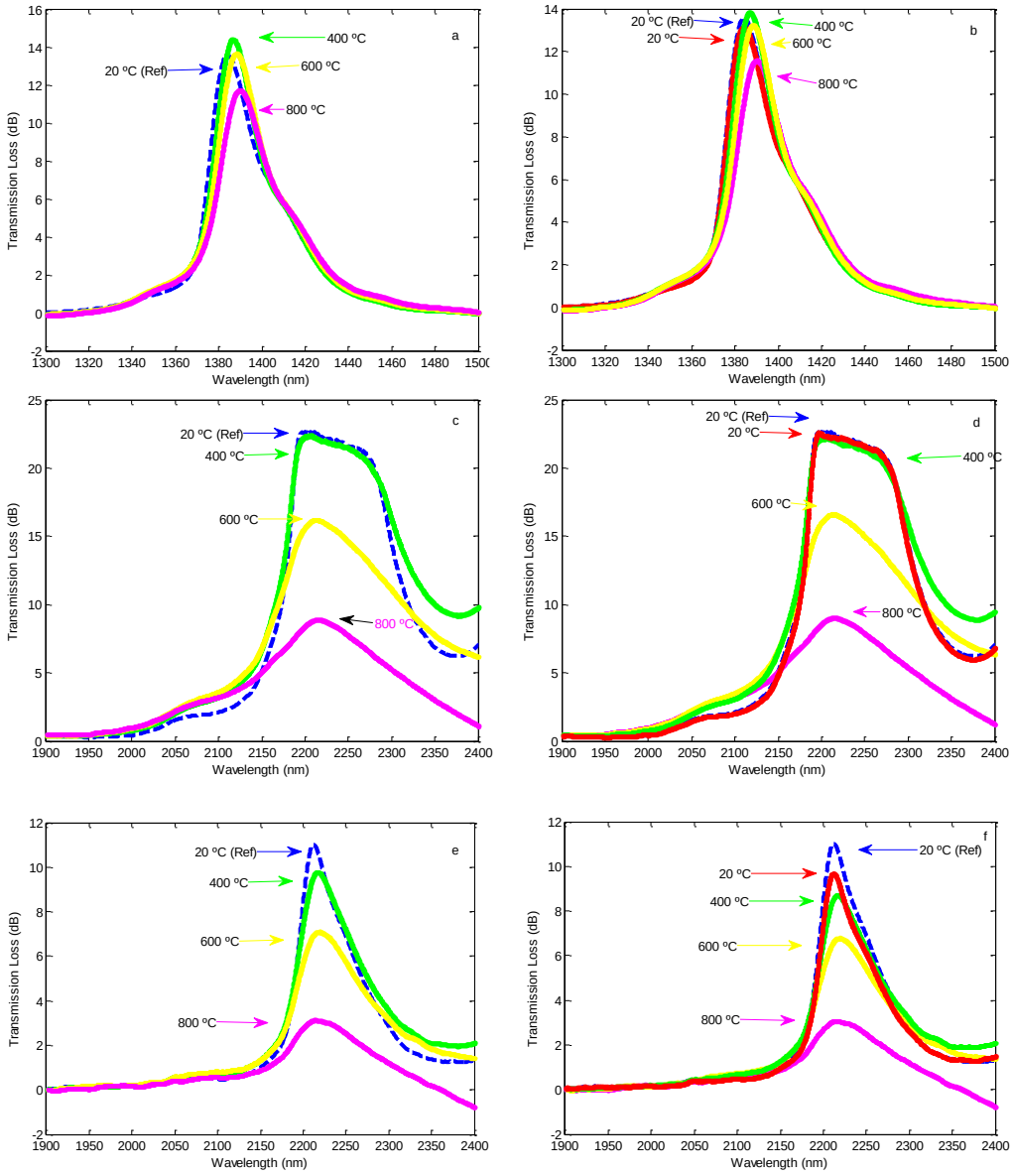

Figure 19 Treated Ge doped 50/125 graded index fiber with continuous hydrogen exposure (a) spectra at 1389 during heating; (b) spectra at 1389 nm during cooling; (c) spectra at 2211 nm during heating; (d) spectra at 2211 nm during cooling; (e) spectra at 2211 nm of shorter segment during heating; (f) spectra at 2211 nm of shorter segment during cooling

It was also seen in a pure silica core step index 50/125 multimode fiber that was manufactured with high OH content. The temperature dependence appears regardless of the formation process of the OH. That is,

if OH is generated through hydrogen exposure or through the fabrication process of the fiber, the absorption bands due to OH will exhibit this same temperature dependent behavior. The only difference between the two spectra is the GeOH related shoulder does not appear in the pure silica fiber because there is no Ge dopant with which to form GeOH.

5.4 High Temperature Cycling

In order to verify that this temperature dependence was repeatable as opposed to something that can be conditioned out of the fiber, experiments in which the temperature was cycled multiple times were performed (see Figure 15 for example of cycling temperature profile). Because the largest change in peak height was seen between 600 and 800 °C and the furnace has accurate cooling capabilities in this temperature regime, those two temperatures were chosen for the cycling profile. For the cycling temperature profile the ramp rate for both heating and cooling was set to 30 minutes, which is well within the capability of the furnace. This cycling temperature profile was performed with and without hydrogen flowing.

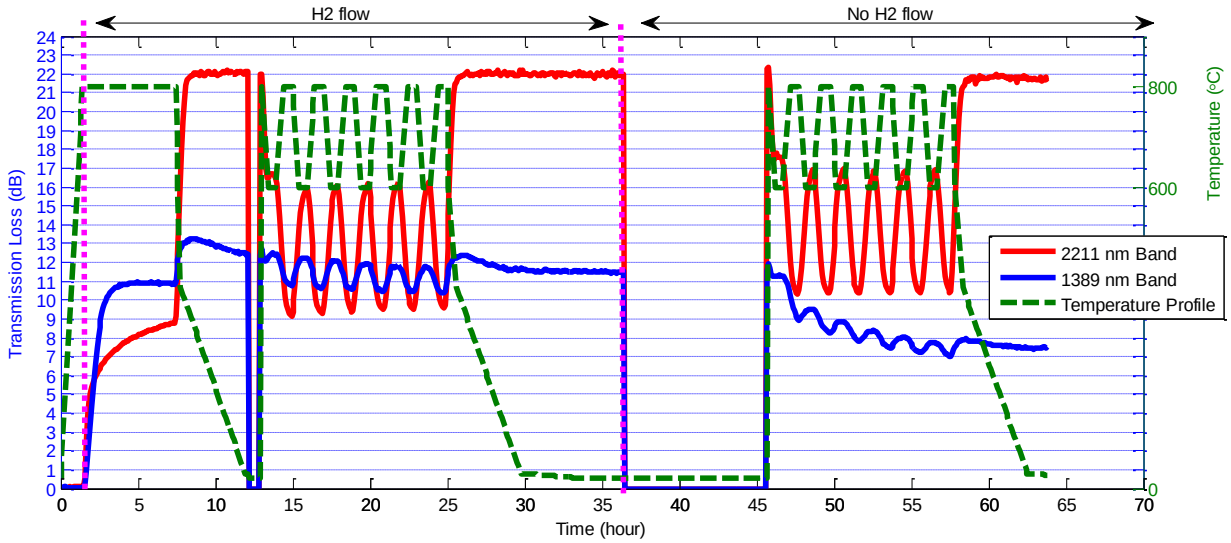

Figure 20 Peak track plot for 2211 nm band (red) and 1389 nm band (blue) through initial hydrogen heat treatment, tempearture cycle with hydrogen still flowing, and a temperature cycle without hydrogen flowing; Spectra was not recorded between treatments

The temperature dependent behavior continued even through repeated cycling of the temperature. In Figure 20 the maximum absorption for each of the two bands is plotted against time. The 1389 nm band is shown in blue, the 2211 nm band in red and the temperature profile is shown as a green dashed line. Figure 20 shows absorption maxima for a fiber that went through an initial hydrogen treatment, was allowed to cool to room temperature, was subjected to a cycling temperature treatment, and allowed to cool to room temperature again with the hydrogen gas flowing the entire time. After this second cooling the hydrogen gas was turned off. The fiber rested in the furnace for nine hours and then a second cycling temperature treatment was performed. Locations in time where the hydrogen is turned on and off are labeled on the plot. Spectra were not recorded between temperature treatments thus the heights of each band are left at zero on the plot.

For all temperature profiles the temperature dependent behavior persisted. However, the 1389 nm peak height exhibited different behavior in the hydrogen and no hydrogen cases. The peak height for points at each 600 °C dwell segments are plotted against time and then fitted. The peak height decreased in intensity linearly in the hydrogen case and followed a power model decrease in the no hydrogen case. The peak height for each 800 °C dwell segment followed the same behavior as the 600 °C peak height for the with and without hydrogen cases. This difference in their behavior is a very surprising result. Possible reasons will be discussed further in the following chapter.

Figure 21 shows the fits for the 1389 nm band peak height maximums. Figure 21 (a) shows the case where hydrogen is flowing, plotting the 1389 nm peak height in each of the 600 °C segments (top in blue) and each of the 800 °C segments (bottom in purple). The purpose of the fit was to compare the decrease behaviors of the hydrogen and no hydrogen cases, not to derive physical meaning from the fit.

The change over time for the 1389 nm peak height is a linear decrease at both temperatures for the cycling temperature profile in a hydrogen environment, following the form of Equation (37).

$$I_\lambda = -at + b \tag{37}$$

Figure 21 (b) shows the case where no hydrogen is flowing, plotting the 1389 nm peak height in each of the 600 °C segments (top in blue) and each of the 800 °C segments (bottom in purple). The change over time for the 1389 nm peak height is a power model decrease at both temperatures for the case where hydrogen is not present following the form of Equation (38).

$$I_\lambda = at^{-b} \tag{38}$$

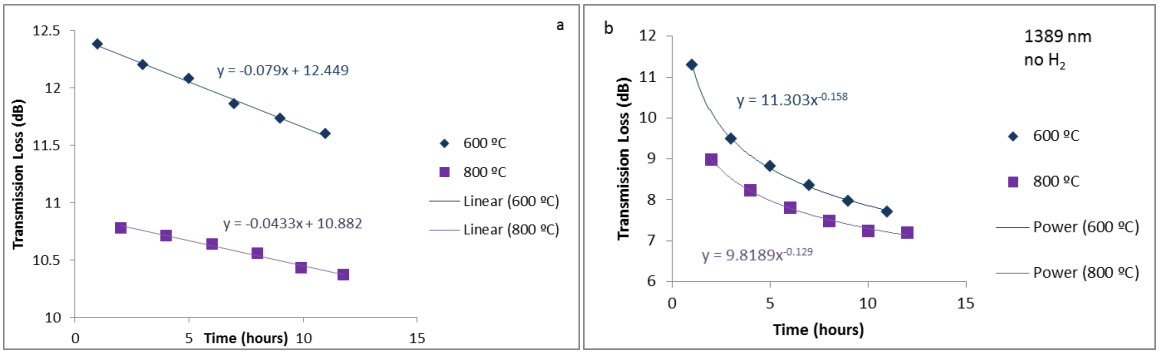

Figure 21 1389 nm peak height from points in cycling temperature profiles (a) case with H_2 exposure linear fit for 600 and 800 °C segments; (b) case without H_2 power fit for 600 and 800 °C segments

In both cases, with and without H_2, the final 20 °C max intensity for the 1389 nm peak was smaller than its initial 20 °C in intensity.

The 2211 nm peak shows uniform behavior in all cases neither appreciably increasing nor decreasing regardless of whether hydrogen was present in the environment. The only notable non-uniform behavior of the 2211 nm peak maximum is at 800 °C in the hydrogen case it increases linearly very slightly. At 600 °C the 2211 nm peak maximums do not increase or decrease for either case of hydrogen and no hydrogen. Figure 22 shows the behavior of the 2211 nm peak height behaviors for points from the 600 °C segments shown in orange, points from the 800 °C segments shown in red. Figure 22 (a) is the case with H_2 exposure and (b) is the case with no H_2 in the environment. The peak maximums at both temperatures show a very flat behavior suggesting that it does not change with time or with temperature cycling.

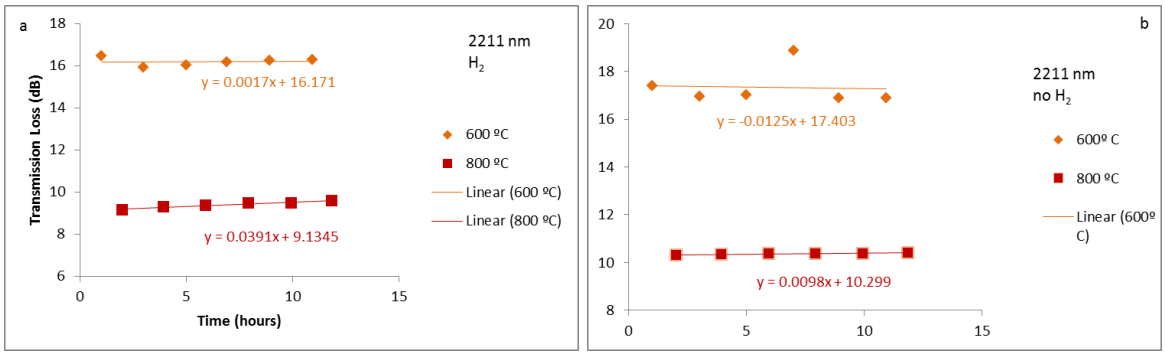

Figure 22 2211 nm peak height from points in cycling temperature profiles (a) case with H_2 exposure 600 °C segments show no change, 800 °C segments slightly increase ; (b) case without H_2 neither show any change

Even as the 1389 nm peak height over time decreases in intensity, changes in the shape or structure of the band do not occur. Compare Figure 23 with Figure 19 (a) & (b). Figure 23 shows the entire 1389 nm band for each of the 600 °C segments in the cycle temperature profile with hydrogen. No shape change or center wavelength shift occurs over time for each of the 600 °C segments (even though there is a slight change in peak height). Contrast this with the shape and height change that with temperature change as seen in Figure 19 (a) and (b). The same is the case for 800 °C segments and the no hydrogen case as well as for the 2211 nm peak at 600 and 800 °C segments with and without hydrogen.

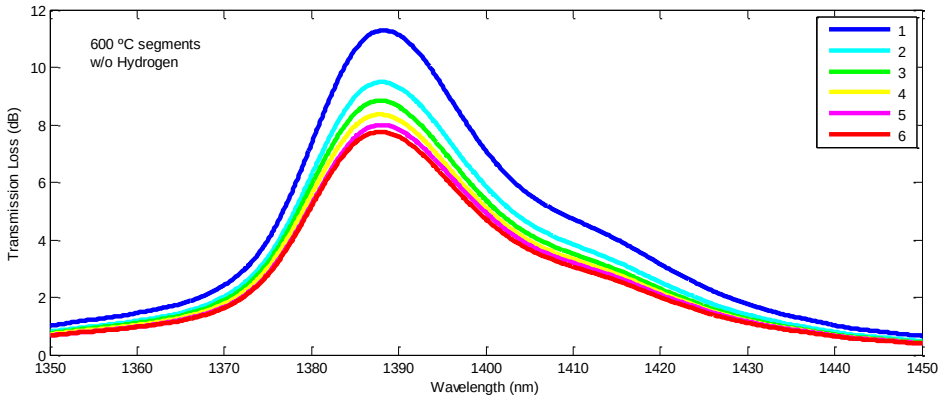

Figure 23 Spectra from the six 600 °C dwell sections of cycle temperature profile with hydrogen flow

To examine whether the peak height for the 1389 nm peak changes during a long dwell at 600 °C with no hydrogen, a test was performed where a previously hydrogenated fiber was set to dwell for 10 hours at 600 °C followed by cycling the temperature between 600 and 800 °C (60 minute dwell at each temperature 30 minute ramp between temperatures). During the 10 hour dwell period the 1389 nm peak reduced very slightly in a linear fashion and the 2211 nm peak did not change during the 10 hours at 600 °C with no hydrogen flowing. Figure 24 shows the maximum for each peak (1389 nm in blue and 2211 nm in red) plotted against time for the ten hour dwell at 600 °C.

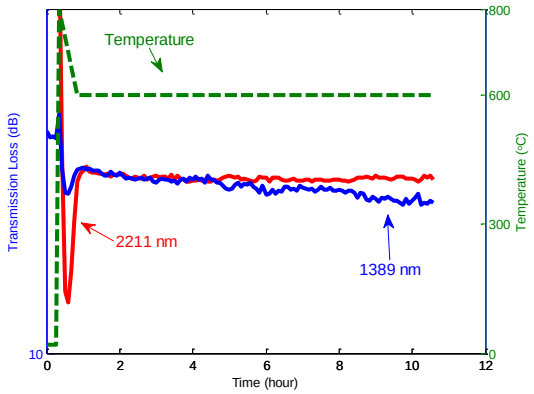

Figure 24 Zoom in to 600 °C dwell for 10 hours with no hydrogen for previously hydrogenated fiber; 2211 nm band (red) and 1389 nm band (blue)

As can be seen in Figure 25, during the following temperature cycling, the 1389 nm peak did decrease following the same power model as in previous cycled temperature profiles without hydrogen. The 2211 nm peak did not change in height as was previously seen.

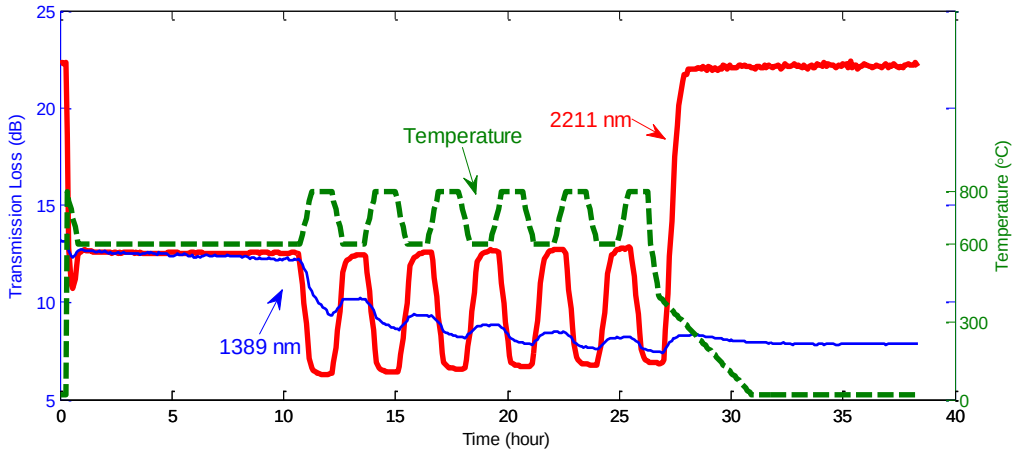

Figure 25 Peak track plot for 2211 nm band (red) and 1389 nm band (blue) against time no hydrogen exposure; Ten hour dwell at 600 °C followed by cycle profile btween 600 and 800 °C with hour dwel for each temperature 30 minute ramp between temperatures; Fiber with previous hydrogen exposure and heat treament

To verify if the decrease is due to temperature cycling or temperature higher than 600 °C another hydroxylated fiber was subject to a ten hour dwell at 800 °C in an ambient air environment. As can be seen in Figure 26 the 1389 nm band decreases in intensity at high temperature. Cycling temperature is not a necessary condition for its decrease. The 2211 nm band appears to decrease slightly over time as well during this dwell period. However the shapes of the decay of the two bands are different.

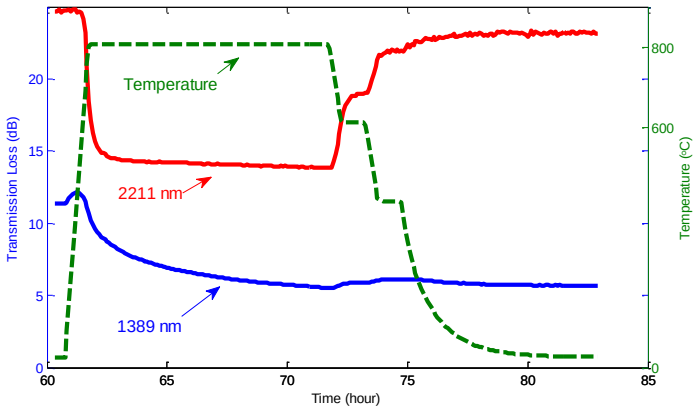

Figure 26 Zoom in to 600 °C dwell for 10 hours with no hydrogen for previously hydrogenated fiber; 2211 nm band (red) and 1389 nm band (blue)

6. Discussion

6.1 Control and Light Source Stability

As an experimental control, a fiber was heated to 800 °C with no hydrogen exposure for 12 hours. No structure or peaks appeared anywhere in the spectrum with the exception of a tail developing in the long wavelength range of the spectrum near 2400 nm. That tail appears to be an increase in signal, which may in part be due to blackbody radiation. But a large portion of the data from that long wavelength tail lie outside of the standard deviation as well as with the mean of the data and at both ends of the spectrum, suggesting that the OSA has poorer performance at its detection limits. Figure 27 shows each of the spectra taken over the 12 hour test period, referenced to the spectra taken at room temperature with the standard deviation shown in cyan and the mean shown in yellow as a dotted line. The flatness of the spectrum suggests that the light source is very stable over time. This light source stability is important because all data is referenced to an initial spectrum at 20 °C as opposed to a reference taken synchronously with each spectrum.

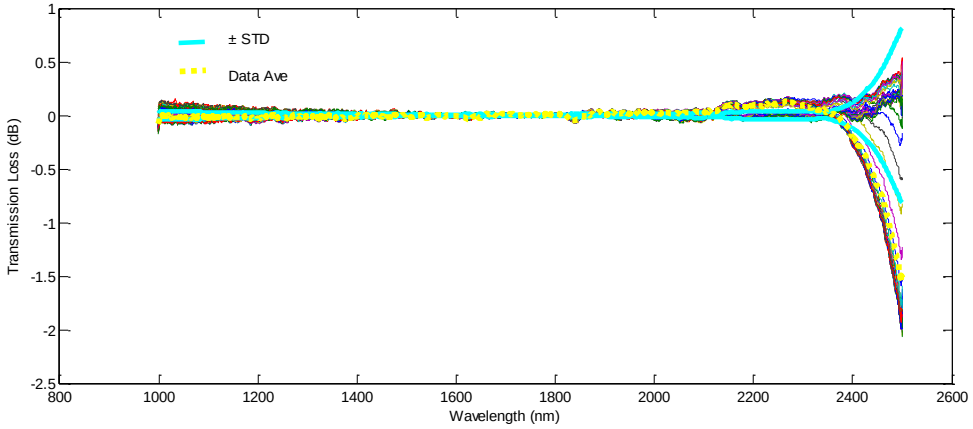

Figure 27 Spectra of fiber heated to 800 °C in ambient air including ±standard deviation and data average

6.2 Blackbody Radiation

Blackbody radiation was examined as a possible suspect for the temperature dependent behavior of the OH related absorption bands at 1389 nm and 2211 nm. As part of quantum theory, thermal radiation emitted by a body at a uniform temperature is known as blackbody radiation. It gets its name from the model that a perfectly opaque body will absorb all radiation, which is incident upon it. That absorbed radiation causes atomic oscillations about the atoms' equilibrium positions causing an effective change in the kinetic energy of the atoms. Recall from thermodynamics that the temperature of a body is determined by the average translational kinetic energy of its atoms. Thus absorbing radiation increases the temperature of the body. But atoms in motion are not rigid spheres. They have a charge distribution that is

also in motion when the atoms are in motion and will thus emit radiation as required by electromagnetic theory. Upon emitting radiation, its atoms will lose kinetic energy thus lowering the temperature of the body. At thermal equilibrium radiation absorbed equals radiation emitted [67]. Blackbody radiation is sort of a misnomer for the phenomenon that might be more simply stated: "hot things glow." The radiation emitted obeys a very specific spectral distribution, which follows Planck's law. When put in a form to equal watt emitted per volume the spectral distribution is as follows:

$$\frac{\Delta P}{\Delta l}(\lambda, T) = \frac{hc^3}{\lambda^5}\frac{1}{e^{\left(\frac{hc}{\lambda kT}\right)} - 1} * A$$

(39)

Where $\frac{\Delta P}{\Delta l}$ is the power per length emitted in watts, **h** is Planck's constant, **c** is the speed of light, **k** is Boltzmann's constant, **l** is wavelength, **T** is absolute temperature, and **A** is the cross sectional area of the body, and .

Wilhelm Wien recognized that the relationship between temperature and peak wavelength of the emitted spectrum is that their product is a constant. In other words, as temperature increases the peak wavelength of the emitted spectrum will decrease. Equation (40) is known as Wien's displacement law [67].

$$\lambda_m \times T = Constant = 2.898 \times 10^{-3} mK$$

(40)

For the case of a heated fiber some of the emitted radiation can be guided by the light guiding portion of the fiber that emitted radiation then being included in the transmitted optical signal. As the temperature increases, the blackbody radiation distribution encroaches further upon the wavelength range of interest for this study. It is worthwhile to evaluate the possibility that blackbody radiation could be to blame for the temperature dependent behavior observed in this work.

Evaluating Wien's displacement law for the temperatures at which these experiments take place shows the maximum wavelength of the emission spectra of the blackbody radiation listed in Table 5. Considering the proximity of the peak wavelengths for blackbody radiation at each temperature to range of interest for this study it can be seen that all peak wavelengths are longer than the pertinent range and only the 800 °C peak wavelength is anywhere near the upper bound. As the long tail is on the long wavelength side of the blackbody radiation spectral distribution and the short wavelength side cuts off sharply, blackbody radiation is only a possible concern for the highest temperature of the experiment.

Table 5 Blackbody radiation peak wavelengths for selected temperatures

Temperature (°C)	l (nm)
20	9891
400	4306
600	3320
800	2701

To determine the maximum effect of blackbody radiation on the optical signal in the wavelength of interest for this study Equation (39) must be evaluated at each temperature for the entire spectra range. In order to compare this result to the collected data it must be turned into dB gain, which can be done by referencing the power of the 800 °C blackbody spectrum to that of 20 °C via the same reference relationship standard for comparing fiber optic signals:

$$dB = 10log_{10}\left(\frac{P_{800}}{P_{20}}\right)$$

(41)

The result is an enormous power increase on the order of 60–150 dB increase across the spectral range of this study. If this type of power increase were actually occurring then no spectral signal would be resolvable at these temperatures as the signal would saturate the OSA at all wavelengths. The problem with the model is it assumes the fiber is a perfect blackbody radiator and that all radiation generated throughout the entire volume of the fiber is guided and thus contributing to the signal. Both assumptions are false and grandiose compared to the real objects involved.

In order to realistically rule out blackbody radiation the spectrum at 800 °C was taken for a fiber with neither initial measurable OH content nor hydrogen exposure during the experiment. In comparing the two spectra it becomes immediately obvious that there is no significant contribution from control data to the OH absorption spectrum at 800 °C from blackbody radiation or any other source. When subtracting the control data from the absorption spectra there remains very good agreement with the original spectrum. The only area that shows poor agreement is in the long wavelength limits of the range. This area is likely to be most affected by blackbody radiation. However, there is enough noise in the detector in this region that it would be impossible to determine the exact source of the disagreement. Ultimately blackbody radiation is not a cause for the temperature dependence observed.

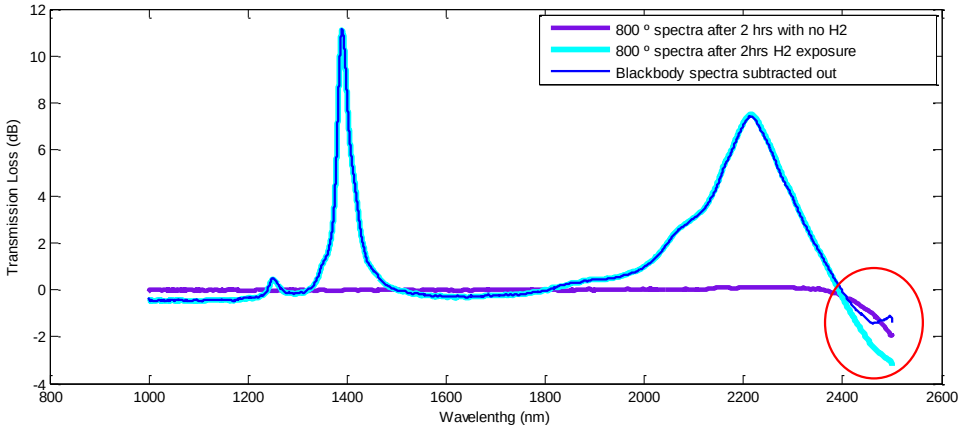

Figure 28 Blackbody approximation subtracted out of OH absorption spectrum

6.3 Change in Number of Modes versus Temperature

It is important to examine the change in number of modes with temperature in order to rule it out as the cause of the observed temperature dependent behavior. Modeling would be necessary to know the exact number of modes for this fiber, but it will be sufficient to use some convenient estimations. Because this phenomenon was observed in step index fibers as well as graded index fibers, and no convenient form of modal estimation is available for graded index fibers, the step index formulas will suffice. The number of modes in a step index multimode fiber can be estimated using the V number of the fiber using

$$M = \frac{V^2}{2} \tag{42}$$

where **M** is the number of modes and **V** is the V number parameter of the fiber. The V number is related to the indices of refraction of the core and cladding by

$$V = \frac{2\pi a}{\lambda}(n_1^2 - n_2^2)^{\frac{1}{2}} \tag{43}$$

where **a** is the radius of the core, $\mathbf{n_1}$ is the index of refraction of the core, $\mathbf{n_2}$ is the index of refraction of the cladding, and **λ** is the wavelength. If the index of refraction changes by **ε** as temperature increases then the index of refraction of the core is

$$n_{1_B} = n_{1_A} + \varepsilon_1 \tag{44}$$

Where **A** is the initial temperature and **B** is the final temperature. Then the change in the number of modes will be

$$M_B - M_A = \frac{2\pi^2 a^2}{\lambda^2}\left[(\varepsilon_1^2 - \varepsilon_2^2) + \left(n_{1_A}\varepsilon_1 - n_{2_A}\varepsilon_2\right)\right] \tag{45}$$

Because the core and cladding are made of the same kind of glass the only difference between them being a small amount of dopant in the cladding for the pure silica core fibers, the indices of refraction of the core and cladding are likely to change by nearly the same amount making $(\varepsilon_1^2 - \varepsilon_2^2) = 0$ and $(n_{1A}\varepsilon_1 - n_{2A}\varepsilon_2) = \varepsilon(n_{1A} - n_{2A})$. According to the manufacturer's specifications, the refractive index difference is typically 1%. In a previous study measuring the change in refractive index with temperature of several different silica based glasses [68], we can infer that $\varepsilon \approx 0.01$making $\varepsilon(n_{1A}–n_{2A}) \approx 0$. Thus the change in the number of modes as temperature increases is negligible.

6.4 Time Dependence

The experiments performed in this work have shown a variety of time dependent behaviors including the initial OH absorption band increase due to diffusion of hydrogen into the fiber, the stability over time of the behavior of the 2211 nm peak, and the different time dependent behaviors of the 1389 nm peak

depending on the presence of hydrogen in the environment. The time dependent behaviors will be discussed here.

6.4.1 Initial Hydrogen Diffusion and OH Peak Increase

Hydrogen diffuses into silica very quickly even at room temperature [44] and even more rapidly at 800 °C. See Table 6 for diffusivities at 21, 600 and 800 °C. In the case of this work the geometry of the silica is a solid cylinder whose radius is 62.5 μm. The core has a radius of 25 μm thus the minimum distance hydrogen molecules must diffuse to reach the core is 37.5 μm. At elevated temperatures (above 150 °C) molecular hydrogen physically dissolved in the fiber reacts with the glass network at defect sites, such as E' centers, forming hydrogen species, predominately hydroxyl species such as SiOH but other hydrides form as well, e.g., SiH. In the case of Ge doped fiber GeOH and GeH are also formed, but the doping concentration limits the concentration of these species that can be formed along with the dopant's participation in a defect site [11, 12, 17, 54]. Since the fiber length exposed to hydrogen is a little less than a meter with the heated region being only 15 cm, it is too short to see absorption caused by molecular hydrogen even at saturated solubility. Although many OH and H_2 peaks overlap the peaks associated only with H_2 absorption are missing most notably are those in the 1.6–2 μm range (see Table 1 for H_2 absorption bands). Absorption due to molecular hydrogen is too small for this length of fiber thus observed loss can be assumed to be due solely to OH. As transmission loss at the OH related peaks appears to saturate the fiber within a few hours at 800 °C the reaction rate must necessarily also be fast in comparison to the diffusion rate. To examine which of the processes, the reaction process or the diffusion process, might be the rate limiting process the initial absorption increase at 1389 nm and 2211 nm can be compared to the diffusion model.

Diffusion of hydrogen through silica follows the ordinary diffusion process defined by the diffusion equation or Fick's second law, the dimensionless solution to the same in cylindrical coordinates [5, 34] when initial concentration inside the cylinder is constant , is shown in Equation (46),

$$\frac{\mathrm{C}-C_1}{C_0-C_1}=1-\frac{2}{a}\sum_{n=1}^{\infty}\frac{e^{(-D\alpha_n^2 t)}J_o(r\alpha_n)}{\alpha_n J_1(a\alpha_n)} \tag{46}$$

where **C** is the concentration at radius **r**, $\mathbf{C_1}$ is the initial concentration inside the cylinder, $\mathbf{C_0}$ is the concentration outside of the cylinder held constant over time, **a** is the radius of the cylinder, **D** is the diffusivity, **t** is time, and $\boldsymbol{\alpha_n}$ is the nth root of the zero order Bessel function. Diffusivity is given in the form of an Arrhenius equation as seen in Equation (47).

$$D_H = D_0 e^{\frac{-E}{kT}} \ \ cm^2 \cdot s^{-1} \tag{47}$$

Where $\mathbf{D_0}$ is a constant, **E** is the activation energy, **k** is the gas constant, and **T** is absolute temperature. $\mathbf{D_0}$ is widely reported as 5.65×10^{-4} [11, 37, 65, 69]. The activation energies reported in the literature,

shown in Table 6, vary very little. The calculated expected diffusivities for H_2 into glass at 600 and 800 °C are also reported in Table 6.

Table 6 Activation energies reported in literature and calculated diffusivities for 600 and 800 °C

Reference	Activation energy (kcal/mol)	Calculated D for 21 °C (cm^2/s)	Calculated D for 600 °C (cm^2/s)	Calculated D for 800 °C (cm^2/s)
[11, 37]	10.4	1.05E-11	1.41E-06	4.30E-06
[69]	10.37	1.11E-11	1.43E-06	4.36E-06
[18, 29]	10.8	5.29E-12	1.12E-06	3.57E-06
[65]	10.36	1.12E-11	1.44E-06	4.38E-06

In order to use Equation (46) to calculate the diffusivity of the initial hydrogen exposure from the data the transmission loss or absorption must be turned into concentration. Absorbance is proportional to concentration by the Beer-Lambert law [22, 28-30]

$$A(\lambda) = \epsilon(\lambda) C x \tag{48}$$

where $\boldsymbol{A(\lambda)}$ is the absorbance at the band maximum, $\boldsymbol{\epsilon(\lambda)}$ is the molar extinction coefficient, $\boldsymbol{C}$ is the concentration of the absorbing species, and $\boldsymbol{x}$ is the optical path length through the sample. Because of this proportionality, and the fact that the concentration side of the equation is dimensionless, all these proportionality constants will cancel and it will suffice to use transmission loss in the diffusivity calculation. To further simplify the calculation the transmission loss can be normalized to the saturation loss thus making the initial concentration inside the fiber $\mathbf{C_1 = 0}$ and the initial concentration at the surface of the fiber $\mathbf{C_0 = 1.}$ The left hand side of Equation (46) then becomes % concentration increase. This normalization simplification can actually work for both diffusion directions, into and out of the fiber, provided that for in-diffusion or concentration increase, there is a constant source of hydrogen in the environment and for out-diffusion or concentration decrease, there is no hydrogen in the environment. The initial concentration profiles for these diffusion directions are thus depicted in Figure 29.

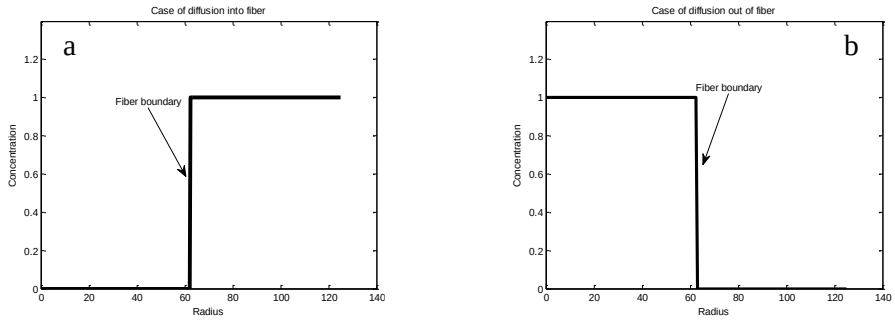

Figure 29 Normalized initial concentration profiles for (a) the case of in- diffusion and (b) out- diffusion.

These simplifications turn Equation (46) into

$$\frac{C}{C_0} = 1 - \frac{2}{a}\sum_{n=1}^{\infty} \frac{e^{(-D\alpha_n^2 t)} J_o(r\alpha_n)}{\alpha_n J_1(a\alpha_n)}$$

(49)

for in-diffusion and

$$\frac{C}{C_0} = \frac{2}{a}\sum_{n=1}^{\infty} \frac{e^{(-D\alpha_n^2 t)} J_o(r\alpha_n)}{\alpha_n J_1(a\alpha_n)}$$

(50)

for out-diffusion, where the left hand side for both is percent change from initial concentration.

In order to apply these equations to the optical fiber in this study the other constants in Equations (49) and (50) are prescribed thusly: Take the radius of the fiber to be **a = 62.5x10^{-4} cm**. The concentration distribution across the cylinder per the solution in Equation (46) follows the contours displayed in Figure 5 from Section 2.3.2. The concentration profile contours show that the concentration profile near the center of the solid cylinder is nearly flat. Instead of needing to integrate over **r** to find an average concentration in the core of the fiber, using **r = 12.5 x10^{-4} cm** (half the radius of the core) will be sufficient to represent the concentration in the entire core. Then **r/a = 0.2** on the x-axis of the concentration distribution plot in Figure 5.

Although diffusivity should not be wavelength dependent, it was solved for separately for the 1389 nm and 2211 nm peaks because their vibrational mode assignments are so different. The 1389 nm band is almost certainly due to the first overtone OH stretch. But the 2211 nm band has a wide variety of assignments relating to OH and could also overlap with non-OH related hydrogen species such as SiH. Their absorption growth need not fit the same model.

The initial absorption increase was modeled for four different experiments. All showed the same behavior for clarity of presentation the calculation results for only one experiment, representative of all four, is shown here.

Consider the very beginning of the hydrogen treatment, the peaks begin to grow as hydrogen diffuses into the fiber and reacts with the glass network until they reach saturation as featured in Figure 30. Using that beginning time period and normalizing the peak height to the saturation intensity, diffusivity for each peak can be calculated. Seven different points at seven different times were selected. Using the normalized loss and the time in seconds Equation (46) was solved for **D**, diffusivity for each of the selected times for each of the peaks. The time resolution for the calculation is ±150 s. The sum was taken out to **n = 3**.

Those diffusivities are plotted against time in Figure 31 (a) and (b). As can be seen in (a) the statistical error for diffusivities calculated from the 1389 nm band is random. The random error suggests that simple diffusion may be a good model for the 1389 nm band absorption increase. But the error in the diffusivities calculated from the 2211 nm band is systematic. The systematic error suggests that the peak growth with time cannot be modeled solely with a simple diffusion process. Using the mean calculated diffusivity for each band a diffusion model fit can be made for each peak. Comparing the fits to the data confirms what the error suggested. The 1389 nm fits the diffusion model quite well, shown in Figure 31 (c). The 2211 nm band does not, shown in Figure 31 (d).

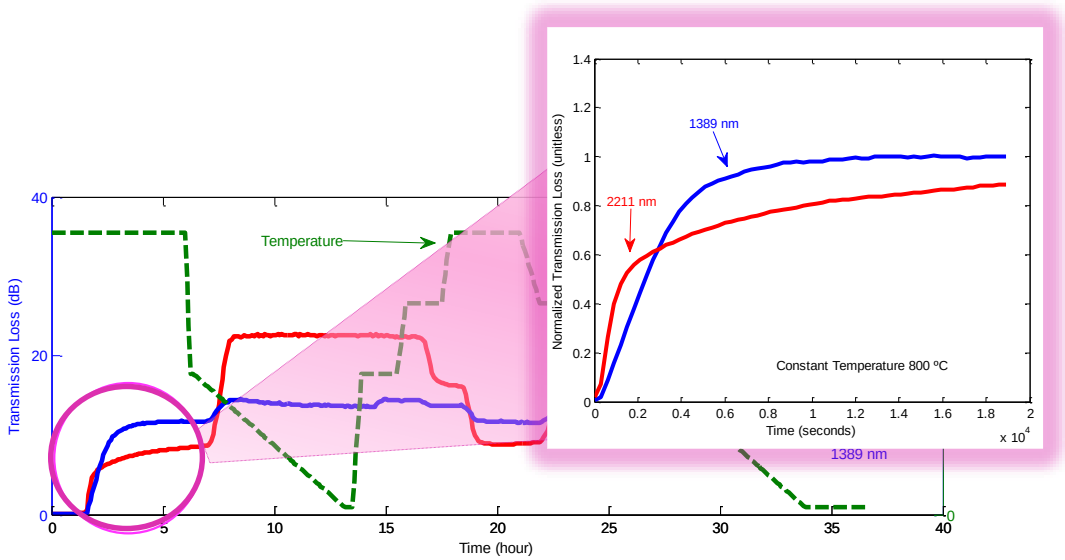

Figure 30 Absorption normalized to saturation intensity for loss increase for initial hydrogen diffusion. 1389 nm band max intensity plotted in blue. 2211 nm band max intensity plotted in red.

It is very interesting that the 1389 nm absorption band is modeled so well with diffusion. The reaction of molecular hydrogen with defect sites in the silica network is certainly dependent on the diffusion of hydrogen into the glass but that does not mean that the loss increase rate should be controlled by diffusion. It then makes sense to compare the mean of the calculated diffusivities for the 1389 nm absorption band shown in Figure 31 (a) with the diffusivity calculated from Equation (47), using 10.4 kcal/mole as the activation energy. The comparison is shown in Table 7. Because the 2211 nm absorption growth had such poor agreement with the diffusion model it is meaningless to compare its mean diffusivity to the diffusivity predicted from the literature.

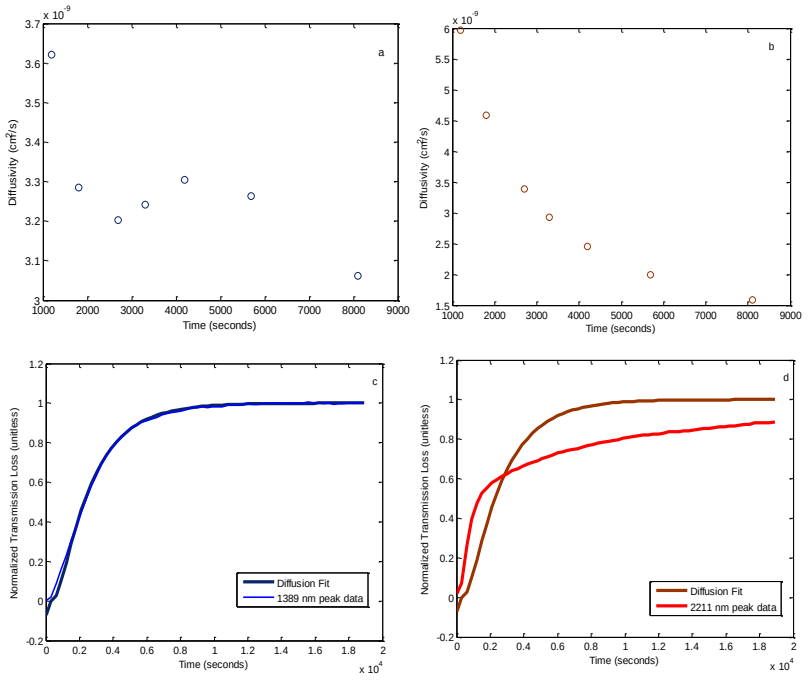

Figure 31 (a) Diffusivities calculated from 1389 nm peak height maximum at seven different times; (b) Diffusivities calculated from 2211 nm peak height maximum at seven different times; (c) Comparison of diffusion model fit to data for 1389 nm band; (d)Comparison of diffusion model fit to data for 2211 nm band.

Table 7 Diffusivity comparison

Diffusivity predicted from Eqn. (47)	Diffusivity calculated from 1389 nm data
4.30E-06	3.2829e-09

From Table 7, the two diffusivities are clearly not the same order of magnitude. This order of magnitude disagreement means that the even though the rate of increase in peak height for the 1389 nm absorption band is modeled very well with the cylindrical solution to the diffusion equation, its rate not governed purely by the molecular hydrogen diffusion process. The calculated diffusivity is smaller than that of hydrogen diffusing in glass. Recall the definition of diffusivity is the rate of transfer of a diffusing substance across a unit of area divided by the gradient of the concentration per unit volume. If the rate of transfer is constant but transferred particles participate in a reaction then the concentration gradient will increase. That would lower the diffusivity. So the diffusivity calculated being lower than that of the pure hydrogen diffusion process is exactly what would be expected if a reaction were taking place provided the reaction rate was close to the rate of diffusion.

The extremely poor agreement between the growth rate of the 2211 nm peak and the diffusion model means that the growth of this peak is far more complicated than that of the combination of diffusion and reaction process seen in the 1389 nm peak. As this peak is very poorly understood and many different modes may lie in this absorption band, it would be necessary to deconvovle the band into its constituents in order to determine a model that would describe its growth. Doing that deconvolution and modeling of this peak is a great opportunity for future work.

6.4.2 Peak Height Change Over Time at 600 °C

A previously heat treated and hydroxylated fiber was set to dwell at 600 °C for ten hours followed by a cycle temperature profile cycling between 600 and 800 °C in ambient air with no hydrogen present to better examine the decrease in peak height for the 1389 nm peak observed during the multiple cycle temperature profile without hydrogen present in the environment. The result was only a very slight decrease in the 1389 nm band and no discernable change in the 2211 nm peak after ten hours. See Figure 32 for zoom-in on the dwell region. It was very obvious that an out-diffusion process did not occur during this ten hour dwell at 600 °C. Nor did any fast reaction process occur. The change in this case was so slow and so small, especially compared to an 80% increase as was seen in 1.5 hours for the 1389 nm absorption band for in-diffusion, that it is easy to conclude that this behavior is not diffusion. If any reaction is occurring, it is also very slow.

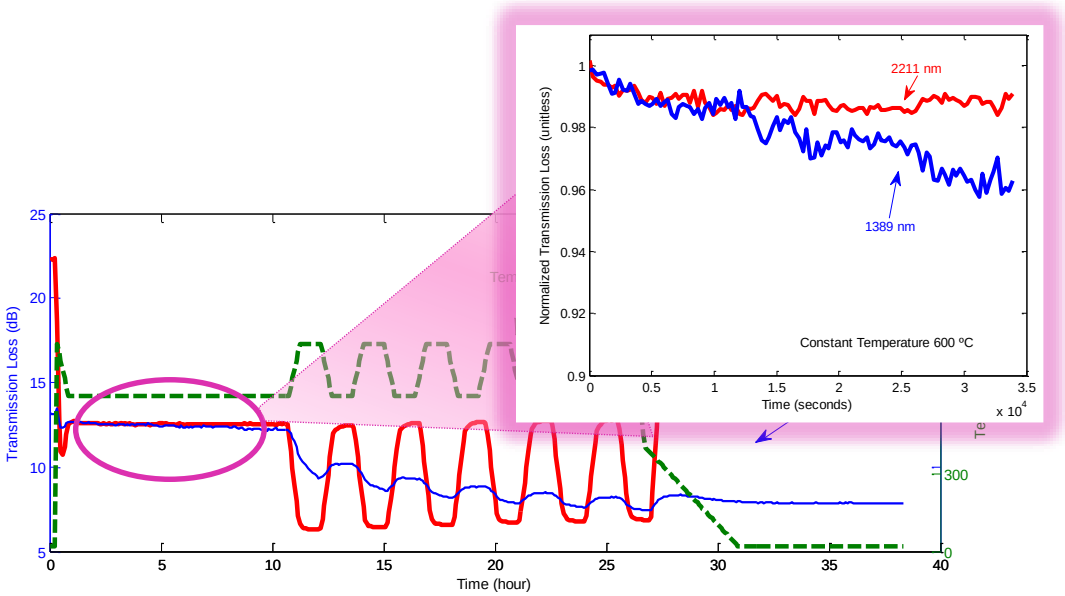

Figure 32 Absorption normalized to saturation intensity for loss increase for initial hydrogen diffusion; 1389 nm band max intensity plotted in blue; 2211 nm band max intensity plotted in red

600 °C was selected as the dwell temperature because the absorption in the previous cycle experiments was much larger at 600 °C than that at 800 °C. Thus it was expected that any decrease in absorption intensity would be more distinctly visible at 600 °C. In retrospect, this temperature was an unwise choice for at least two reasons. The first reason is the obvious inability to compare this result to the in-diffusion that took place at 800 °C. But the second is that, even though, in general, OH absorption is considered an irreversible consequence of hydrogen ingress at high temperatures [11, 17], there have been reported results of removing OH from the fiber [20, 29, 36, 55]. This removal process, however, is always reported at temperatures greater than 700 °C. In the temperature range where hydroxyl is claimed to be removed from fiber or glass the temperature range is 700–1000 °C based on the reaction

$$\equiv Si - OH + \equiv SiH \rightarrow \equiv Si - O - Si \equiv + H_2 \quad \textbf{(51)}$$

which is just the reverse reaction of one of the reactions reported that produced OH absorption from hydrogen ingress in the first place. But again, this reverse reaction is said to take place at temperatures >700 °C [29, 55]. In work done by Yonheng, et al. in removing hydroxyl groups from silica glass approximately a 60% decrease from initial concentration was achieved at 800 °C as measured by a decrease in the height of the peak caused by the fundamental OH stretch (~3672 cm^{-1}) [36]. This removal process was performed on glass slides whose hydroxyl content originated from the fabrication process. It would be interesting future work to see if this same process works at a similar rate for fibers whose hydroxyl content originated from hydrogen ingress at high temperatures. The current results at 600 °C are too ambiguous to provide any comparison or prediction.

In order to verify whether the decrease in intensity over time for the 1389 nm absorption band is due to temperature cycling or due to higher temperatures, a hydrogenated fiber was set to dwell at 800 °C for 10 hours. The expected decrease did occur but it did not follow any of the fit curves previously discussed. Its decrease shape was compared to out-diffusion from Equation (50) and power model from Equation (38). As expected the 2211 nm band does not fit the diffusion model either. It does not change similar to its behavior during the 600 °C dwell. Figure 33 compares the fit and the data for both bands. Previously reported in the literature, decrease in intensity of the fundamental OH stretch absorption band in silica glass at temperatures higher than 700 °C was well modeled by out-diffusion [36] making this result surprising. However, this particular experiment had a thermocouple in the furnace when the data was taken. The material in the chromel – alumel type K thermocouple may have interacted with the system in such a way as to skew the results.

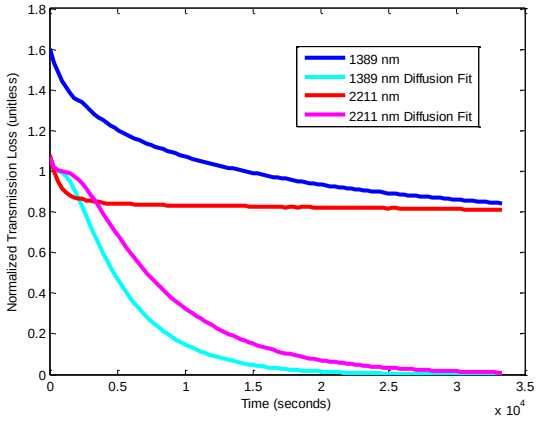

Figure 33 Comparison of diffusion model fit with data for each absorption band

Another indication that this particular result may be abnormal was the growth rate of the 1389 nm peak at the initial hydrogen treatment. It began growing normally but where it had flattened in previous experiments, in the experiment in which the thermocouple was present in the furnace it decreased after its initial increase in a linear fashion as can be seen in Figure 34.

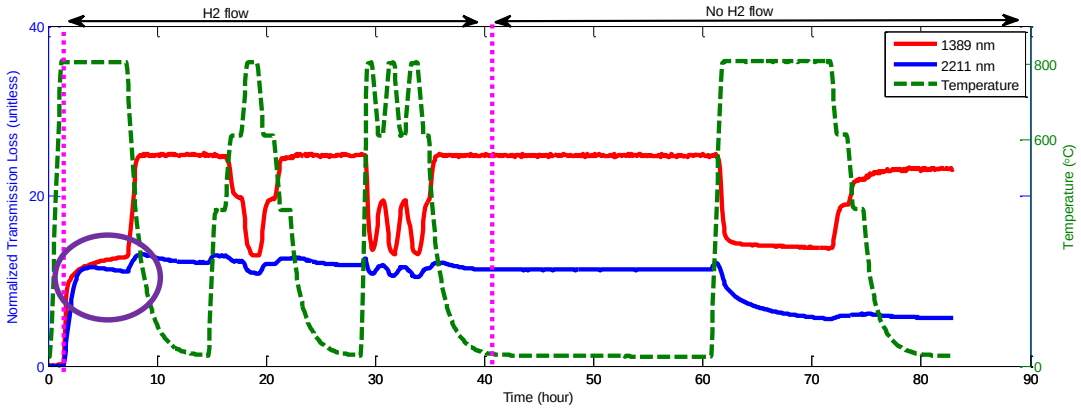

Figure 34 Peak track for fiber with thermocouple present in furnace. Fiber went through an initial hydrogen treatment, a step temperature profile and a cycling profile in a hydrogen environment. The fiber was allowed to cool to room temperature. The hydrogen source was removed and the system rested at room temperature in ambient air for twenty hours. The fiber was then heated to 800 °C to dwell for ten hours in ambient air. The final cool to room temperature went through a step profile.

6.4.3 Time Dependent Loss Decrease During Cycling Temperature Without Hydrogen

During the experiments with a temperature profile cycling between 600 and 800 °C and no hydrogen present, a noticeable decrease in absorption over time occurred for the 1389 nm absorption band while the 2211 nm band did not decrease. The absorption at room temperature following the temperature cycle is also much lower than it was prior to the cycle. See Figure 35 showing the maxima of each peak plotted against time during a cycle temperature profile where the temperature is cycled between 600 and 800 °C, dwelling for two hours at 600 °C and dwelling for one hour at 800 °C. The ramp time between

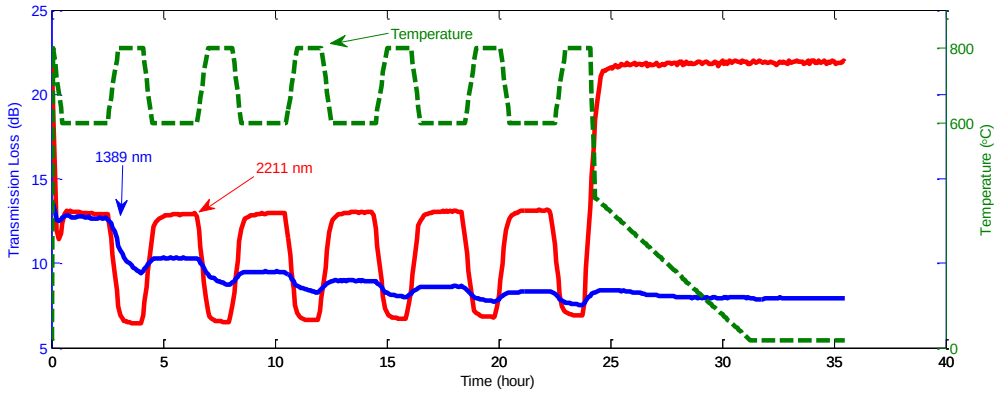

Figure 35 Temperature profile cycling between 600 and 800 °C; Two hour dwell at 600 °C; One hour dwell at 800 °C; 30 minute ramp between temperatures

temperatures is 30 minutes.

As can be seen in Figure 35, neither the 1389 nm nor the 2211 nm peak height change much during each two hour dwell period during the 600 °C segments. This result is consistent with the incredibly slow change in intensity exhibited by the 1389 nm peak when the fiber was allowed to dwell at 600 °C for ten

hours. The reduction in this band's absorption over time is due to the portions of the cycling temperature profile above 700 °C rather than the fact that the temperature is cycled as was shown in the previous section. Previous studies attempting to remove OH from silica glass have shown a reduction in the fundamental OH stretch absorption band [20, 36], which is then consistent with a reduction in the first overtone of the OH stretch observed here. When looking at the changes between each 600 °C dwell segment by taking the peak maximum from the end of each dwell segment and plotting them against time, (similarly for the 800 °C dwell segments) it looks like the 1389 nm peak reduces in height following a power model (see Figure 21, model following the form of Equation (38)). However, that model does not necessarily have any physical significance. It could be the impact of temperature fluctuation on the out-diffusion model of Equation (50). The first step to analyzing the cause of the reduction in peak height would be to analyze the behavior of this absorption band at constant temperature with no hydrogen present.

It is actually surprising that the 2211 nm band does not seem to respond in a time dependent way to the fact that no hydrogen is present in the environment, especially in light of the fact that the 1389 nm reduces in intensity over time under the same conditions. The height of the 2211 nm peak obviously responds to temperature changes, but over time its height does not change. If there is any reduction in OH concentration in the core of the fiber affecting the height of the 1389 nm peak height, it is not affecting the height of the 2211 nm absorption band. The fact that the two absorption bands do not respond the same way is because their mode assignments are so different. However, since they are both assigned to some form of OH related absorption, the fact that one reduces in height while the other stays the same is quite puzzling. Deconvolving the 2211 nm peak into constituents and watching how each behaves over time at constant temperature above 800 °C compared to the 1389 nm band would be a great place to start to dig into this mystery. Perhaps such work could aid in identifying the constituents of the 2211 nm peak that pertain specifically to OH concentration and those which do not. The contrast between the behaviors of these two peaks offers a starting place for plunging deeper into the cause of the poorly understood 2211 nm absorption band.

6.5 Temperature Dependence

In addition to any diffusion and reaction time dependent processes going on, there is obviously a temperature dependent behavior to the peak height for the two absorption bands at 1389 nm and 2211 nm. In Figure 36 this temperature dependence is shown when the maximum peak height is plotted against time. The temperature profile is plotted in green. When the temperature increases the transmission loss at these two absorption bands decreases. The temperature dependence appears to be completely reversible, even if the temperature is cycled multiple times (see Figure 35), so no permanent change to the chemical composition of the glass or the chemistry of the absorbing species is taking place. Because the absorption is less at lower temperatures if the initial absorption due to hydrogen diffusion occurs at a high temperature, the absorption will increase when the temperature is lowered at a rate precluding the possibility of an increase due to hydrogen diffusion and chemical reaction within the glass network. In previous studies where temperature dependence was observed a structural change in the glass was postulated as the cause [1, 24]. This structural change viewpoint will be examined here in light of data from the current study.

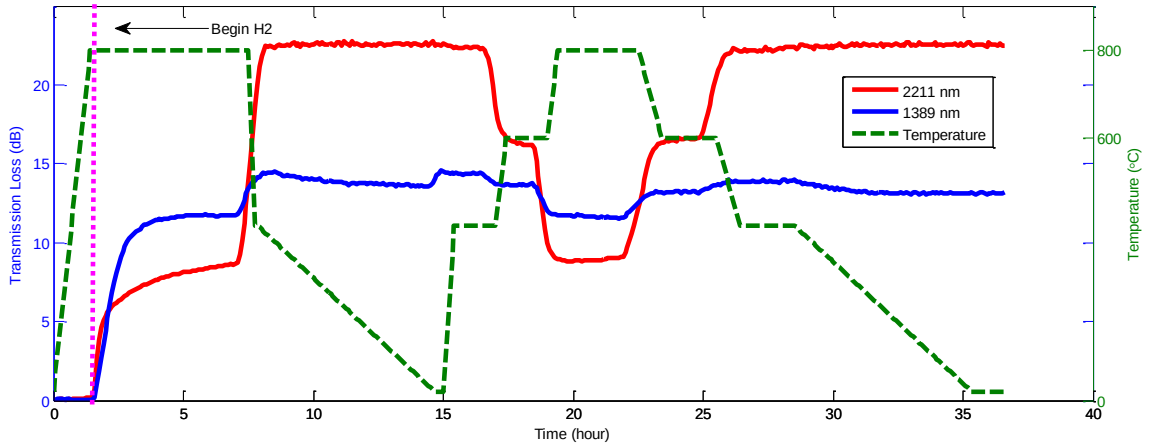

Figure 36 Maximum peak height of 1389 nm (blue) and 2211 nm (red) absorption bands plotted against time for initial hydrogen treatment at 800 °C and then through a step temperature profile

The two structural postulations made to explain this temperature dependent behavior are structural relaxation around hydroxyl groups [24] and a change in hydrogen bonding state [1]. The in depth literature review of each explanation is accounted in Section 3.7. Structural Relaxation Usually Requires a Fast Quenching, which was not part of the current study. The slow cool rate in this study makes it difficult to compare to structural relaxation reports in the literature. Differences in absorption band shape at different temperatures seen in this study may provide some information as to the structural changes taking place in the glass.

6.5.1 Heating Versus Cooling

When the temperature is changed, there are changes in the shape of both the 1389 nm and 2211 nm absorption bands. But there does not seem to be a difference between heating and cooling. The shape of the 1389 nm band at 600 °C appears to be the same whether the fiber was heated to 600 °C or cooled to 600 °C. Consider the spectra at each absorption band when the temperature is cycled between 600 and 800 °C: For each of the 600 °C sections, the shapes of the absorption bands are the same; see Figure 37 (a) and (c). The same is true for the 800 °C segments (Figure 37 (b) and (d)). This behavior suggests that the structure change in the glass is not dependent on whether it is being heated or cooled. Additionally, it shows that the structure change is reversible. This reversibility would imply that there is a preferential structural configuration for each temperature rather than a permanent alteration caused by heating the fiber.

A preferential structural configuration for the glass at different temperatures is not unheard of but it is interesting [70-73]. It means that the temperature dependent behavior here is not a result of annealing or glass transition properties. However, most of the available literature focuses on structural changes at the glass transition and in particular with respect to changes in cooling rate; as opposed to these changes which are below the glass transition and do not appear to depend heavily on the rate of change of temperature. It would be important to further explore the kind of structures that exist at each temperature and what their properties are. Any application calling for high temperature use cannot depend on the structural properties of the fiber at room temperature. Design of fiber optic systems intended to operate

over a wide range of temperatures would be impacted if the structural changes in the glass at different temperatures greatly impacts the properties of the fiber necessary for the application. Exploring these preferential structural configurations and their properties is an exciting area for future research.

6.5.2 First Overtone OH Stretch: 1389 nm Band

Unfortunately when analyzing the data for the 1389 nm peak for temperature dependent behavior there is a confounding factor in that its height changes over time. Fortunately, the shape of the peak for each

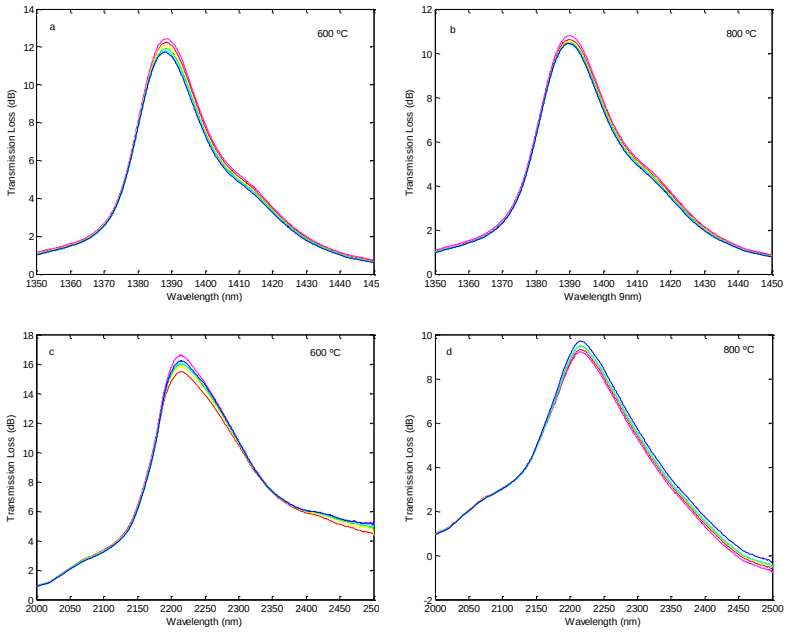

Figure 37 Temperature cycling between 600 and 800 °C, 30 minute dwell at each temperature;
30 minute ramp between temperatures for six cycles; (a) 1389 nm band at each 600 °C dwell; (b) 1389 nm band at each 800 °C dwell; (c) 2211 nm band at each 600 °C dwell; (d) 2211 nm band at each 800 °C dwell

temperature does not seem to change over time so structural information may be preserved, but the overall height change makes it confusing to compare spectra taken at different times. It is especially confusing for experiments where no hydrogen was flowing because during the tests where no hydrogen was flowing there is such a dramatic change in the height of this peak over time. Even though it is obvious that there is a peak height change with temperature and that the height at 800 °C is smaller than that of lower temperatures, there are points from 800 °C dwell segments throughout an experiment where the 1389 nm peak height is larger than that of the final 20 °C peak height such as can be seen in Figure 38. When comparing peaks of different temperatures, it is best to use data from experiments where hydrogen was present. Even though a quantitative comparison of peak height differences is quite imprudent qualitative comparisons can be made.

There is a shoulder visible on the longer wavelength side of the absorption band which can be seen in Figure 39. Its location is very near to 1414 nm, which is claimed to be the vibrational frequency of hydroxyl groups whose hydrogen is participating in hydrogen bonding [1]. However, this shoulder is more likely the contribution from hydroxyl groups bonded to germanium whose absorbance is centered near 1420 nm [17] because it did not appear in spectra from pure silica core fiber. As the fiber is heated, the entire band seems to shift towards longer wavelengths, but the shoulder does not appear to grow in comparison to the main peak.

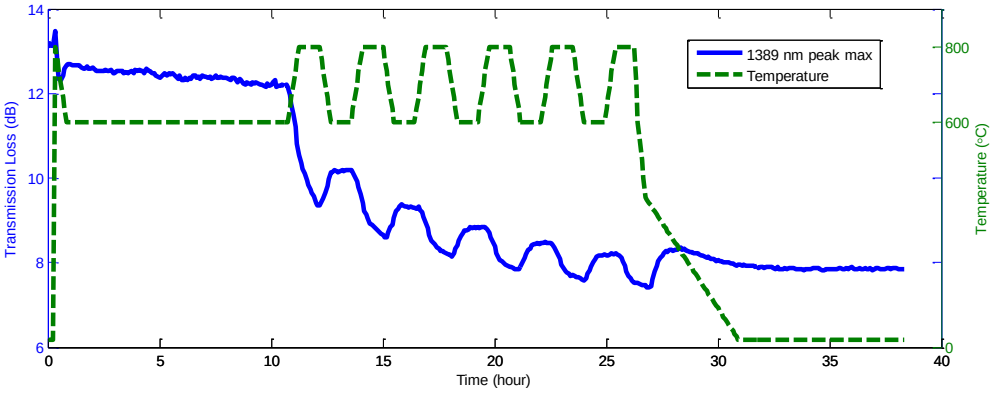

Figure 38 Maximum absorption of 1389 nm peak tracked with time (no hydrogen flowing); Temperature profile cycling between 600 and 800 °C with 30 minute ramp between temperatures and one hour dwell at each temperature

Also visible in Figure 39, the entire band seems to shift to longer wavelengths without tremendous change in the overall shape of the band. The top portion of the band may spread out slightly but the shape is not largely changed even if this spreading out does occur. The shoulder to the longer wavelength end is still clearly visible.

When the temperature is raised, it appears that initially the absorption begins to increase. The maximum

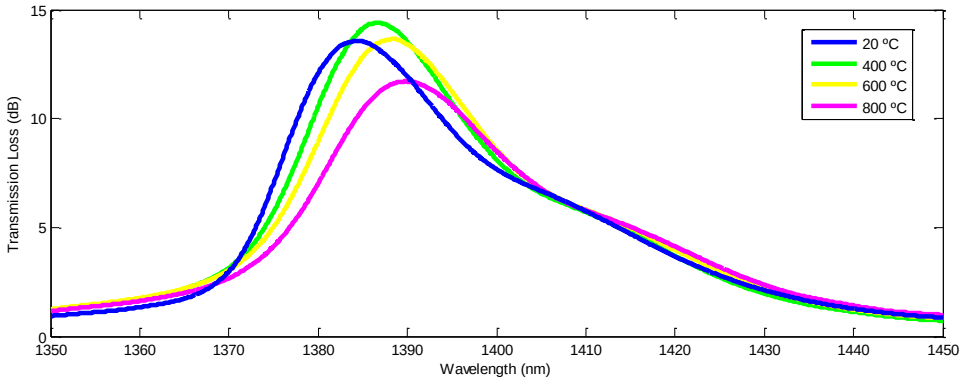

Figure 39 Shape of 1389 nm band at different temperatures

at 400 °C is greater than that at 20 °C. As the temperature is further raised the absorption goes down until it is much lower than the initial room temperature height at 800 °C. This height is behaving differently with temperature than the center of the band. The band at 400 °C, although larger in absorption intensity than at 20 °C, is shifted towards longer wavelengths.

The way this band changes with temperature suggests strongly that there is a change to the overall structure of the glass rather than to the hydroxyl bond itself. If great changes to the hydroxyl bond were taking place the shape of the band would distort rather than the shift seen here. Small changes to the hydroxyl bond, such as energy leaving the hydroxyl bond going into a hydrogen bond with neighboring oxygen could cause a shift like this. However hydrogen bonding should decrease with increasing temperature [1] thus hydrogen bonding increasing is a very unconvincing reason for the shift.

6.5.3 Combination Absorption Band at 2211 nm

The 2211 nm absorption band has much stronger absorption at room temperature than at higher temperatures, so much so that when the fiber is cooled, the transmission loss saturates the detector at 400 °C and below. In order to make comparisons between lower temperatures and higher temperatures, a 6 cm segment of Ge-doped fiber was used, spliced to pure silica core 50/125 fiber, which shows a much smaller hydrogen response. Effects of the pure silica fiber are considered negligible as shown in Figure 40 (a). For features of the band near the long and short wavelength edges more absorption is necessary to see some details so the full length of the heating area, 15 cm is shown in Figure 40 (b).

Figure 40 shows the 2211 nm band at 20, 400, 600, and 800 °C. The band shifts ever so slightly to the longer wavelength, but it is far smaller a shift than that of the 1389 nm band. This band spreads out considerably as temperature is increased. At lower temperatures there is a distinction between this band and another at longer wavelengths centered beyond the range of the OSA. This distinction disappears as temperature increases. The longer wavelength band may be another combination band of the fundamental OH stretch with a different silica network vibration than that of the 2211 nm or it may be the tail of the fundamental OH stretch. It is impossible to determine the cause of the cessation of the distinction because there is considerable noise in the signal at the end of the range of the detection limits of the instrument and there is some distortion due to blackbody radiation in that region as well. Thus, changes with temperature beyond 2350 nm cannot be considered for evidence of structural changes. However, from Figure 40 it is possible to see that at the longer wavelength portions of the band, absorption increases slightly as temperature increases. This increase could be a result of the band broadening.

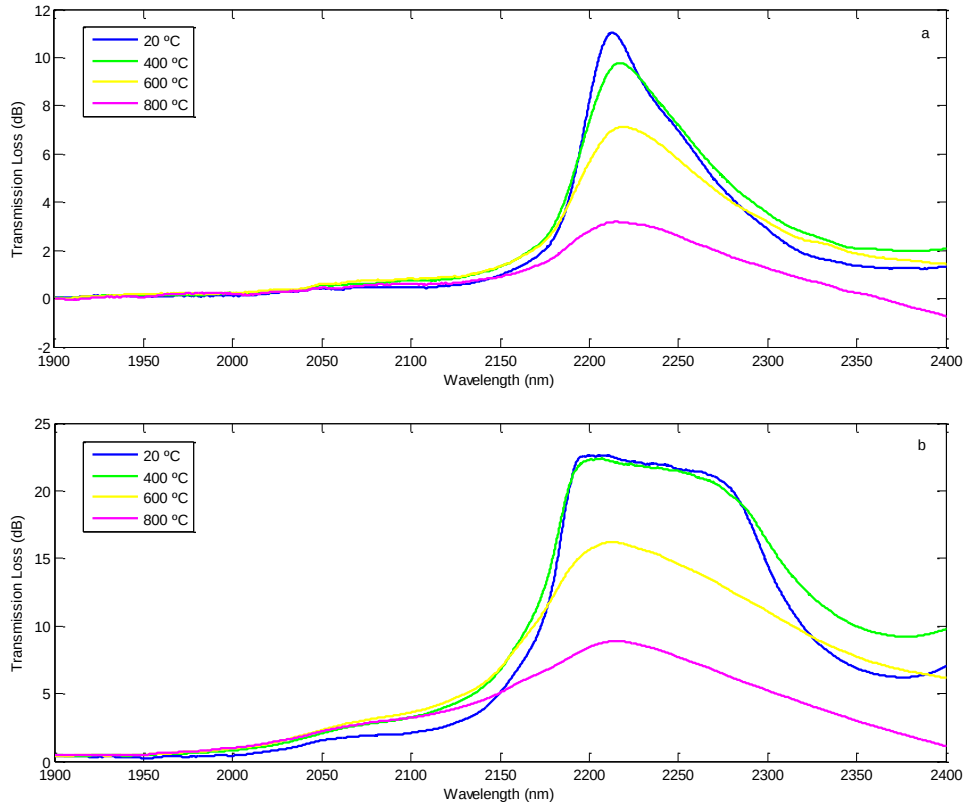

Figure 40 Shape of 2211 nm band at different temperatures, Ge doped 50/125 graded index fiber (a) 6 cm length; (b) 15 cm length

There is the slightest shoulder visible on the long wavelength side of the absorption band near 2066 nm, which can be seen on the blue curve in Figure 40 (b). The absorption in this area is too weak to be seen in the 6 cm piece of fiber shown in (a). The intensity of the shoulder increases as temperature increases just like the long wavelength side of the band. It looks like a separate band at room temperature and as the whole band broadens the distinction between this shoulder area and the bulk of the main band becomes less distinct. The various changes to the shape of this band as temperature changes could imply the glass network is changing or that there are changes in the vibrational mode of a particular absorbing species. This band has so many different assignments. Decomposing it and considering the changes of each component with temperature is an open area for future research.

6.5.4 Hydrogen Bonding

Changes in hydrogen bonding are one scheme that has been suggested to account for the changes in spectral features in OH absorption bands. When the hydrogen in a hydroxyl group participates in hydrogen bonding energy is removed from the OH bond shifting its absorption to longer wavelengths. More hydroxyl groups participating in hydrogen bonding as temperature increases would qualitatively account for the shift to longer wavelengths seen in the 1389 nm absorption band. However, the number of hydroxyl groups participating in hydrogen bonding are not expected to increase with temperature [1]. Glass expands as it is heated, thus if proximity between hydroxyl groups were to change it would not

change in favor of increasing hydrogen bonding. Additionally, the viscosity would go up if more hydrogen bonding were occurring. Testing viscosity could be a helpful test for confirming or disproving an increase in hydroxyl groups participating in hydrogen bonding. However, with so many other factors against the possibility of an increase in hydrogen bonding it is likely that is not the cause of the shift to longer wavelengths with increase in temperature. Additionally, a change in the amount of participation in hydrogen bonding does not, it itself, account for the changes in peak intensity seen with changes in temperature.

In an effort to suggest a better model than simply an increase or decrease in the number of hydroxyl groups participating in hydrogen bonding another hydrogen bond model for the temperature dependent behavior of the absorption peaks has been reported. In a similar observance of decrease in band absorption intensity with increase of temperature, Yokomachi, et al. [1] employed a model to explain both the shift to longer wavelengths and decrease in intensity as temperature is increased. The model assigns each of the components of the 1389 nm band to one of four different hydrogen bonding schemes originally posed by Walrafen, et al. [3] for interpreting the fundamental OH stretch absorption band with respect to the interactions of OH groups with silica glass. The first two hydrogen bond states are the hydroxyl group whose hydrogen is not participating in hydrogen bonding, and the hydroxyl group in which the hydrogen is participating in hydrogen bonding, which would then absorb at a longer wavelength. Those two states are as depicted in Figure 41 (a). The second two states have the same structure but different vibrational frequencies. The structure is a symmetric non-linear bidentate ring with in-phase and out of phase vibrational states as shown in Figure 41 (b).

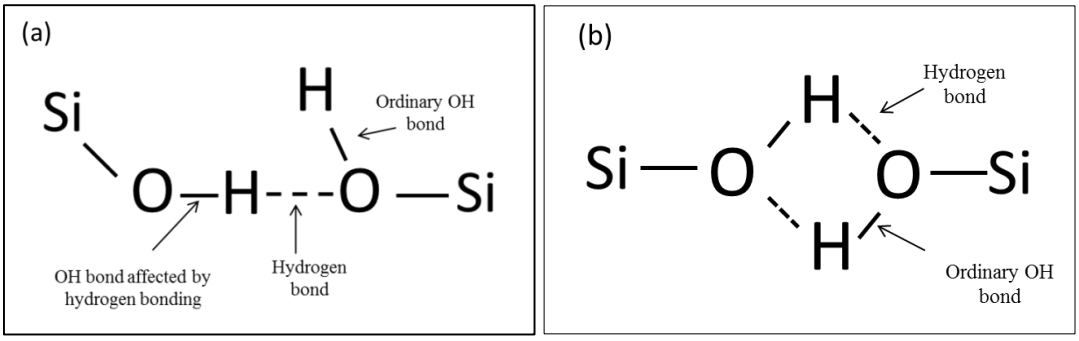

Figure 41 (a) asymmetric bindentate structure yielding only one linear hydrogen bond with oxygen in neighboring silanol group whose hydroxyl group has an ordinatry OH bond, (b) symmetric bidentate structure where hydrogens of two neighboring silanol groups are close enough to neighboring oxygen to form hydrogen bonds having in-phase and out-of-phase vibrational modes
[1-3]

This model is a reasonably attractive explanation for the temperature dependent behavior but an understanding of what the in-phase and out-of-phase vibrational states are like is not immediately accessible. Another problem with this model is there is no obvious reason why hydrogen bonding should decrease molar absorptivity of hydroxyl atoms. In the current study, the combination band at 2211 nm also decreases in absorption intensity with increase in temperature. It is not immediately obvious how a transition from in-phase to out-of-phase for the symmetric bidentate ring structure will produce a decrease in such a complex absorption band. Finally, the band at 1389 nm decreases in intensity when there is no hydrogen present in the environment suggesting that some hydroxyl groups are able to dissociate and the hydrogen diffuse out of the fiber. Meanwhile the 2211 nm band does not exhibit this behavior. The 2211

nm band is so much more complex than the 1389 nm band having so many more constituent vibrational modes it is not unreasonable that they should behave differently. However, if the temperature dependence were due only to this transition between in-phase and out-of-phase for the symmetric bidentate structure there is no necessity that both bands should behave the same way with respect to temperature changes.

6.5.5 Structural Changes Within the Glass Network

To account for two very different absorption bands behaving very similarly with respect to temperature (i.e., decreasing in absorption intensity as temperature increases), it seems necessary that some structural change in the glass is taking place as opposed to merely a change in the bonding of the absorbing species. It is likely that this change is not specific to the OH bond itself as suggested by the hydrogen bonding hypothesis but rather global to the glass network and then consequently affects the OH bond. Viscosity studies at different temperatures could be instrumental in confirming whether structural changes have taken place. Electron density distribution modeling would be extremely helpful in conventionalizing and visualizing the nature of the structural changes that might be taking place. Such models could predict expected viscosities, which could then be measured to confirm the models. Electron density distribution models may also predict the locations of absorption bands, which could be measured farther in the infrared or perhaps by Raman spectroscopy.

6.6 Conditions for Absorption Intensity to Change with Temperature

The slight shifts to longer wavelengths suggest structural changes that are slightly adjusting the absorption frequency of the absorbing species. But that shift still does not explain why structural changes would cause the absorption intensity at the two bands in the 1–2.5 μm range to decrease so dramatically as temperature increases. Several conditions and their respective consequences must be considered to explore the connection between structural changes and decrease in absorption.

Although the chemistry of the glass is not changing, it is now necessary to move beyond chemistry to describe the species present instead defining a species by the frequency of light it absorbs. Using this definition of species, the consequences of the following two conditions will be examined in light of the observed temperature dependent behavior: concentration of absorbing species remains the same and concentration of absorbing species changes.

6.6.1 The Concentration of Absorbing Species Does Not Change

If the concentration of the absorbing species does not change, one of two things must happen for the decrease of absorption with temperature to occur. Either the molar absorptivity of the species must be temperature dependent or absorption must deviate from Beer's law (Equation (48)). Since the molar absorptivity is an intrinsic property of the material it should be well known in the literature if this property is temperature dependent. As it is not reported as such, this possibility is highly unlikely. The alternative, that the absorbance deviates from Beer's law, is not, however, impossible. Deviations from Beer's law are not unheard of and can certainly occur because of a chemical or physical effect of the material or be caused by an instrumental effect [74]. In the case of this work instrumental effects can

effectively be ruled out as a cause for the temperature dependence because the instrumentation (i.e., the light source and detector) do not suffer any changes when the fiber is heated. Additional evidence for ruling out instrumental causes is this temperature dependent behavior has been observed by others [1, 66]. To carefully quantify the deviation from Beer's law evaluation of any instrumental effects is in order, but instrumental effects can be eliminated as the cause for deviation.

6.6.1.1 Deviation from Beer's Law

Deviation from Beer's law simply means that absorbance no longer has a linear proportionality to concentration of absorber. An example of a non-linear relationship is [74]

$$A = aCl + bC^2l + \cdots + gC^ml \quad \textbf{(52)}$$

where $\boldsymbol{A}$ is absorbance, $\boldsymbol{C}$ is concentration, $\boldsymbol{l}$ is optical path length, and $\boldsymbol{a,b,..,g}$ are constants similar to molar absorptivity. Absorbing species no longer acting independently of each other could be a cause for deviation from the linear relationship in Beer's law, as is the case in symmetric bidentate hydrogen bonded ring proposed by Walrafen, et al. [3] depicted in Figure 41 (b). However, in that model the absorbers never act independently of each other and thus may not obey Beer's law at room temperature either. Studies to measure molar absorptivity have confirmed Beer's law for hydroxyl concentration in glass at room temperature [30]. It is possible that the change in glass structure with temperature creates codependency of absorbers in some fashion creating a deviation from Beer's law at higher temperatures. This codependency would need to affect species causing both absorption bands seen in this experiment. If it is a global change in glass structure it is possible for both to be affected.

In situ measurements of concentration might be necessary for confirmation that concentration of absorbing species are not changing. Raman spectroscopy would be a useful tool in examining this situation because it is also sensitive to changes in absorption frequency. Mass spectrometry would only be sensitive to chemical changes which are clearly not occurring due to the reversibility of the phenomenon.

Discovering a deviation from Beer's law for hydroxyl related species in glass at high temperature would be an exciting discovery for both sensing technology applications and for fiber optic system design.

6.6.2 The Concentration of Absorbing Species Changes

If the concentrations of the absorbing species are changing, then according to our new definition of species (although the chemistry of glass is not changing) the frequencies at which the chemical species absorb are changing. An example of a mechanism which could cause such a change would be the case of hydrogen bonding. The hydrogen atom of a hydroxyl group participating in hydrogen bonding would remove energy from the OH bond reducing the frequency of the vibrational mode and lengthening the wavelength at which it absorbs light. The chemistry has not changed but the absorbing species has changed because the wavelength of light absorbed has changed. Models for changes in hydrogen bonding have been explored in previous sections. The necessary conditions of a change in absorbing species (i.e., a change in wavelength of absorption) to result in the observed temperature dependent behavior will be examined in this section.

In order for a change in absorbing species to result in the observed temperature dependent behavior one or more of the following conditions must be met.

6.6.2.1 Change to Infrared Inactive

The change in species must be a change to an infrared inactive species. If the species changes such that its vibrational mode no longer has an oscillating dipole moment, then it will no longer be infrared active. Should species become infrared inactive the intensity of the observed infrared absorbance bands would be reduced. A change to infrared inactivity need not change the vibrational frequency of the species; it must merely change the vibrational mode such that it no longer has an oscillating dipole moment. For example, there are two silicate vibrational modes, namely symmetric stretch and symmetric bending (see Figure 3) that are infrared inactive because the modes do not have oscillating dipole moments. Hydroxyl groups, on the other hand, only have one vibrational mode, stretching, and an inherent dipole moment, thus hydroxyl groups seem destined to always be infrared active. However, it is not inconceivable that some coupling between hydroxyl groups and the SiO_4 network could produce an infrared inactive vibrational mode. If such a coupling were a result of a temperature dependent structure change in the glass network, it could result in the observed phenomenon. But any such behavior would necessarily require a symmetric bonding structure involving the hydroxyl group such that its vibrational mode did not have an oscillating dipole moment. Hydroxyl groups being so heavily polarized, the lack of any core electrons to shield the hydrogen's proton, and the random nature of the glass network in terms of long range order seem to preclude this situation from occurring for a large majority of hydroxyl groups present in the glass. It seems very unlikely that some structural change to the glass could cause a large portion of the hydroxyl groups to become part of some unit with vibrational modes that have no oscillating dipole moment. Modeling of electron density distributions could be helpful if the prospect of a shift to infrared inactive were a motivating notion as a cause for the observed reduction in absorption intensity with increase in of temperature. Raman spectroscopy could potentially be helpful in investigating this possibility as well if it can be done in situ. But interpreting Raman results might be complicated and it would still be necessary to know if there is a difference in vibrational frequency between the room temperature and high temperature species. If the room temperature species and the high temperature species were both Raman active and they have the same vibrational frequency, the high temperature Raman spectra should remain the same. If they are both Raman active, and they have different vibrational frequencies a shift in the Raman spectra would be expected. If the room temperature species is not Raman active, an increase in the Raman spectra at high temperature would be expected at the high temperature species' absorption frequency. These complex conditions would make the remote possibility that hydroxyl related species are shifting to an infrared inactive structure complicated to verify.

6.6.2.2 Shift in Infrared Absorbance Wavelength

If a change in absorbing species occurs and the species is still infrared active, only two possibilities for the amount of change in absorption frequency exist. Either it must change to a frequency very close, within 150 nm of the previous species, or it must change by at least a micron. The reason the shift is limited to these two possibilities is that no additional peaks form in the high temperature absorbance spectrum in the 1–2.5 μm range. So the new frequencies must either be very close to room temperature frequencies or else at least one micron shorter for the 1389 nm band and one micron longer for the 2211

nm band, otherwise new peaks would appear. Figure 42 shows the full spectral range at 20, 400, 600, and 800 °C. No new absorption bands appear throughout the temperature range.

A one micron change in absorption frequency would seem to necessitate a chemical change, which is not likely due to the reversibility of this phenomenon. Expanding the spectral range of detection could verify whether new peaks appear as the 1389 nm and 2211 nm peaks reduce as temperature is increased. A study of this nature could be complicated by the presence of other OH related peaks on either end of the region studied here, namely the second overtone stretch at 950 nm [11], the first overtone stretch near 2700 nm [47], and another combination mode near 2440 nm [59].

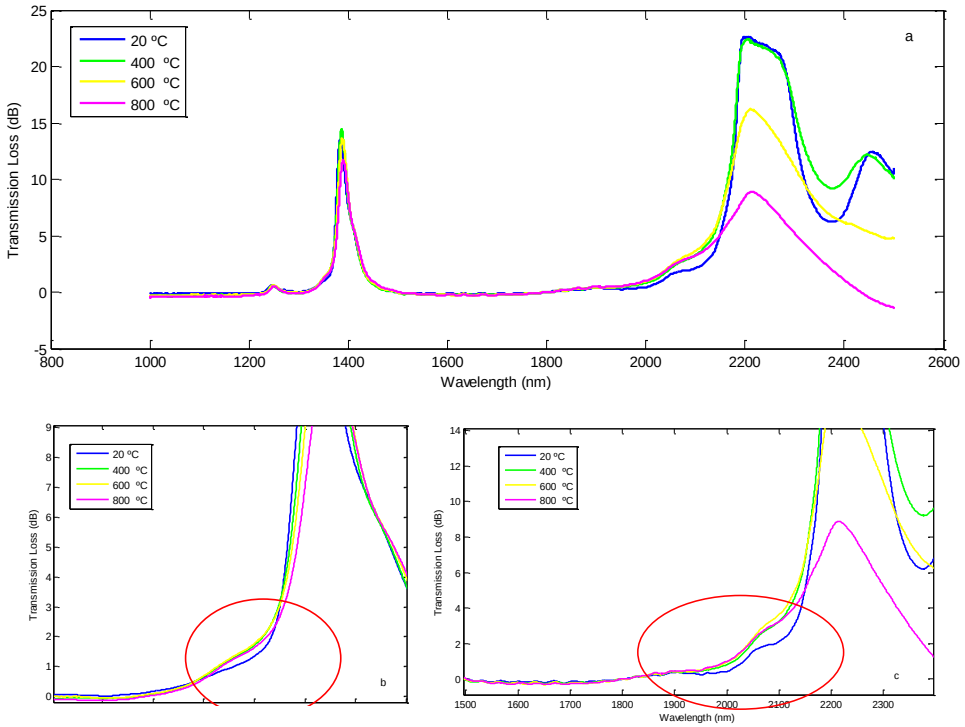

Figure 42 (a) Full spectral range at different temperatures; (b) Zoom in on shoulder of 1389 nm band near 1350 nm; (c) Zoom in on shoulder of 2211 nm band near 2066 nm

If there is a shift in the absorbing wavelength by a few nanometers, then the molar absorptivity of the high temperature species must be much greater than that of the low temperature species or else absorbance deviates from the linear relationship to concentration as stated in Beer's law (Equation (48)). Estimating the needed difference in molar absorptivities will require knowledge of how many of the room temperature species make the shift and at what new frequency they absorb. There does appear to be a slight increase in absorption as temperature increases in the shoulder around 2066 nm on the short wavelength side of the 2211 nm absorption band, which can be seen in Figure 42 (c). This increase in the shoulder could be a candidate frequency range for high temperature species. However, it looks like a separate absorption band at low temperatures and as the larger band broadens at high temperatures the distinction is blurred, which may be a feature of peak broadening rather than a species shift. There is visible gain in intensity as temperature increases, but it is very small compared to the reduction in intensity of the larger band. A corresponding shoulder can be seen on the 1389 nm band near 1350 nm shown in Figure 42 (b). Again, absorption in this shoulder area increases as temperature increases. But the

increase is very small compared to that of the rest of the absorption band. It is not impossible that there is a shift of some of the species causing the larger peaks to these smaller shoulders but the requirements that the species making up the shoulders must have much smaller molar absorptivities still holds. Alternatively, even if species shift into the shoulder regions, absorption across the entire spectrum may deviate from Beer's law.

If there is a shift as temperature increases in order to accommodate the observed behavior that both peaks reduce in height and shift to some degree over a range of temperatures it is most likely that the shifting occurs by degrees as opposed to all species shifting to a different bonding state at the same time. Also, a range of states could be available. Alternatively, even if the species do shift slightly in vibrational frequency, absorbance could still begin to deviate from Beer's law. The small gain on the short wavelength side of each band is certainly not enough to make up for the loss of intensity in the bulk of the band.

7 Conclusions and Future Work

In this study the temperature dependent behavior of absorption bands in a germanium doped silica 50/125 optical fiber caused by hydrogen at high temperature were studied. The two main bands that appeared upon exposure to hydrogen at 800 °C were located at 1389 nm and 2211 nm. The increase of the 1389 nm band, assigned to the first overtone OH stretch, could be modeled well with the cylindrical coordinate solution to the diffusion equation. The 2211 nm band did not follow a diffusion model, which was surprising because diffusion should not be wavelength dependent. However, the poor agreement between the growth increase of the 2211 nm band and the diffusion model is comprehensible because its assignments are much more complicated than the 1389 nm band. Assignments for the 2211 nm band include SiOH stretch and bend [19, 59] and a combination vibration of OH and a SiO_4 tetrahedral vibration [2, 47, 59]. A third band appeared at 1.24 μm, but its absorption was too small for reliable modeling and was not considered further.

These absorption bands proved to be permanent in that long periods of time in ambient air at room temperature did not decrease their absorption. Several fibers treated at high temperature, developing absorption in these bands, were left in ambient air for months and then returned to the furnace for more heat treatments. Their room temperature and high temperature absorption spectra were unchanged by the lengthy hiatus at room temperature without hydrogen exposure. Based on results shown in Figure 32 it is unlikely that the long periods of time at higher temperatures possibly even as high as 600 °C will cause much change to the absorption spectra. The persistence of these bands over time must be considered for longer term reliability when designing fiber optic systems that could be exposed to hydrogen, especially exposure at high temperatures.

In this work these absorption bands appeared during hydrogen exposure at 800 °C. But when the temperature was lowered to room temperature the loss at these bands increased dramatically and at a rate too fast to be consistent with hydrogen diffusion. This temperature dependence was then studied further by raising and lowering the temperature of the fiber while measuring the spectra in situ. Both bands decrease in absorption intensity as temperature is increased from room temperature to 800 °C. The 2211 nm band decreased monotonically as temperature increased while the 1389 nm band first increased up to 400 °C and then decreased in intensity as the fiber was heated further to 800 °C. This temperature dependent behavior was reversible. When the fiber was cooled the intensity increased to its position before heating. And it was repeatable as the absorption would return to its previous value at each temperature as it was heated or cooled. The temperature gradient direction did not appear to affect the phenomenon, i.e., the result was the same whether the fiber was being heated or cooled. Another important observation to note was when initial increase of the two bands occurred during hydrogen exposure at 800 °C the absorption at the 2211 nm was smaller than that of the 1389 nm band, showing a more dramatic change with temperature for the 2211 nm band. Upon cooling the 2211 nm band's absorption increased so dramatically it exceeded the detection limit for loss of the OSA. The 1389 nm band, although higher at high temperature, did not come close to saturating the detector upon cooling. In fact, in order to understand the full effect of the temperature range on the 2211 nm band a shorter piece of fiber was needed to reduce attenuation to within detection limits. On the other hand, fiber reaching the

full length of the furnace's heated region provided better signal to noise ratio for studying the 1389 nm band in the whole temperature range.

When designing a fiber optic system for communication or sensing it is important to account for the temperature dependence of the bands in this wavelength region. If the fiber is exposed to hydrogen at high temperatures absorption in these bands will occur and may even saturate after a few hours. But the absorption will increase if the fiber is cooled, even if it ceases to be in a hydrogen environment. The transmission loss at high temperatures cannot be relied on for understanding the hydroxyl concentration of the fiber. If a certain amount of power loss is budgeted for the system it is possible to meet the power budget at high temperature but not at low temperatures. Additionally, considering the difference in temperature response of the 2211 nm band and the 1389 nm band, if the attenuation changes due to temperature are all within the acceptable ranges for system design at the 1389 nm band they may not be for the 2211 nm band. When designing a system it is important to keep this phenomenon in mind.

Though the two absorption bands in this study are both related to hydroxyl concentration they do not behave the same way under the same circumstances. In addition to the difference in their growth behaviors when forming, there is a difference in their decrease in an environment when no hydrogen is present. Hydroxyl groups were generated in this fiber by heating it in an environment containing hydrogen. [36]So over time at high temperature the 1389 nm band decreased in absorption intensity, but this total decrease persisted to room temperature when the fiber was cooled. The high temperature absorption was still lower than the room temperature absorption but the final room temperature attenuation was lower than prior to the heating in ambient air. This change over time suggests a reduction in the hydroxyl content of the fiber In a hydroxyl concentration measurement two bands could show different results. So, it would be best to use the 1389 nm first overtone hydroxyl stretch band to measure hydroxyl content.

Although reduction in the height of the absorption bands was the most dramatic change due to increase in temperature it was not the only changed observed. The 1389 nm band may have broadened slightly as well but quantification of broadening is problematic without decomposition modeling. It also has a small shoulder near 1350 nm, which increased very slightly as temperature increased. The increase of this shoulder is not enough to account for the decrease of the bulk portion of the band and may be a result of band broadening as opposed to an increase at the particular wavelength of the shoulder. The 2211 nm band also shifted to longer wavelengths although its shift was not as pronounced and not unmistakably monotonic. It also had a shoulder, near 2066 nm, that increased with increasing temperature slightly. Both of these shoulders behaved the same with temperature, but it was difficult to tell if the shoulder was increasing specifically or if there was a general broadening of the band resulting in an increase in that area. Finally, because the two bands do not behave the same in terms of rate of hydroxyl formation and removal, and even monotonic increase in absorption as temperature increases, it is unlikely that change in structure affecting only the hydroxyl groups is the cause of this temperature dependent behavior. Instead it is likely that the entire glass network is changing in structure as it is heated and that change is in turn affecting these two hydroxyl related absorption bands. These changes with temperature were reversible, implying that a chemical change is not taking place but rather a structural change is affecting the absorption frequencies of the chemical bonds. The repeatability of these changes with temperature

indicates that, at each temperature, there is a preferential structure the network will take on for each temperature.

But even a change in glass structure or local environment for hydroxyl groups does not completely explain this massive reduction in peak height. If the frequency of vibration for the absorbing species at room temperature is not changing or changing only by a few nanometers in terms of wavelength, then something else must be occurring for the peak to reduce in height so dramatically. Some promising explanations, explored in detail in the previous section, are a change in molar absorptivity, a deviation from the linear relationship of Beer's law, or a change to an infrared inactive species. Investigating these possibilities is an excellent opportunity for future work. Even eliminating some of them would contribute markedly to the understanding of glass science and the expected performance of fiber optic systems which may become hydroxylated.

References

[1] R. T. Yukihiro Yokomachi, Kaya Nagasawa, and Yoshimichi Ohki, "Hydrogen Bond of OH groups in Silica Glass and its relation to the 1.39 um absorption," *Journal of Non-Crystalline Solids,* vol. 95 & 96, pp. 663-670, 1987.

[2] J. Stone and G. E. Walrafen, "Overtone Vibrations of OH Groups in Fused-Silica Optical Fibers," *Journal of Chemical Physics,* vol. 76, pp. 1712-1722, 15 February 1982 1982.

[3] G. E. Walrafen and S. R. Samanta, "Infrared absorbance spectra and interactions involving OH groups in fused silica," *The Journal of Chemical Physics,* vol. 69, pp. 493-495, 1978.

[4] L. Yu, "Experimental Setup," in *Powerpoint*, ed, 2014.

[5] J. Crank, *The Mathematics of Diffusion: 2d Ed*: Clarendon Press, 1975.

[6] Stefan. (2009, 3 June 2014). *Water is blue ... because water is blue*.

[7] "0.20 and 0.27 NA Graded-Index Multimode Fibers," 2015.

[8] (2015). *Refraction, reflection, and what is total reflection?* Available: http://physics.stackexchange.com/questions/37731/refraction-reflection-and-what-is-total-reflection

[9] R. M. Atkins and P. J. Lemaire, "Effects of elevated temperature hydrogen exposure on short-wavelength optical losses and defect concentrations in germanosilicate optical fibers," *Journal of Applied Physics,* vol. 72, p. 344, 1992.

[10] Q. Williams, "Infrared, Raman and Optical Spectroscopy of Earth Materials," in *Mineral Physics & Crystallography: A Handbook of Physical Constants*, ed: American Geophysical Union, 2013, pp. 291-302.

[11] J. Stone, "Interactions of Hydrogen and Deuterium with Silica Optical Fibers - a Review," *Journal of Lightwave Technology,* vol. 5, pp. 712-733, May 1987.

[12] H. Itoh, Y. Ohmori, and M. Nakahara, "Chemical change from diffused hydrogen gas to hydroxyl ion in silica glass optical fibres," *Electronics Letters,* vol. 20, pp. 140-142, 1984.

[13] K. Mochizuki, Y. Namihira, M. Kuwazura, and Y. Iwamoto, "Behavior of Hydrogen Molecules Adsorbed on Silica in Optical Fibers," *Ieee Journal of Quantum Electronics,* vol. 20, pp. 694-697, July 1984 1984.

[14] C. McDonagh, "Optical Chemical Sensors," *Chemical reviews,* vol. 108, pp. 400-422, 2008.

[15] K. S. P. Hae Young Choi, Seong Jun Park, Un-Chul Paek, Byeong Ha Lee, and Eun Seo Choi, "Miniature fiber-optic high temperature sensor based on a hybrid structure fabry-perot interferometer," *Optics Letters,* vol. 33, July 22 2008 2008.

[16] B. Lee, "Review of the present status of optical fiber sensors," *Optical Fiber Technology,* vol. 9, pp. 57-79, Apr 2003.

[17] P. J. Lemaire, "Reliability of optical fibers exposed to hydrogen: prediction of long-term loss increases," *Optical engineering,* vol. 30, pp. 780-789, 1991.

[18] N. S. Kazuhiro Noguchi, Naoshi Uesugi, and Yukiyasu Negishi "Loss Increase for Optical Fibers Exposed to Hydrogen Atmosphere," *Journal of Lightwave Technology,* vol. LT-3, April 1985 1985.

[19] R. D. Aines, S. H. Kirby, and G. R. Rossman, "Hydrogen Speciation in Synthetic Quartz," *Physics and Chemistry of Minerals,* vol. 11, pp. 204-212, 1984 1984.
[20] Y. Morimoto, T. Igarashi, H. Sugahara, and S. Nasu, "Analysis of gas release from vitreous silica," *Journal of Non-Crystalline Solids,* vol. 139, pp. 35-46, // 1992.
[21] G. Herzberg and S. Mrozowski, "Molecular Spectra and Molecular Structure. I. Spectra of Diatomic Molecules," *American Journal of Physics,* vol. 19, pp. 390-391, 1951.
[22] D. W. Ball, *The basics of spectroscopy* vol. 49: Spie Press, 2001.
[23] H. Yamagishi, S. Nakashima, and Y. Ito, "High temperature infrared spectra of hydrous microcrystalline quartz," *Physics and Chemistry of Minerals,* vol. 24, pp. 66-74, Jan 1997.
[24] H. Kakiuchida, K. Saito, and A. J. Ikushima, "Local structural relaxation around OH in silica glass," *Japanese Journal of Applied Physics Part 1-Regular Papers Short Notes & Review Papers,* vol. 41, pp. 2993-2998, May 2002.
[25] H. D. Young, R. A. Freedman, A. L. Ford, and F. W. Sears, *Sears and Zemansky's University physics*. San Francisco: Pearson Addison Wesley, 2008.
[26] R. Salh, *Defect Related Luminescence in Silicon Dioxide Network: A Review*, 2011.
[27] D. J. Griffiths, *Introduction to electrodynamics*. Upper Saddle River, N.J: Prentice Hall, 1999.
[28] G. Herzberg, *Molecular spectra and molecular structure I. Spectra of Diatomic Molecules*. Ney York NY: Van Nostrand Reinhold Company, 1950.
[29] J. E. Shelby, "Protonic species in vitreous silica," *Journal of Non-Crystalline Solids,* vol. 179, pp. 138-147, 11/4/ 1994.
[30] K. M. Davis, A. Agarwal, M. Tomozawa, and K. Hirao, "Quantitative infrared spectroscopic measurement of hydroxyl concentrations in silica glass," *Journal of Non-Crystalline Solids,* vol. 203, pp. 27-36, 8/1/ 1996.
[31] E. Hecht, *Optics*. Reading, Mass: Addison-Wesley, 2002.
[32] G. Keiser, *Optical fiber communications*. New York, NY: McGraw-Hill Companies, 2011.
[33] A. E. Lobkovsky, A. Karma, M. I. Mendelev, M. Haataja, and D. J. Srolovitz, "Grain shape, grain boundary mobility and the Herring relation," *Acta Materialia,* vol. 52, pp. 285-292, 1/19/ 2004.
[34] H. Mehrer, *Diffusion in solids: fundamentals, methods, materials, diffusion-controlled processes Springer series in solid-state sciences v. 155*. DE: Springer Verlag, 2007.
[35] J. Stone, A. R. Chraplyvy, and C. A. Burrus, "Gas-in-glass--a new Raman-gain medium: molecular hydrogen insolid-silica optical fibers," *Optics Letters,* vol. 7, pp. 297-299, 1982/06/01 1982.
[36] Z. Yongheng and G. Zhenan, "The study of removing hydroxyl from silica glass," *Journal of Non-Crystalline Solids,* vol. 352, pp. 4030-4033, 10/15/ 2006.
[37] R. W. Lee, "Diffusion of Hydrogen in Natural and Synthetic Fused Quartz," *The Journal of Chemical Physics,* vol. 38, p. 448, 1963.
[38] D. M. C. K. J. BE ALES, J. D. RUSH, "Increased attenuation in optical fibers caused by diffusion of molecular hydrogen at room temperature," *Electronics Letters,* vol. 19, 20th September 1983 1983.
[39] Y. M. K. Noguchi, K. Ishihara, "Infra-red loss spectrum of hydrogen molecules in a silica fibre," *Electronics Letters,* vol. 19, 24 November 1983 1983.

[40] R. H. Doremus, "Physical Solubility of Gases in Fused Silica " *Journal of American Ceramic Society,* vol. 49, September 21 1966 1966.
[41] J. E. Shelby, "Molecular diffusion and solubility of hydrogen isotopes in vitreous silica," *Journal of Applied Physics,* vol. 48, p. 3387, 1977.
[42] A. Iino, M. Kuwabara, and K. Kokura, "Mechanisms of Hydrogen-Induced Losses in Silica-Based Optical Fibers," *Journal of Lightwave Technology,* vol. 8, pp. 1675-1679, Nov 1990.
[43] C. M. Hartwig, "Raman-Scattering from Hydrogen and Deuterium Dissolved in Silica as a Function of Pressure," *Journal of Applied Physics,* vol. 47, pp. 956-959, 1976.
[44] Y. Mitsunaga, T. Kuwabara, T. Abe, and Y. Ishida, "Molecular hydrogen behaviour for loss increase of silica fibre in cable filled with water," *Electronics Letters,* vol. 20, pp. 76-78, 1984.
[45] J. F. Shackelford, "Solubility of Gases in Glass. II. He, Ne, and H2 in Fused Silica," *Journal of Applied Physics,* vol. 43, p. 1619, 1972.
[46] N. J. Pitt and A. Marshall, "Long-term loss stability of single-mode optical fibres exposed to hydrogen," *Electronics Letters,* vol. 20, pp. 512-514, 1984.
[47] H. F. O. Humbach, U. Grzesik, U. Haken, W. Heitmann, "Analysis of OH absoprtion bands in synthetic silca," *Journal of Non-Crystalline Solids,* vol. 203, pp. 19-26, 1996 1996.
[48] K. K. Unger, "Surface Structure of Amorphous and Crystalline Prous Silicas Status and Prospecs," in *In the Colloid Chemistry of Silica,* ed Washington DC: American Chemical Society, 1994, pp. 165-176.
[49] F. L. Galeener, "The Structure and Vibrational Excitations of Simple Glasses," *Journal of Non-Crystalline Solids,* vol. 123, pp. 182-196, Aug 1990.
[50] D. Griscom, "Defect Structure of Glasses Some outstanding questions in regards to vitreous silica," *Journal of Non-Crystalline Solids,* vol. 73, pp. 51-77, 1985 1985.
[51] X. Yuan and A. N. Cormack, "Si–O–Si bond angle and torsion angle distribution in vitreous silica and sodium silicate glasses," *Journal of Non-Crystalline Solids,* vol. 319, pp. 31-43, 2003.
[52] F. Mauri, A. Pasquarello, B. G. Pfrommer, Y. G. Yoon, and S. G. Louie, "Si-O-Si bond-angle distribution in vitreous silica from first-principles Si-29 NMR analysis," *Physical Review B,* vol. 62, pp. R4786-R4789, Aug 15 2000.
[53] V. G. Plotnichenko, V. O. Sokolov, and E. M. Dianov, "Hydroxyl groups in high-purity silica glass," *Journal of Non-Crystalline Solids,* vol. 261, pp. 186-194, 1// 2000.
[54] J. E. Shelby, "Reaction of Hydrogen with Hydroxyl-Free Vitreous Silica," *Journal of Applied Physics,* vol. 51, pp. 2589-2593, May 1980 1980.
[55] M. Tomozawa, H. Li, and K. M. Davis, "Water diffusion, oxygen vacancy annihilation and structural relaxation in silica glasses," *Journal of Non-Crystalline Solids,* vol. 179, pp. 162-169, 11/4/ 1994.
[56] M. Tomozawa, "Concentration Dependence of the Diffusion Coefficient of Water in SiO2 Glass," *Journal of American Ceramic Society,* vol. 68, pp. C251-C252, May 3 1985 1985.
[57] W. A. P. a. R. J. B. K W Hutt, "Far-infrared properties of dilute hydroxyl groups in an amorphous silica matrix," *Journal of Physics: Condensed Matter,* vol. I, pp. 4767-4772, 16 March 1989 1989.

[58] A. Tomita and P. J. Lemaire, "Hydrogen-induced loss increases in germanium-doped single-mode optical fibres: long-term predictions," *Electronics Letters,* vol. 21, pp. 71-72, 1985.
[59] K. M. Davis and M. Tomozawa, "An infrared spectroscopic study of water-related species in silica glasses," *Journal of Non-Crystalline Solids,* vol. 201, pp. 177-198, Jun 1996.
[60] A. Efimov and V. Pogareva, "IR absorption spectra of vitreous silica and silicate glasses: The nature of bands in the 1300 to 5000 cm−1 region," *Chemical Geology,* vol. 229, pp. 198-217, 2006.
[61] S. P. Z. L. S. K. a. T. I. Titova, "IR Study of Hydroxylated Silica," *Langmuir,* vol. 3, pp. 960-967, 10 September 1986 1987.
[62] J. H. Anderson jr and K. A. Wickersheim, "Near infrared characterization of water and hydroxyl groups on silica surfaces," *Surface Science,* vol. 2, pp. 252-260, // 1964.
[63] G. Lucovsky, R. J. Nemanich, and J. C. Knights, "Structural interpretation of the vibrational spectra of a-Si: H alloys," *Physical Review B,* vol. 19, pp. 2064-2073, 02/15/ 1979.
[64] M. H. Moore, T. Tanabe, and J. A. Nuth, "The SiH vibrational stretch as an indicator of the chemical state of interstellar grains," *The Astrophysical Journal,* vol. 373, pp. L31-L34, 1991.
[65] V. Lou, R. Sato, and M. Tomozawa, "Hydrogen diffusion in fused silica at high temperatures," *Journal of Non-Crystalline Solids,* vol. 315, pp. 13-19, 1// 2003.
[66] O. J. Edwards, "Optical Transmittance of Fused Silica at Elevated Temperatures," *Journal of the Optical Society of America,* vol. 56, 25 January 1966 1966.
[67] P. A. Tipler and R. A. Llewellyn, *Modern physics*. New York: W.H. Freeman, 2003.
[68] J. H. Wray and J. T. Neu, "Refractive Index of Several Glasses as a Function of Wavelength and Temperature," *Journal of the Optical Society of America,* vol. 59, pp. 774-776, 1969/06/01 1969.
[69] R. W. Lee, R. C. Frank, and D. E. Swets, "Diffusion of Hydrogen and Deuterium in Fused Quartz," *The Journal of Chemical Physics,* vol. 36, pp. 1062-1071, 1962.
[70] L. P. Huang and J. Kieffer, "Amorphous-amorphous transitions in silica glass. I. Reversible transitions and thermomechanical anomalies," *Physical Review B,* vol. 69, Jun 2004.
[71] L. P. Huang and J. Kieffer, "Amorphous-amorphous transitions in silica glass. II. Irreversible transitions and densification limit," *Physical Review B,* vol. 69, Jun 2004.
[72] C. T. Moynihan, A. J. Easteal, M. A. De Bolt, and J. Tucker, "Dependence of the Fictive Temperature of Glass on Cooling Rate," *Journal of the American Ceramic Society,* vol. 59, pp. 12-16, 1976.
[73] C. L. R Le Parc, J Pelous, V. Martinez, and B Champagnon, "Influence of fictive temperature and composition of silica glass on anomalous elastic behaviour," *Journal of Physics: Condensed Matter,* vol. 18, 30 March 2006 2006.
[74] K. Buijs and M. J. Maurice, "Some considerations on apparent deviations from lambert-beer's law," *Analytica Chimica Acta,* vol. 47, pp. 469-474, 10// 1969.